



Title	Ultra High-Speed Optical Soliton Transmission in Dispersion Managed Fibers
Author(s)	廣岡, 俊彦
Citation	大阪大学, 2000, 博士論文
Version Type	VoR
URL	https://doi.org/10.11501/3169410
rights	
Note	

The University of Osaka Institutional Knowledge Archive : OUKA

<https://ir.library.osaka-u.ac.jp/>

The University of Osaka

Doctoral Dissertation

**Ultra High-Speed Optical Soliton Transmission
in Dispersion Managed Fibers**

Toshihiko Hirooka

**Department of Electronics and Information Systems
Graduate School of Engineering
Osaka University**

January 2000

Man cannot survive except through his mind. He comes on earth unarmed. His brain is his only weapon. Animals obtain food by force. Man has no claws, no fangs, no horns, no great strength of muscle. He must plant his food or hunt it. To plant, he needs a process of thought. To hunt, he needs weapons, and to make weapons — a process of thought.

— Ayn Rand, *The Fountainhead*

Preface

The content of this thesis, a study of ultra high-speed optical soliton transmission in dispersion managed fibers, is based on the research I carried out during my Ph. D. course at the Department of Electronics and Information Systems, Graduate School of Engineering, Osaka University. The theoretical studies herein attempt to give general guidance for the developments of soliton based fiber-optic communication systems, for applications to long-haul point-to-point transmission links as well as the next generation all-optical networks, with much larger information carrying capacity.

The organization of the thesis is as follows.

Chapter 1 summarizes the history of fiber-optic communication systems, and solitons in optical communications. Physical properties of optical fibers are reviewed; in particular, the role of group velocity dispersion (GVD) and nonlinearity of fibers is highlighted to introduce the concept of solitons and dispersion management. It is then clarified what remains to be explored in the area covered by the thesis.

Chapter 2 presents a theory for modeling dispersion managed (DM) soliton transmission systems. In this model, the modified nonlinear Schrödinger equation that describes propagation of optical solitons in dispersion managed fibers is formulated in terms of Euler-Lagrange equation. By means of the variational method, a set of ordinary differential equations is obtained to describe the evolution of the parameters which characterize the pulse. This reduced model, where the pulse is characterized mainly by its width and frequency chirp, helps to elucidate the fundamental dynamics of DM solitons. Perturbation theory is also introduced to study the adiabatic evolution of the parameters under the influence of higher order effects and external perturbations. The results obtained in this chapter are applied to the analyses in the subsequent chapters.

In Chapter 3, the increase of transmission capacity in the soliton systems is addressed by channel multiplexing in the wavelength domain with strong dispersion management. The impact of cross phase modulation, which is known to limit transmission capacity in conventional soliton transmission lines, is studied analytically. As a result of strong dispersion management, solitons in different wavelength channels collide repeatedly with each other due to periodic variation of the sign of GVD, which leads to a residual frequency shift and timing jitter even in an ideal lossless transmission line. This frequency shift, however, is shown to be reduced significantly by strong dispersion management, indicating the potential applicability of DM solitons for massive wavelength division multiplexing (WDM).

In Chapter 4, the increase of transmission capacity per single-channel by means of dense dispersion management is discussed. Optimal design of densely dispersion managed line is shown to minimize nonlinear interactions between neighboring solitons in the same channel. The feasibility of single-

channel 160 Gbit/s soliton transmission by the use of the dense dispersion management in a practical situation is then numerically investigated. Taking advantage of the large tolerance of solitons to GVD variation, high-speed soliton transmission is shown to be possible in a practical dispersion-flattened fiber even in the presence of GVD variation and polarization mode dispersion.

Chapter 5 deals with the further improvement of transmission performance, for both single-channel and multi-wavelength DM soliton transmissions, with the help of transmission control schemes such as nonlinear gain elements, optical phase conjugation, and optical bandpass filters. Nonlinear gain elements, which selectively amplify the soliton component while suppressing the growth of background radiation, are shown to be beneficial in stabilizing the amplitude, frequency, and chirp fluctuations of the DM soliton. We also study ultra fast single-channel transmission over thousands of kilometers with a help of properly programmed GVD profile and optical phase conjugation. Thanks to the pulse confinement by means of the particular GVD profile combined with the optical phase conjugation, the stationary pulse called the quasi-soliton is shown to exhibit less variation of pulse width and suffers less interaction between adjacent pulses, which are beneficial for long-haul high-speed transmission links as well as for network applications. We further demonstrate that the instability observed in conventional control schemes such as the use of guiding filters may be avoided by the help of the cross phase modulation of the linearly unstable mode by solitons in other wavelength channels. Noise growth, which may eventually destroy solitons, is suppressed due to the spectral diffusion caused by the cross phase modulation. This result manifests a substantial advantage for application of DM solitons to massive WDM transmission.

Chapter 6 summarizes the overall results.

All the results obtained in this thesis are either published in Optics Letters and Electronics Letters, presented at Optical Fiber Communication Conference 1998 and Nonlinear Guided Waves and Their Applications 1999, or in press.



Osaka, Japan
December 1999

Toshihiko Hirooka

Acknowledgments

The present research has been carried out during my tenure of doctoral study at the Department of Electronics and Information Systems, Graduate School of Engineering, Osaka University, under the guidance of Prof. Akira Hasegawa (presently with Kochi University of Technology and NTT Science and Core Technology Laboratory Group).

I would like to express my deepest sense of appreciation to Prof. Akira Hasegawa for his professional instruction, continuous encouragement, and a number of stimulating discussions not only in the field of fiber optics but also in general physics. His keen insight and a wealth of creative ideas, to my surprise, have always provided me precise guiding frameworks for understanding complicated phenomena. I have learned many valuable lessons through my collaboration with him, which have further developed my abilities. I have been extremely fortunate to have been able to work with an authority in the fields of physics and engineering.

I wish to express my sincere thanks to Prof. Stefan Wabnitz, Université de Bourgogne (presently with Alcatel Corporate Research Center) for guidance during my short visit to Dijon and for ongoing collaborations, constant encouragement, and his hearty hospitality in Dijon. His fervent activities have always inspired me. The one month I spent in Bourgogne surrounded by autumn leaves and vineyards is certainly one of the more memorable times in my life.

I am profoundly indebted to the supervisor of my thesis, Prof. Ken-ichi Kitayama, for his constructive comments and suggestions, which have improved this thesis. Acknowledgment also goes to Prof. Kenji Taniguchi for his careful review on this thesis.

I have many people to acknowledge in the faculty of the Department of Electronics and Information Systems and the Department of Communication Engineering. Prof. Yuji Kodama (presently with Ohio State Univ.) gave me helpful and valuable suggestions based on his wealth experience in mathematics. The discussions with him intrigued my interest to the mathematical aspects of solitons. Prof. Masayuki Matsumoto, who also read through this thesis carefully as one of the reviewers, has generously spent a lot of time answering my question and providing technical advice. Prof. Shinsuke Hara frequently stopped by my office and always encouraged me. He also provided me with valuable comments from his experience in the area of wireless communications. Prof. Hiroyuki Toda has always been a source of guidance whenever I have had questions about experimental aspects of fiber optics. He generously provided me with a number of related references and data, which have been helpful to me. Dr. Akihiro Maruta has patiently devoted many hours to me in various technical discussions. His comments, criticism, and his kind hospitality in the laboratory have been invaluable in accomplishing this thesis.

I would like to express my gratitude to all the past and present colleagues in the Research Group of Advanced Communications Engineering in the Department of Electronics and Information Systems (Kitayama Laboratory) and the Research Group of Fundamentals of Communications Engineering in the Department of Communications Engineering. They have always provided encouragement and their friendship have given me strength through the difficult times. Special thanks go to Drs. Shiva Kumar (presently with Corning Inc.), An Hui Liang (with Tyco Submarine Systems), Hiroto Sugahara, Takeshi Nakada (with Hitachi, Ltd.), Hiroki Kato (with NTT West Corporation), Takashi Inoue, Itaru Nishioka, and Satoru Hattori (with Sumitomo Electric Industries, Ltd.), for their assistance and from a number of fruitful discussions.

There are many others to thank outside of the laboratory who have been a great encouragement personally. I especially thank Ivan Setiawan for his deep friendship ever since my undergraduate years.

I wish to acknowledge the Japan Society for the Promotion of Science (JSPS) Research Fellowships for their grants and financial support, which have been helpful in continuing this research without economic concerns.

Last but by no means least, I would like to thank my parents, Masahiko and Keiko, my sister, Yoko, and my grandmother, Shizu, for their unwavering love, patience, and support during the whole period of my education. They have been a source of great strength, enabling me to complete this endeavor.

Contents

Chapter 1	Introduction	1
1.1	Historical perspective	1
1.2	Overview	9
Chapter 2	Dynamics of dispersion managed solitons	13
2.1	Introduction	13
2.2	Lagrangian formulation	13
2.3	Fast and slow dynamics of dispersion managed solitons	18
2.4	Lagrangian perturbation method	19
2.5	Conclusion	24
Chapter 3	Wavelength division multiplexing of dispersion managed solitons	25
3.1	Introduction	25
3.2	Soliton interaction in WDM systems	25
3.3	Soliton interaction in strongly dispersion managed WDM systems	27
3.4	Numerical results	28
3.5	Conclusion	31
Chapter 4	Densely dispersion managed soliton transmission	33
4.1	Introduction	33
4.2	Dispersion managed soliton interaction in the same channel	33
4.3	Densely dispersion managed soliton	35
4.4	Numerical results	40
4.5	Conclusion	41
Chapter 5	Transmission control of dispersion managed solitons	43
5.1	Introduction	43
5.2	Stabilization of dispersion managed soliton transmissions by nonlinear gain	43
5.3	Quasi-soliton propagation with periodic optical phase conjugation	48
5.4	Stable filter control of wavelength division multiplexed soliton systems	51
5.5	Conclusion	53

Chapter 6	Conclusions and discussions	57
6.1	Conclusions	57
6.2	Discussions	57
Appendix	Nonlinear Schrödinger equation	63
A.1	Maxwell equation	63
A.2	Quasi monochromatic approximation	64
A.3	Linear and nonlinear polarization	65
A.4	Asymptotic expansion	68
A.5	Nonlinear Schrödinger equation in optical fibers	75
A.6	Normalization of the nonlinear Schrödinger equation	77
Bibliography		79

Chapter 1

Introduction

1.1 Historical perspective

This section presents a historical perspective on the development of fiber-optic communication systems and optical solitons. Particular emphases are made to clarify the role of dispersion management in soliton transmission.

Optical fibers can transmit information with extremely low loss over a wide range of wavelengths. By virtue of this outstanding property, fiber-optic communication technologies have been applied to a variety of transmission systems throughout the world, such as international undersea networks, terrestrial links, and access networks [1, 2]. The invention of the erbium doped fiber amplifiers (EDFAs) in the late 1980's, in particular, has brought remarkable progress in this field. EDFAs have played a critical role in constructing fiber-optic communication systems with remarkably large capacity over much longer distance, allowing transmission of multiple wavelength channels by the use of wavelength division multiplexing (WDM). A recent surge of data traffic due to the widespread use of Internet, on the other hand, has accelerated demands for much larger capacity in transmission links. As this trend grows continuously, fiber-optic communication systems are expected to mature into an infrastructure of the next generation, which will revolutionize our society in the 21st century. In order to meet the explosive growth of demands, terrestrial links will be required to support more than 1 Tbit/s transmission capacity in the near future. In constructing such high-speed transmission systems, lying far beyond the limit of electronic signal processing, it is important to understand extensively the physical properties of optical fibers in order to take full advantage of their potential.

Physical properties of optical fibers have been studied since the 1960's, such as their waveguide characteristics, chromatic dispersion, loss, and nonlinearity [3, 4].

Optical fiber cables guide waves by total internal reflection at the interface between the core layer having higher refractive index and the cladding layer having lower index. Boundary condition at the core-cladding interface permits a finite number of guided modes supported by fibers. The lowest mode is known as HE_{11} mode, and as the core radius gets larger, higher modes such as TE_{01} and TM_{01} are also allowed to be guided. When more than two guided modes propagate simultaneously in fibers, signals get distorted at the receiver because each mode propagates with different speed, which is the phenomenon known as multimode dispersion.

In addition, chromatic dispersion of optical fibers brings about the dependence of group velocity on frequency. In the presence of dispersion, different spectral components of an optical pulse propagates at different group velocities, which leads to pulse broadening. As a result, a signal is distorted at the receiver in a way similar to the multimode dispersion. This phenomenon is referred to as group-velocity dispersion (GVD). Chromatic dispersion has two contributions: material dispersion and waveguide dispersion. Material dispersion originates from a physical property of the silica, i.e. a retarded response of bound electrons in silica for lightwave electric field, which gives frequency dependence of the refractive index. Waveguide dispersion arises from the geometry of the guided structure such as a core radius.

Fiber loss, another limiting factor of transmission distance, originates from material absorption in the far-infrared region and Rayleigh scattering arising from random density fluctuation that takes place during fiber fabrication. Pure silica absorbs light at the wavelength $\sim 2 \mu\text{m}$, while Rayleigh scattering loss is dominant at short wavelengths since it increases as λ^4 . Hence the fiber exhibits a minimum loss at the wavelength in the vicinity of $1.55 \mu\text{m}$.

Nonlinear effects in optical fibers [5–7] have two major contributions: nonlinear refractive index arising from nonlinear electric polarization of bound electrons in the silica, and stimulated inelastic scattering arising from the excitation of vibrational mode of the silica. Since silica fibers do not exhibit second order nonlinear effects due to the inversion symmetry of the molecular, third order nonlinear electric polarization (Kerr nonlinearity) contributes to the lowest order nonlinear effect in fibers. Since the Kerr effect induces intensity dependence of the refractive index of silica, it brings about intensity dependent phase shift. The nonlinear phase shift introduced by the optical field itself is called self phase modulation, whereas the cross phase modulation is a phase shift which is induced by the other light copropagating with different frequencies or polarization components. These nonlinear phase shifts result in spectral broadening during propagation and, by the interplay with GVD, may produce considerable waveform distortion. In addition to phase modulations, once the phase matching conditions are satisfied, third order nonlinearity induces a parametric process called four wave mixing, where three copropagating optical fields generate the fourth electric field with a different frequency. This leads to inter-channel crosstalk in WDM systems as a result of energy transfer between neighboring wavelength channels, and imposes a limit on WDM transmission performance such as the number of channels or channel spacing.

In an inelastic scattering process, as a result of transferring a part of the incident energy to vibrational mode excitation in the silica, the incident light suffers from a loss of power and generates a scattered light wave whose frequency is downshifted by the amount equal to the number of phonons transferred from the incident photons. Furthermore, once the incident power exceeds a threshold value, the power of the scattered light grows exponentially due to stimulated scattering. Stimulated Raman scattering (SRS) causes the energy transfer to optical phonons, whereas stimulated Brillouin scattering (SBS) transfers the energy to acoustic phonons. Since SBS scatters light in the backward direction, the threshold of SBS limits the launched optical power.

Although silica fibers do not intrinsically exhibit high nonlinearity (Kerr coefficient of the silica is the

magnitude of 10^{-20} m²/W), nonlinear effects accumulate over a long distance of propagation and may have a considerable impact because of its rather high efficiency due to the low loss and high density of lightwave over a small cross section in waveguide geometry. Nevertheless, as described below, they had not been taken into consideration carefully before the development of EDFA.

To overcome the limitations imposed by the physical properties of optical fibers, there have been made a number of technical advances.

To avoid multimode dispersion, waveguide geometry of optical fibers has to satisfy the single mode condition, which is determined by the condition that TE₀₁ and TM₀₁ modes reach cutoff. This requires a core radius < 10 μ m and fractional index change $< 1\%$ at the core-cladding interface. Thus the multimode dispersion can be avoided by the use of single mode fibers (SMFs) that satisfy the cutoff condition. Since SMF exhibits zero dispersion at the wavelength of 1.3 μ m, lightwave systems at the early age was operated at this wavelength.

Such primary systems, however, were limited mostly by fiber loss. Advances in fabrication technology of fibers had made it possible to achieve the minimum loss of 0.2 dB/km at the wavelength of 1.55 μ m [8]. On the other hand, at this wavelength, GVD exceeds 15 ps/nm/km for SMF and brings about significant pulse broadening during propagation. This difficulty was overcome by the use of dispersion shifted fibers (DSFs) having minimum dispersion at 1.55 μ m by a careful design of the index profile such that the zero dispersion wavelength is shifted from 1.3 μ m to the vicinity of 1.55 μ m. Now that we have almost precise control over the arbitrary choice of GVD value, it is possible to fabricate fibers even with negative GVD that compensates for the high value of GVD in SMF installed. These fibers are referred to as dispersion compensating fibers (DCFs).

In such lightwave systems using DSF at the operating wavelength of 1.55 μ m, electronic regeneration was employed to compensate for the loss at intervals of 60–80 km, where the input optical signal is detected, converted to an electronic signal, and then after reshaping and retiming it at the electronic circuit, regenerated as a brand-new optical signal at the output. The electronic regenerators, however, include complicated signal processing, and they are not only less cost-effective but also impose a limit on transmission speed.

The invention of an optical amplifier in 1987 operating at 1.55 μ m making use of the Erbium doped fiber [9, 10] was thus welcome and excited considerable enthusiasm among the worldwide researchers involved in the field of lightwave systems. The development of EDFA has accelerated the experimental research toward longer distance and larger capacity thanks to its compatibility with WDM and contribution to improved receiver sensitivity.

EDFA solved the loss problem, however EDFA restated the significance of nonlinear effects at the same time, as lightwave systems making use of EDFA operate at relatively high power in order to maintain the average power without being buried by noise. In addition to the nonlinear effects, amplified spontaneous emission (ASE) noise accumulate over multiple amplification stages, which was absent in conventional systems employing the electronic repeaters. Since nonlinear effects cannot be compensated by passive methods, the only approach to cope with them is to reduce the fiber nonlinearity itself by the use

of fibers with large core area or by keeping local GVD relatively large on purpose to suppress the nonlinear effects while minimizing the average GVD by compensating for the cumulative GVD. The latter approach, referred to as dispersion management, reduces nonlinear effects by the help of GVD.

Pioneering works on nonlinear effects in fibers back in the 1970's have recently been revived as nonlinear effects have induced considerable attention especially in long-haul transmission systems using EDFA. Among those contributions, theoretical prediction of optical solitons by Hasegawa and Tappert in 1973 [11] is now attracting profound interest as an ultimate solution to overcome the nonlinear effects [12–14]. Hasegawa and Tappert derived the nonlinear Schrödinger equation for the propagation of the slowly varying envelope of an optical pulse in a fiber with dispersion and nonlinearity and demonstrated the soliton solutions to be effective in high-speed signal transmission in optical fibers. Optical soliton preserves its shape during propagation, where the nonlinear chirp arising from Kerr effect counteracts with the dispersion-induced chirp. Solitons thus do not suffer from either the pulse broadening in the presence of GVD or the spectral broadening due to the self phase modulation. This indicates their potential application to high-speed optical transmission. The important thing is that, theoretically speaking, the integrability of the nonlinear Schrödinger equation [15] guarantees the stability of soliton propagation and, at the same time, indicates that any pulse of arbitrary shape launched with a proper amount of power evolves itself to a soliton (or solitons) during propagation whenever the nonlinearity is maintained large enough by loss compensated by amplifiers. The flexibility of solitons is an important property not only from a mathematical but also from a technical point of view.

As a result of technical advances in lightwave systems, such as the development of semiconductor lasers with high power, optical fibers with low loss, and optical amplifiers, there have been a large number of theoretical as well as experimental contributions toward the application of optical solitons to long-haul high-speed transmission systems. One important theoretical discovery is that the averaged dynamics of optical pulses in the presence of periodic perturbations such as non-adiabatic loss and lumped amplifications or weak dispersion management is also described by the nonlinear Schrödinger equation by means of the guiding center theory, as long as the periodicity is much shorter than the characteristic distance called the soliton period [16–18]. Hereafter we generally refer to the soliton solution of the nonlinear Schrödinger equation as a ‘classical’ soliton, whether it is the solution of the unperturbed equation or the averaged equation.

Soliton based communications also face some technical difficulties unique to solitons. One of the most serious issues is the phenomenon referred to as the Gordon-Haus effect [19]. Gordon-Haus effect is a timing jitter which originates from random fluctuation of the carrier frequency of solitons caused by the nonlinear interaction with ASE noise. Gordon-Haus effect crucially limits the available capacity and transmission distance in soliton based systems. Nonlinear interaction between two neighboring solitons in a single channel also degrades the performance [20, 21], since two solitons, when they are in-phase, attract with each other during propagation, resulting in their complete overlap at some distance. To avoid the attraction, the interval between solitons should be set at least five times as large as the pulse width of the soliton. Moreover, in WDM transmissions, solitons in different wavelength

channels could induce their timing jitter. Since the nonlinear Schrödinger equation is integrable, solitons interact elastically and their amplitudes and velocities remain the same as those prior to the collision. A collision, however, can introduce nonlinear interactions between the wavelength channels through cross phase modulation and four wave mixing. These effects affect soliton transmission in a manner slightly different from the case of the conventional linear systems [22–29]. Cross phase modulation and four wave mixing bring about central frequency shift [22–26] and the sideband generation [27–29], respectively, during the collision process. In a lossless fiber, these nonlinear effects are canceled out completely after the collision is over because of the symmetry of the whole collision process [26, 29]. As a consequence of the integrability, the colliding pair of solitons preserves their amplitudes and velocities, but they experience temporal displacement after the collision by the amount which is given by the integral of the temporary frequency shift along the distance. The situation, however, gets much worse in the case of the collision process within periodically inserted lumped amplifiers because of the breakdown of the symmetry [23]. Here we consider two cases. When the walk-off distance of the two colliding solitons is sufficiently large compared with the amplifier spacing, which is the case of narrower channel spacing, solitons do not recognize the perturbation since the effect of the lumped amplifications are averaged out. On the other hand, two solitons with wide channel spacing may experience asymmetric collision process (partial collisions) because of the walk-off distance comparable to the amplifier spacing. In the latter case, central frequency shift due to the cross phase modulation is not canceled out after the collision is over, resulting in residual frequency shift. The residual frequency shift leads to the shift of their temporal position increasing in proportional to the distance and causes considerable timing jitter. Note that even for narrow channel spacing, another limitation comes from the overlap of multi-solitons at the input of a transmission line, referred to as the initial overlap [22, 25]. This is another consequence of the asymmetric collision process, since the first part of the collision is absent. As a result, they experience a residual shift of the central frequency which is given by the amount of the temporary frequency shift that would have been offset in a complete collision process. In this case, the temporary frequency shift, which is significant for narrower channel spacing, is responsible for timing jitter during the whole propagation.

Spatial frequency as a result of the periodic variation of optical power in the presence of the periodic damping and lumped amplifications may help satisfy the phase matching condition responsible for the accumulation of the four wave mixing component [27, 28]. Such pseudo phase matching may enhance the sideband generation within the collision process, resulting in inter-channel crosstalk as an additional noise. It is difficult to control these nonlinear effects because they depend on data pattern of the individual channels.

Several techniques have been proposed to overcome these limitations. The simplest method is to combine a bandpass filter with an amplifier [30, 31]. Filters with narrow bandwidth inserted periodically are able to stabilize the amplitude and frequency of a soliton. This takes advantage of a unique property of the optical solitons that their amplitude is always proportional to the inverse of their pulse width. Excessive amplification, for instance, leads to the narrowing of the bandwidth according to this property,

thus the spectrum broadens. This broadened spectrum then goes through the bandpass filter where the spectral components outside the bandwidth are eliminated. The excess amplitude therefore can be diminished. In this principle, the guiding filters give feedback against the variation of soliton amplitude and frequency. Linear waves such as ASE noise, on the other hand, are diffused in time domain by the filters, making it possible for only solitons to be selectively controlled in principle. The guiding filter, however, requires excess gain in EDFA, which is necessary to compensate for the loss of soliton energy lost by the filtering action. However, the excess gain, at the same time, amplifies linear waves within the filter bandwidth every time the pulse goes through a filter. This leads to significant growth of the noise and may even destroy the soliton [32]. To avoid the instability, several methods have been studied, such as sliding frequency guiding filter [33] and synchronized amplitude [34] and phase [35] modulation, which attempt to separate noise from solitons. These schemes have demonstrated successful soliton transmission over a long distance, far beyond the limitation imposed by the instability [36, 37]. However, the sliding frequency filters, which require precise control of the central frequency at every stage, are troublesome in a practical application. The synchronous modulation is not compatible with WDM transmission, since the pulses in different channels propagating with different speeds have to be retimed separately, which requires demultiplexing and multiplexing of all the channels every time they go through modulators.

Through a number of attempts to overcome these limitations, a significant breakthrough has finally come about in soliton transmissions: the discovery of dispersion managed (DM) solitons. DM soliton is a new stable nonlinear pulse which propagates in a dispersion managed fiber that consists of multiple sections of positive and negative GVD. The dispersion management, which is originally introduced to suppress nonlinear effects in linear transmission systems, is demonstrated to be beneficial also in soliton transmission systems. In 1993, Forysiak et al. proposed post transmission compensation of cumulative GVD altogether by connecting DCF prior to the receiver [38]. Their motivation was to reduce the Gordon-Haus effect, noting that the timing jitter decreases by reducing the total amount of GVD. Suzuki et al., in 1995, succeeded in the reduction of Gordon-Haus jitter experimentally by periodically compensating for the GVD accumulation by the use of DCF [39]. Also in 1995, Knox et al. demonstrated numerically that solitons can propagate with reasonable power in conventional SMF with large GVD by periodic dispersion compensation with DCFs at every amplifier and reducing the average dispersion [40]. Furthermore, in 1996, Smith et al. numerically showed that a chirped quasi-stationary pulse, now referred to as the DM soliton, exists in a periodically dispersion managed fiber, whose shape is close to Gaussian. The DM soliton has enhanced energy compared with the energy of the classical solitons in a fiber with the constant GVD equal to the average GVD of the dispersion managed line [41]. The energy enhancement is a particularly important property in soliton transmission, since it allows the suppression of Gordon-Haus jitter by reducing the average GVD without sacrificing the degradation of the signal-to-noise ratio [42].

Since then, it has been clarified by a number of theoretical and experimental studies that the DM solitons have remarkable properties that are not observed in the classical solitons [43–45]. One of their

outstanding properties is the large margin for initial conditions, such as launched power, pulse width, and prechirp. This flexibility is an important issue in practice. Experimental studies have verified their superb characteristics and have been demonstrating their feasibility for practical transmission systems. The DM soliton evolution and interactions have also been elucidated by theoretical studies based on the variational method [46, 47], Lie transformation [48, 49], and multiple scale method [50] as well as direct numerical simulations. Some of these features are discussed in detail in the succeeding chapters.

On the other hand, considerable efforts have been made in linear transmission systems to cope with nonlinear effects. In addition to dispersion management or the use of new fibers with reduced nonlinearity, optical modulation in the return-to-zero (RZ) format helps reducing nonlinear effects rather than in the conventional non-return-to-zero (NRZ) format. NRZ had been employed since it requires less bandwidth associated with the bit stream. NRZ had also been considered to suppress nonlinear effects by transmitting continuous waves over the total time slot of successive bits of “1” and thus reducing the peak power. Nonlinearity, however, plays a crucial role even in the NRZ format as the bit rate increases and the peak power is enhanced to keep the average power within one bit slot. For this reason, the RZ format, more tolerant to nonlinearity, has recently been employed. The pulse modulated in the RZ format propagating in a dispersion managed line is sometimes called the chirped RZ pulse or the nonlinear supported RZ pulse.

Dispersion management is now regarded as a simple but powerful scheme to deal with nonlinear effects in both linear and nonlinear transmission systems. It is an interesting contrast that linear systems take advantage of GVD to suppress nonlinear perturbations, whereas classical solitons cope with GVD by the help of nonlinearity. The main difference between the chirped RZ pulse and the DM soliton is that the DM solitons positively exploit the self phase modulation whereas the chirped RZ pulses attempt to avoid any kind of nonlinear effects. As in the case of the classical solitons, self phase modulation is beneficial also for the DM solitons, in that it gives a feedback effect against amplitude and frequency fluctuations by the help of the bandpass filtering action.

Figure 1.1 shows the latest results of transmission experiments collected from the postdeadline papers presented at the international conferences held in 1998 and 1999. Open marks represent the results of linear transmission systems, whereas closed circles are for the DM soliton transmission. At present, the performance of linear systems looks superior to that of solitons both in the achievable distance and total capacity. However, solitons can provide higher bit rate per channel in WDM systems and in ultra long transmissions. Furthermore, it should be noted that some of these superior linear transmissions are significantly assisted by forward error correction (FEC). Without FEC, the error-free transmission distance is reduced to less than a half. In addition, some of these experiments combine Raman amplification with EDFA in order to reduce the ASE noise generated from EDFA as a result of its reduced gain. These sophisticated techniques are expected to be helpful also to improve the performance of the DM soliton systems. One of the advantages of DM solitons is that, in contrast to those linear systems employing post transmission compensation of GVD, they are intrinsically a periodic system, giving more flexibility in constructing practical systems including network applications.

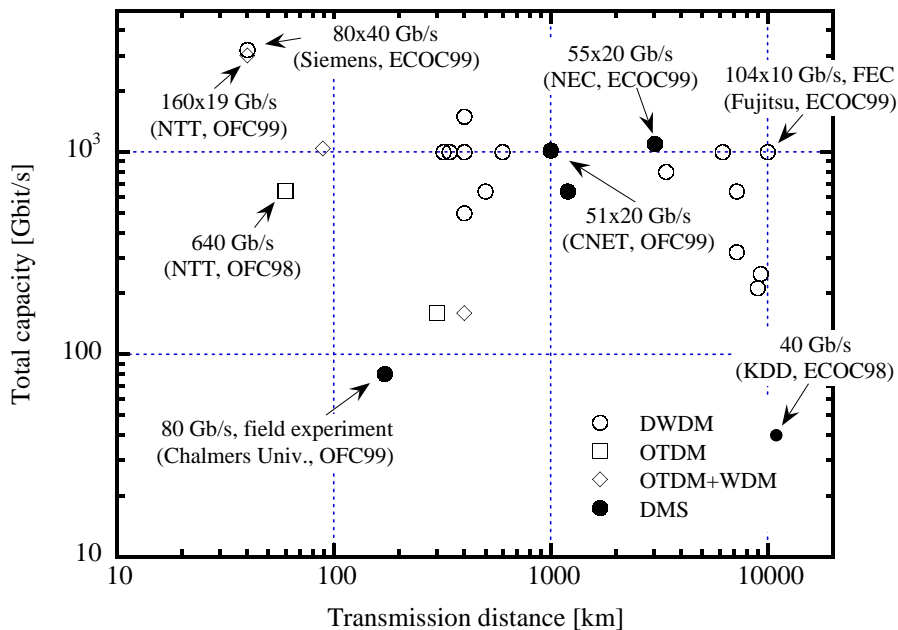


Figure 1.1: Recent experimental results of high-speed optical transmissions. Total capacities are denoted as the number of wavelength channels times the bit rate per single channel.

OFC: Optical Fiber Communication Conference,

ECOC: European Conference on Optical Communication,

DWDM: Dense Wavelength Division Multiplexing, OTDM: Optical Time Division Multiplexing,

DMS: Dispersion Managed Soliton, FEC: Forward Error Correction.

The further increase of transmission capacity beyond Tbit/s gives rise to other limiting issues and requires a more careful study of optical fibers. As short optical pulses are used to increase the bit rate per channel up to 40 Gbit/s or even more, the bandwidth occupied by the individual pulse becomes considerably large, resulting in a relatively large influence of higher order effects in fibers such as third order dispersion, nonlinear retarded response, and polarization mode dispersion (PMD). Third order dispersion, often referred to as dispersion slope, brings about pulse distortion as a result of the dependence of GVD on the frequency component within its own spectrum. Retarded response of nonlinear electric polarization is responsible for Raman effect observed within the spectrum, known as the self-induced Raman effect, i.e. a continuous downshift of the frequency. Polarization mode dispersion induces signal distortion as a consequence of stochastic group velocity difference and coupling between the two orthogonal polarization components in a birefringent optical fiber. Compared with linear pulses, solitons are more tolerant to PMD owing to the self confinement of the two orthogonal modes by cross phase modulation. However, the energy loss induced by PMD generates dispersive radiation, resulting in interference with other solitons. In dense WDM, further expansion of the total bandwidth available to WDM transmission is an important issue. Gain flattening over the whole bandwidth of EDFA as well as GVD equalization is thus required, while taking into account the impact

of nonlinear crosstalk to decrease the channel spacing.

The scope covered by this thesis and its objectives are now ready to be clarified. The discussions in this section so far have focused on how nonlinear effects in optical fibers affect and why they play an important role in constructing high-speed optical communication systems. Particular emphasis has been placed on the claim that the DM soliton is a natural solution to cope with these perturbations. Yet there still remains much clarification with respect to the feasibility of its employment in practical systems. In particular, the study of DM soliton interaction in single-channel as well as multi-channel transmissions is an important subject. Improvements of the transmission control schemes which take advantage of self phase modulation should also be pursued. Theoretical studies on these issues are expected to provide guidance to experimental developments, just as the classical solitons have owed much of their improvement to a number of theoretical indications. These are the main aspect what the thesis aims for.

1.2 Overview

Reflecting on the recent trends in fiber-optic communication systems described in the previous section, this thesis provides a theoretical investigation on the feasibility of ultra high-speed fiber-optic transmission by the use of dispersion managed (DM) solitons. Applications to all-optical network systems are taken into account consistently in the thesis as well as point-to-point transmission links. We first clarify the physical and technical restrictions on the increase of transmission capacity in DM soliton transmission, by means of optical time and wavelength division multiplexing. Based on the theory, we present practical configuration of dispersion managed transmission lines especially with respect to an arrangement of the GVD profile. We further study several control schemes to stabilize DM soliton transmissions to improve their performance, by taking advantage of the identity of DM solitons as a nonlinear stationary pulse. The overall results obtained in the thesis are devoted to motivate developments of soliton based fiber-optic transmission systems in the next generation with much larger capacity and improved stability.

Chapter 2 provides an analytical model that describes the pulse dynamics of DM solitons. DM solitons in optical fibers with damping, lumped amplification, and periodic dispersion management behave according to the modified nonlinear Schrödinger equation where the coefficients of the dispersion and nonlinear terms are given by periodic functions of distance. Although the equation is written in Hamiltonian form, it is not integrable because of the inhomogeneity in the dispersion and nonlinear coefficients, making it difficult to treat mathematically. We demonstrate that the DM soliton evolution is described, with good accuracy, simply by a finite number of ordinary differential equations which is reduced via the variational method from the nonlinear Schrödinger equation, namely by trailing the evolution of parameters that identify the DM soliton (typically its pulse width and frequency chirp). Based on the obtained reduced model, we study fast (within one period) and slow (averaged over one period) dynamics of the DM solitons, and elucidate their peculiar characteristics that are not observed

in the classical solitons. We further derive ordinary differential equations that describe the adiabatic behavior of these parameters under the influence of higher order effects and external perturbations. The analytical results obtained in this chapter not only provide a deep insight on understanding fundamental dynamics of DM solitons but also are frequently referred to in the analyses in the subsequent chapters.

In Chapter 3, we analytically study the impact of the cross phase modulation for DM solitons in WDM transmissions, which has been one of the major limitations on transmission performance in classical soliton WDM systems. We employ the perturbation method introduced in Chapter 2 to evaluate the frequency shift caused by the cross phase modulation in a strongly dispersion managed transmission line. As a result of the strong dispersion management, solitons in different wavelength channels collide repeatedly with each other due to the periodic variation of the sign of GVD, which leads to a residual frequency shift even in an ideal lossless transmission line. This frequency shift, however, is shown to be reduced significantly by employing strong dispersion management, indicating its potential applicability for soliton WDM systems.

In Chapter 4, the interaction between neighboring DM solitons in the same channel is studied, and a properly designed densely dispersion managed transmission system is demonstrated to overcome the limitation. DM soliton is also known to suffer from the nonlinear interaction between neighboring bits, and the impairment may be more significant than classical solitons especially for strongly dispersion managed lines. Meanwhile in a sufficiently weak dispersion management regime, where the pulse dynamics are described in the frame of the guiding center theory, the interaction is shown to be reduced thanks to the faster decaying tail of the stationary core pulse compared with the sech shape of the classical soliton. Therefore the optimal strength of dispersion management exists that minimizes the interaction, which has been verified by numerical simulations. The optimal condition is, however, difficult to meet in a conventional two-step GVD profile over one or more amplifier spacing as the bit rate increases, because the optimization imposes a lower limit on the pulse width available for a given GVD profile, or equivalently, requires sufficiently small GVD for a short pulse width. In order to satisfy the both demands simultaneously, dense dispersion management (sometimes referred as short scale dispersion management) has been successfully demonstrated to suppress the interaction without these restrictions. On the other hand, DM soliton transmission at higher bit rate per channel up to 160 Gbit/s, supported by the dense dispersion management, is required to cope with the above mentioned higher order perturbations that explicitly influence the performance. Among them, dispersion slope may be the dominant perturbation, leading to considerable pulse distortion. We therefore take into account these perturbations in arranging GVD profile of dense dispersion management and study the feasibility of 160 Gbit/s transmission in the revised profile.

Chapter 5 deals with the improvement of DM soliton systems, both in single-channel and WDM transmission, by means of the transmission control schemes such as nonlinear gain elements, optical phase conjugations, and guiding filters. Nonlinear gain elements combined properly with guiding filters, realized by fast saturable absorbers, are shown by the perturbative analysis and numerical simulations to improve considerably the DM soliton stability in a single-channel transmission. The nonlinear gain

helps suppress the growth of background radiation even for nearly-zero average dispersion, allow the large tolerance with respect to the initial energy or chirp fluctuations, and avoid the instability caused by lumped filtering actions in an inadequate location within one dispersion management period. From a point of view of the suppression of the pulse-to-pulse interactions, we next consider the application of optical phase conjugation (OPC) to the ‘quasi-soliton’ transmission, where the GVD profile is properly programmed so that the pulse is confined by a trapping potential, suppressing the pulse width oscillation within one period, thus reducing the interaction. OPC provides not only compensation of cumulative dispersion, but also contributes to form the trapping potential. The quasi-soliton supported by OPC is shown through numerical simulations to provide ultra-fast single-channel transmission over thousands of kilometers. This scheme is also compatible with WDM transmission. Finally, we return to the conventional scheme of the guiding filter. Guiding filter with excess gain provides instability caused by the noise growth that is induced by the amplification of dispersive wave within the bandwidth of the filter by the excess gain. We demonstrate that, in WDM DM soliton systems, the instability may be avoided by the help of the cross phase modulation of the linearly unstable mode induced by other WDM solitons channels. Numerical simulations are carried out to observe the evolution of initially generated noise and to demonstrate successful suppression of the noise growth. This result presents a substantial advantage of dense WDM soliton transmission systems supported by guiding filters.

Chapter 6 summarizes the overall results obtained in the thesis.

Chapter 2

Dynamics of dispersion managed solitons

2.1 Introduction

As described in Chapter 1, periodic dispersion management is attracting profound interest in soliton based communication systems for the past few years. It has been found that there exists a quasi-stationary pulse known as dispersion managed (DM) soliton in periodically dispersion compensated systems that has features more attractive than a classical soliton such as the reduced timing jitter caused by amplifier noise (Gordon-Haus effect) or the improved signal to noise ratio. The waveform deviates from the classical soliton (sech-type pulse) and is closer to Gaussian. A unique feature common to such a pulse is a periodically changing chirp along its propagation. The strong chirp helps reduce effective nonlinearity which is necessary for balancing the local dispersion. In this chapter, we present the result on the study of fundamental dynamics of the DM solitons and the influence of perturbative effects in transmission lines by means of the variational method. (See also [46, 51].)

2.2 Lagrangian formulation

Propagation of optical pulses in fibers with variable dispersion can be described by the nonlinear Schrödinger equation of the form

$$i \frac{\partial q}{\partial Z} + \frac{d(Z)}{2} \frac{\partial^2 q}{\partial T^2} + |q|^2 q = -i\Gamma q + iG(Z)q, \quad (2.1)$$

where T and Z are the normalized time and distance respectively, Γ is the normalized loss, and $d(Z)$ and $G(Z)$ are periodic functions that represent the normalized dispersion and lumped amplification, respectively. A detail of its derivation and these normalizations can be found in the Appendix. We introduce new amplitude $u(T, Z)$ through $q(T, Z) = a(Z)u(T, Z)$ with $da/dZ = [-\Gamma + G(Z)]a$ in order to remove the oscillating amplitude due to loss and periodic amplification. The newly introduced amplitude $u(T, Z)$ satisfies

$$i \frac{\partial u}{\partial Z} + \frac{d(Z)}{2} \frac{\partial^2 u}{\partial T^2} + a^2(Z)|u|^2 u = 0. \quad (2.2)$$

It should be noticed that (2.2) has a Hamiltonian structure whereas the original equation (2.1) does not. Equation (2.2), however, is not integrable because of the inhomogeneity due to the periodic variation of d and a . Thus we solve the problem approximately by means of the variational method based on the observation that the system described by (2.2) supports a well-defined solution of a chirped pulse whose shape is close to Gaussian. In order to introduce the variational method, we start from Lagrangian formulation of the problem [14, 52].

Suppose we have a functional \mathcal{L} called Lagrangian density which is a function of the field quantity u , u^* , and their derivatives with respect to Z and T . We adopt formulation of the infinite dimensional Euler-Lagrange problem [53]. For infinite dimensional problems, Lagrange's principle of least action is given by

$$\delta I = \delta \int_{-\infty}^{\infty} \int_{-\infty}^{\infty} \mathcal{L}[u, u^*, u_Z, u_Z^*, u_T, u_T^*; Z] dT dZ = 0. \quad (2.3)$$

For the variation of the field δu , that is when u varies to $u + \delta u$, the variation of \mathcal{L} is expressed as

$$\delta \mathcal{L} = \frac{\partial \mathcal{L}}{\partial u} \delta u + \frac{\partial \mathcal{L}}{\partial u_Z} \delta u_Z + \frac{\partial \mathcal{L}}{\partial u_T} \delta u_T + \frac{\partial \mathcal{L}}{\partial u^*} \delta u^* + \frac{\partial \mathcal{L}}{\partial u_Z^*} \delta u_Z^* + \frac{\partial \mathcal{L}}{\partial u_T^*} \delta u_T^*. \quad (2.4)$$

Hereafter in this chapter, the subscripts denote the partial derivative with respect to the coordinate. Then (2.3) leads to

$$\begin{aligned} \delta I &= \int_{-\infty}^{\infty} \int_{-\infty}^{\infty} \delta \mathcal{L} dT dZ \\ &= \int_{-\infty}^{\infty} \int_{-\infty}^{\infty} \frac{\partial \mathcal{L}}{\partial u} \delta u dT dZ + \int_{-\infty}^{\infty} \int_{-\infty}^{\infty} \frac{\partial \mathcal{L}}{\partial u_Z} \frac{\partial(\delta u)}{\partial Z} dZ dT + \int_{-\infty}^{\infty} \int_{-\infty}^{\infty} \frac{\partial \mathcal{L}}{\partial u_T} \frac{\partial(\delta u)}{\partial T} dT dZ \\ &\quad + \int_{-\infty}^{\infty} \int_{-\infty}^{\infty} \frac{\partial \mathcal{L}}{\partial u^*} \delta u^* dT dZ + \int_{-\infty}^{\infty} \int_{-\infty}^{\infty} \frac{\partial \mathcal{L}}{\partial u_Z^*} \frac{\partial(\delta u^*)}{\partial Z} dZ dT + \int_{-\infty}^{\infty} \int_{-\infty}^{\infty} \frac{\partial \mathcal{L}}{\partial u_T^*} \frac{\partial(\delta u^*)}{\partial T} dT dZ \\ &= \int_{-\infty}^{\infty} \int_{-\infty}^{\infty} \frac{\partial \mathcal{L}}{\partial u} \delta u dT dZ - \int_{-\infty}^{\infty} \int_{-\infty}^{\infty} \frac{\partial}{\partial Z} \left(\frac{\partial \mathcal{L}}{\partial u_Z} \right) \delta u dZ dT \\ &\quad - \int_{-\infty}^{\infty} \int_{-\infty}^{\infty} \frac{\partial}{\partial T} \left(\frac{\partial \mathcal{L}}{\partial u_T} \right) \delta u dT dZ + \int_{-\infty}^{\infty} \int_{-\infty}^{\infty} \frac{\partial \mathcal{L}}{\partial u^*} \delta u^* dT dZ \\ &\quad - \int_{-\infty}^{\infty} \int_{-\infty}^{\infty} \frac{\partial}{\partial Z} \left(\frac{\partial \mathcal{L}}{\partial u_Z^*} \right) \delta u^* dZ dT - \int_{-\infty}^{\infty} \int_{-\infty}^{\infty} \frac{\partial}{\partial T} \left(\frac{\partial \mathcal{L}}{\partial u_T^*} \right) \delta u^* dT dZ \\ &= \int_{-\infty}^{\infty} \int_{-\infty}^{\infty} \left\{ \frac{\partial \mathcal{L}}{\partial u} - \frac{\partial}{\partial Z} \left(\frac{\partial \mathcal{L}}{\partial u_Z} \right) - \frac{\partial}{\partial T} \left(\frac{\partial \mathcal{L}}{\partial u_T} \right) \right\} \delta u dT dZ \\ &\quad + \int_{-\infty}^{\infty} \int_{-\infty}^{\infty} \left\{ \frac{\partial \mathcal{L}}{\partial u^*} - \frac{\partial}{\partial Z} \left(\frac{\partial \mathcal{L}}{\partial u_Z^*} \right) - \frac{\partial}{\partial T} \left(\frac{\partial \mathcal{L}}{\partial u_T^*} \right) \right\} \delta u^* dT dZ \\ &= 0, \end{aligned} \quad (2.5)$$

where we took the integration by parts with respect to the T - and Z - derivative, and assumed that the variations δu and δu^* vanish at the boundary of the integration; for instance

$$\begin{aligned} \int_{-\infty}^{\infty} \frac{\partial \mathcal{L}}{\partial u_Z} \frac{\partial(\delta u)}{\partial Z} dZ &= \frac{\partial \mathcal{L}}{\partial u_Z} \delta u \Big|_{-\infty}^{\infty} - \int_{-\infty}^{\infty} \frac{\partial}{\partial Z} \left(\frac{\partial \mathcal{L}}{\partial u_Z} \right) \delta u dZ \\ &= - \int_{-\infty}^{\infty} \frac{\partial}{\partial Z} \left(\frac{\partial \mathcal{L}}{\partial u_Z} \right) \delta u dZ. \end{aligned}$$

Since the variations δu and δu^* are taken to be arbitrary and independent in (2.5), we obtain

$$\frac{\partial \mathcal{L}}{\partial u} - \frac{\partial}{\partial Z} \left(\frac{\partial \mathcal{L}}{\partial u_Z} \right) - \frac{\partial}{\partial T} \left(\frac{\partial \mathcal{L}}{\partial u_T} \right) = 0, \quad (2.6a)$$

and

$$\frac{\partial \mathcal{L}}{\partial u^*} - \frac{\partial}{\partial Z} \left(\frac{\partial \mathcal{L}}{\partial u_Z^*} \right) - \frac{\partial}{\partial T} \left(\frac{\partial \mathcal{L}}{\partial u_T^*} \right) = 0. \quad (2.6b)$$

These equations are Euler-Lagrange equation in infinite dimension. For the case of the nonlinear Schrödinger equation, (2.2) is formulated as Euler-Lagrange equation of the form

$$\frac{\delta \mathcal{L}}{\delta u^*} \equiv \frac{\partial \mathcal{L}}{\partial u^*} - \frac{\partial}{\partial Z} \left(\frac{\partial \mathcal{L}}{\partial u_Z^*} \right) - \frac{\partial}{\partial T} \left(\frac{\partial \mathcal{L}}{\partial u_T^*} \right) = 0 \quad (2.7)$$

with the Lagrangian density defined as

$$\mathcal{L}[u, u^*, u_Z, u_Z^*, u_T, u_T^*; Z] = \frac{i}{2}(u_Z u^* - u_Z^* u) - \frac{d(Z)}{2}|u_T|^2 + \frac{a^2(Z)}{2}|u|^4. \quad (2.8)$$

We now apply the variational method to analyze approximately the dynamics of the DM solitons. We first assume the solution of (2.2) to be given by a chirped pulse of the form

$$u(T, Z) = A(Z) f[p(Z) \{T - T_0(Z)\}] \\ \times \exp \left[iC(Z) \{T - T_0(Z)\}^2 - i\kappa(Z) \{T - T_0(Z)\} + i\theta_0(Z) \right], \quad (2.9)$$

where f is a pulse shape. We use the variational method to (2.2) and the ansatz (2.9) to derive a set of ordinary differential equations for the parameters A , p , C , κ , T_0 , and θ_0 . Integrating \mathcal{L} in (2.8) over T and with this ansatz, we obtain the following form of Lagrangian

$$L = \int_{-\infty}^{\infty} \mathcal{L} dT \\ = -dA^2 \left(\frac{pI_D}{2} + \frac{2C^2 I_C}{p^3} + \frac{\kappa^2 I_L}{2p} \right) + \frac{a^2 A^4 I_N}{2p} - \frac{A^2 I_C}{p^3} \frac{dC}{dZ} + \frac{A^2 I_L}{p} \left(T_0 \frac{d\kappa}{dZ} - \frac{d\theta_0}{dZ} \right), \quad (2.10)$$

where

$$I_L = \int_{-\infty}^{\infty} f^2(\tau) d\tau, \quad I_C = \int_{-\infty}^{\infty} \tau^2 f^2(\tau) d\tau, \quad I_D = \int_{-\infty}^{\infty} \left(\frac{df}{d\tau} \right)^2 d\tau, \quad I_N = \int_{-\infty}^{\infty} f^4(\tau) d\tau. \quad (2.11)$$

The original infinite dimensional problem (2.2) is now reduced to a Lagrangian form in finite dimension whose Lagrangian is given by (2.10), which involves only finite sets of variables.

Euler-Lagrange equation for a finite dimensional problem can be obtained in a way similar to the derivation for the infinite dimensional case. The Lagrange's principle of least action

$$\delta I = \delta \int_{-\infty}^{\infty} L[r, r_Z; Z] dZ = 0, \quad (2.12)$$

where r is one of the parameters in (2.10), gives,

$$\int_{-\infty}^{\infty} \left\{ \frac{\partial L}{\partial r} - \frac{d}{dZ} \left(\frac{\partial L}{\partial r_Z} \right) \right\} \delta r dZ = 0. \quad (2.13)$$

As a result, Euler-Lagrange equation reads

$$\frac{\delta L}{\delta r} \equiv \frac{\partial L}{\partial r} - \frac{d}{dZ} \left(\frac{\partial L}{\partial r_Z} \right) = 0. \quad (2.14)$$

From this expression, we are able to construct a set of equations for the each parameter in Lagrangian (2.10). Equation (2.14) gives the following equations for the each parameter $r = A, p, C, \kappa, T_0,$ and θ_0 .

For $r = A$:

$$\begin{aligned} \frac{\partial L}{\partial A} - \frac{d}{dZ} \left(\frac{\partial L}{\partial A_Z} \right) &= -dA \left(pI_D + \frac{4C^2}{p^3} I_C + \frac{\kappa^2}{p} I_L \right) + \frac{2a^2 A^3}{p} I_N - \frac{2A}{p^3} \frac{dC}{dZ} I_C \\ &\quad + \frac{2A}{p} \left(T_0 \frac{d\kappa}{dZ} - \frac{d\theta_0}{dZ} \right) I_L \\ &= 0. \end{aligned} \tag{2.15a}$$

For $r = p$:

$$\begin{aligned} \frac{\partial L}{\partial p} - \frac{d}{dZ} \left(\frac{\partial L}{\partial p_Z} \right) &= -dA^2 \left(\frac{I_D}{2} - \frac{6C^2}{p^4} I_C - \frac{\kappa^2}{2p^2} I_L \right) - \frac{a^2 A^2}{2p^2} I_N + \frac{3A^2}{p^4} \frac{dC}{dZ} I_C \\ &\quad - \frac{A^2}{p^2} \left(T_0 \frac{d\kappa}{dZ} - \frac{d\theta_0}{dZ} \right) I_L \\ &= 0. \end{aligned} \tag{2.15b}$$

For $r = C$:

$$\begin{aligned} \frac{\partial L}{\partial C} - \frac{d}{dZ} \left(\frac{\partial L}{\partial C_Z} \right) &= -\frac{4dA^2 C}{p^3} I_C + \frac{2A}{p^3} \frac{dA}{dZ} I_C - \frac{3A^2}{p^4} \frac{dp}{dZ} I_C \\ &= 0. \end{aligned} \tag{2.15c}$$

For $r = \kappa$:

$$\begin{aligned} \frac{\partial L}{\partial \kappa} - \frac{d}{dZ} \left(\frac{\partial L}{\partial \kappa_Z} \right) &= -\frac{dA^2 \kappa}{p} I_L - \frac{2AT_0}{p} \frac{dA}{dZ} I_L - \frac{A^2}{p} \frac{dT_0}{dZ} I_L + \frac{A^2 T_0}{p^2} \frac{dp}{dZ} I_L \\ &= 0. \end{aligned} \tag{2.15d}$$

For $r = T_0$:

$$\begin{aligned} \frac{\partial L}{\partial T_0} - \frac{d}{dZ} \left(\frac{\partial L}{\partial T_{0Z}} \right) &= \frac{A^2}{p} \frac{d\kappa}{dZ} I_L \\ &= 0. \end{aligned} \tag{2.15e}$$

For $r = \theta_0$:

$$\begin{aligned} \frac{\partial L}{\partial \theta_0} - \frac{d}{dZ} \left(\frac{\partial L}{\partial \theta_{0Z}} \right) &= \frac{2A}{p} \frac{dA}{dZ} I_L - \frac{A^2}{p^2} \frac{dp}{dZ} I_L \\ &= 0. \end{aligned} \tag{2.15f}$$

From (2.15a)–(2.15f), we obtain

$$\frac{dA}{dZ} = -ACd, \tag{2.16a}$$

$$\frac{dp}{dZ} = -2pCd, \tag{2.16b}$$

$$\frac{dC}{dZ} = \left(\frac{I_D}{2I_C} p^4 - 2C^2 \right) d - \frac{I_N}{4I_C} a^2 A^2 p^2, \tag{2.16c}$$

$$\frac{d\kappa}{dZ} = 0, \tag{2.16d}$$

$$\frac{dT_0}{dZ} = -\kappa d, \tag{2.16e}$$

$$\frac{d\theta_0}{dZ} = \left(\frac{\kappa^2}{2} - \frac{I_D}{I_L} p^2 \right) d + \frac{5I_N}{4I_L} a^2 A^2. \tag{2.16f}$$

We note from (2.16a) and (2.16b) that A and p are not independent since (2.16a) and (2.16b) give the relation

$$A = \alpha\sqrt{p}, \quad (2.17)$$

with some constant α . Thus the dynamics of DM solitons can be described by the two parameters p and C , that is the inverse of the pulse width and the frequency chirp, respectively. We further assume that the pulse shape is approximated as Gaussian, namely $f(\tau) = \exp(-\tau^2)$. With this approximation, the integral constants I_L , I_C , I_D , and I_N are given by

$$\begin{aligned} I_L &= \int_{-\infty}^{\infty} \exp(-2\tau^2) d\tau = \sqrt{\frac{\pi}{2}}, & I_C &= \int_{-\infty}^{\infty} \tau^2 \exp(-2\tau^2) d\tau = \frac{1}{4}\sqrt{\frac{\pi}{2}}, \\ I_D &= \int_{-\infty}^{\infty} \left\{ \frac{d}{d\tau} \exp(-\tau^2) \right\}^2 d\tau = \sqrt{\frac{\pi}{2}}, & I_N &= \int_{-\infty}^{\infty} \exp(-4\tau^2) d\tau = \frac{\sqrt{\pi}}{2}. \end{aligned} \quad (2.18)$$

Equations (2.16a) and (2.16b) now read

$$\frac{dp}{dZ} = -2pCd, \quad (2.19a)$$

$$\frac{dC}{dZ} = 2(p^4 - C^2)d - \frac{\sqrt{2}a^2\alpha^2 p^3}{2}. \quad (2.19b)$$

Note that in the absence of nonlinearity, that is when $a = 0$, we have

$$\frac{dp}{dZ} = -2pCd, \quad (2.20a)$$

$$\frac{dC}{dZ} = 2(p^4 - C^2)d. \quad (2.20b)$$

This can be integrated with the conserved quantity

$$H_0 = p^2 + \frac{C^2}{p^2}. \quad (2.21)$$

H_0 is mathematically a Hamiltonian of the system (2.20a) and (2.20b), and physically corresponds to the spectral width of the pulse.

In the presence of nonlinearity, however, the system can be formally integrated to give

$$\begin{aligned} H_0 &= p^2 + \frac{C^2}{p^2} - \int \frac{a^2\alpha^2}{\sqrt{2}d} dp \\ &= p^2 + \frac{C^2}{p^2} - \int \sqrt{2}a^2\alpha^2 pC dZ \end{aligned} \quad (2.22)$$

and the spectral width is no longer constant during propagation. Equations (2.19a) and (2.19b) admit a periodic evolution of the parameters by a proper choice of the initial conditions, which gives evidence of the stationary propagation of DM solitons.

2.3 Fast and slow dynamics of dispersion managed solitons

In this section, we provide a couple of introductory remarks on dynamics of the DM solitons using (2.19a) and (2.19b) derived in Section 2.2. We solve the equations to study fast (short term) dynamics within one dispersion management period as well as slow (long term) dynamics that is observed, in an averaged form, over multiple dispersion management spans.

We consider an example of the periodic solutions p and C in a lossless dispersion managed line shown in Fig. 2.1. The GVD profile is given by

$$d(Z) = \begin{cases} d_1, & \text{for } nZ_d < Z < nZ_d + \frac{Z_d}{4}, \quad nZ_d + \frac{3}{4}Z_d < Z < (n+1)Z_d \\ d_2, & \text{for } nZ_d + \frac{Z_d}{4} < Z < nZ_d + \frac{3}{4}Z_d \end{cases} \quad (2.23)$$

with $d_1 = 31.0$, $d_2 = -29.0$, and $Z_d = 0.1$. The solution p (C) is shown in Fig. 2.2 (Fig. 2.3). The solid line represents the analytical result obtained from (2.19a) and (2.19b), and circles are obtained by solving (2.1) directly by means of the split-step Fourier method with the same parameters. This result also clarifies the difference between the DM solitons and linear Gaussian pulses in a completely dispersion compensated system. Note that the periodic solution in the nonlinear system (2.19a) and (2.19b) is obtained only for the particular value of the initial conditions, whereas in the linear system (2.20a) and (2.20b) periodic solutions exist for arbitrary values of the initial conditions provided that $\langle d \rangle = 0$. This observation is a consequence of the asymmetric evolution of the parameters on the propagation in the positive and the negative GVD segment in the presence of nonlinearity.

The difference between the linear system and the nonlinear system can be clearly seen by plotting a periodic orbit in the p - C plane [54] as shown in Fig. 2.4. The upper branch (a-b, d-e) is given by the propagation in the positive GVD segment (d_1), whereas the lower branch (b-c-d) corresponds to the propagation in the negative GVD segment (d_2). This means that DM solitons acquire pulse width oscillation and bandwidth broadening in the positive GVD larger than in the negative GVD. Note that the distinction is not observed in the linear case, since the periodic orbit is characterized by the relation in (2.21), and H_0 is a conserved quantity during the whole propagation.

Long range evolution of the DM solitons discloses their peculiar properties that the classical solitons do not exhibit. One of their unique properties is that the nonlinear-induced asymmetric periodic orbit allows stationary propagation of DM solitons in systems with $\langle d \rangle = 0$ or even $\langle d \rangle < 0$ [55]. This can be understood by writing down the propagation equation that the core of the pulse satisfies. Substituting into (2.2) the solution $u(T, Z) = A(Z)v(\tau, Z) \exp(iCT^2)$, $\tau = pT$ with (2.17), one obtains

$$i \frac{\partial v}{\partial Z} + dp^2 \frac{\partial^2 v}{\partial \tau^2} + \alpha^2 a^2 p |v|^2 v - K \tau^2 v = 0 \quad (2.24)$$

with

$$K(Z) \equiv \frac{1}{p^2} \left(\frac{dC}{dZ} + C^2 d \right) = d \frac{I_D}{2I_C} p^2 - a^2 \frac{\alpha^2 I_N}{4I_C} p, \quad (2.25)$$

where we used (2.16b) and (2.16c). Slow scale dynamics of $v(\tau, Z)$ can be well approximated by the equation obtained by averaging the coefficients in (2.25) over Z_d :

$$i \frac{\partial v}{\partial Z} + \langle dp^2 \rangle \frac{\partial^2 v}{\partial \tau^2} + \alpha^2 \langle a^2 p \rangle |v|^2 v - \langle K \rangle \tau^2 v = 0. \quad (2.26)$$

The obtained equation (2.26) describes the evolution of the solution v , supported by the ‘weighted’ dispersion $\langle dp^2 \rangle$ and the self-trapping potential $-\alpha^2 \langle a^2 p \rangle |v|^2$, as well as the linear parabolic potential $\langle K \rangle \tau^2$. We note that, even when $\langle d \rangle \leq 0$, the asymmetric evolution of p within one period can make the average of the weighted potential over one period $\langle dp^2 \rangle$ to be positive. Thus we expect stationary propagation of the DM solitons by the balance between the nonlinear chirp and the linear chirp produced by the weighted dispersion $\langle dp^2 \rangle$, rather than by the intrinsic dispersion $\langle d \rangle$.

Furthermore, the DM solitons possess peculiar characteristics with respect to their large margin of the initial conditions, which are not seen in linear systems. Figures 2.5 and 2.6 show plots of Poincaré section in p - C plane, namely a trajectory of the parameters at every period of the dispersion map (in this case, the middle of d_1 segment) for several different values of the initial condition. Figure 2.5 shows plots for different values of $p(0)$ and $C(0)$ with the fixed energy of $E_0 = 3.629$, whereas Fig. 2.6 is obtained for different values of E_0 with the fixed value of $p(0) = 1/\sqrt{2}$ and $C(0) = 0$. As shown in these figures, evolution of the parameters starting from the vicinity of the stationary state is a closed loop around the fixed point corresponding to the stationary state (i.e. $p(0) = 1/\sqrt{2}$, $C(0) = 0$, $E_0 = 3.629$), and exhibits a long term quasi-periodicity. This is in contrast to the behavior of the classical solitons, where the pulse having parameters deviating from the stationary state generates radiative waves and approaches asymptotically to the stationary solution. Too much deviation from the stationary state, however, results in the collapse of the pulse, as shown in Fig. 2.6 for $E_0 = 1.0$.

Detailed analyses on these interesting properties, however, are out of scope of this thesis. Intensive studies and discussions on the role of the linear parabolic potential or the exact range of $\langle d \rangle$ available to support the stationary solution can be found in [56, 57]. Numerical studies on the chaotic behavior of the Poincaré map can be found in [58]. Integrability of the slow dynamics of DM solitons has also been discussed elsewhere [59–61].

2.4 Lagrangian perturbation method

We extend the problem considered in Section 2.2 to the perturbed system of the form

$$i \frac{\partial u}{\partial Z} + \frac{d(Z)}{2} \frac{\partial^2 u}{\partial T^2} + a^2(Z) |u|^2 u = \varepsilon R[u, u^*], \quad (2.27)$$

where $\varepsilon R[u, u^*]$ represents the perturbation with $|\varepsilon| \ll 1$. Euler-Lagrange equation in infinite dimension which corresponds to (2.7) can now be written as

$$\frac{\delta \mathcal{L}}{\delta u^*} = \varepsilon R. \quad (2.28)$$

We note that the action integral of Lagrangian L is given by the Lagrangian density of the form

$$\begin{aligned} \int_{-\infty}^{\infty} \delta L dZ &= \int_{-\infty}^{\infty} \int_{-\infty}^{\infty} \delta \mathcal{L} dT dZ \\ &= \int_{-\infty}^{\infty} \int_{-\infty}^{\infty} \left(\frac{\delta \mathcal{L}}{\delta u} \delta u + \frac{\delta \mathcal{L}}{\delta u^*} \delta u^* \right) dT dZ. \end{aligned} \quad (2.29)$$

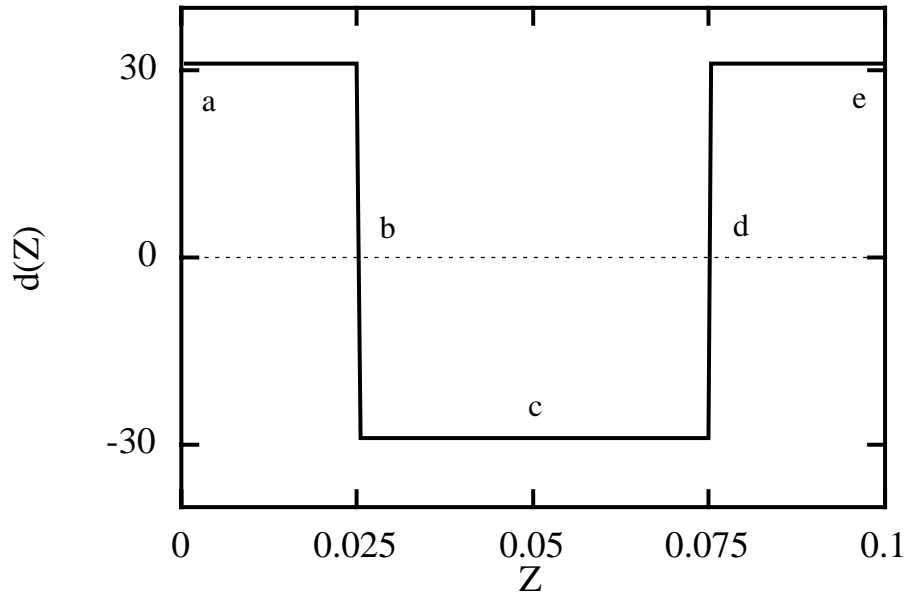


Figure 2.1: Dispersion profile given by (2.23).

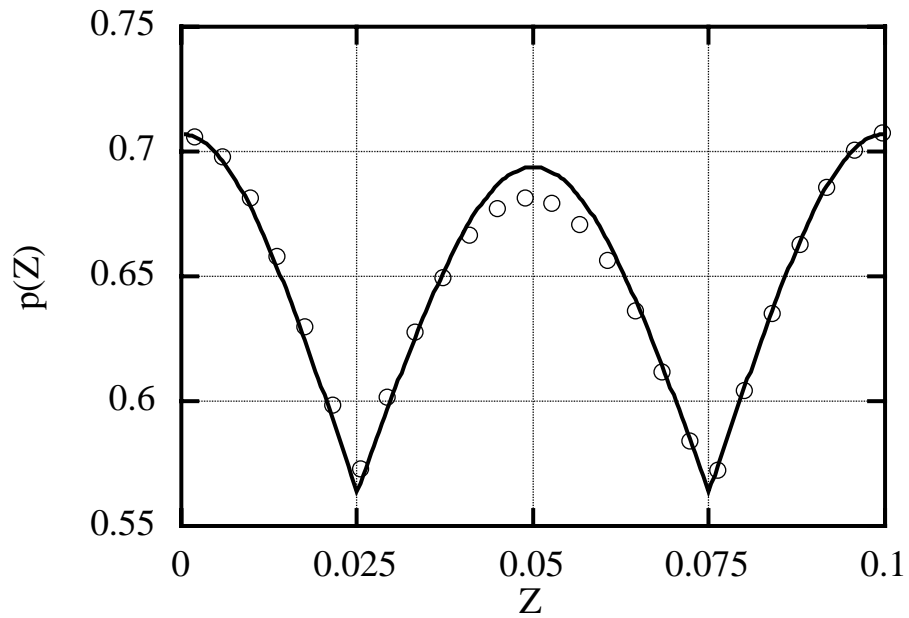


Figure 2.2: The evolution of $p(Z)$ obtained by solving (2.19a) and (2.19b) (solid line) and by a direct numerical simulation of (2.1) with the same initial condition (dots).

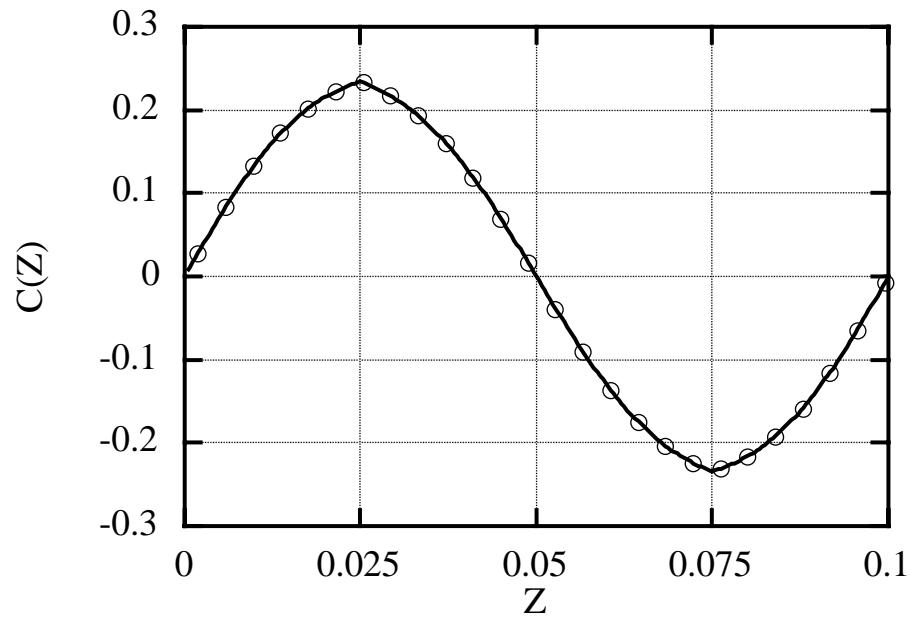


Figure 2.3: The evolution of $C(Z)$. Solid line shows the analytical result obtained by solving (2.19a) and (2.19b), and dots are the numerical result of (2.1) with the same initial condition.

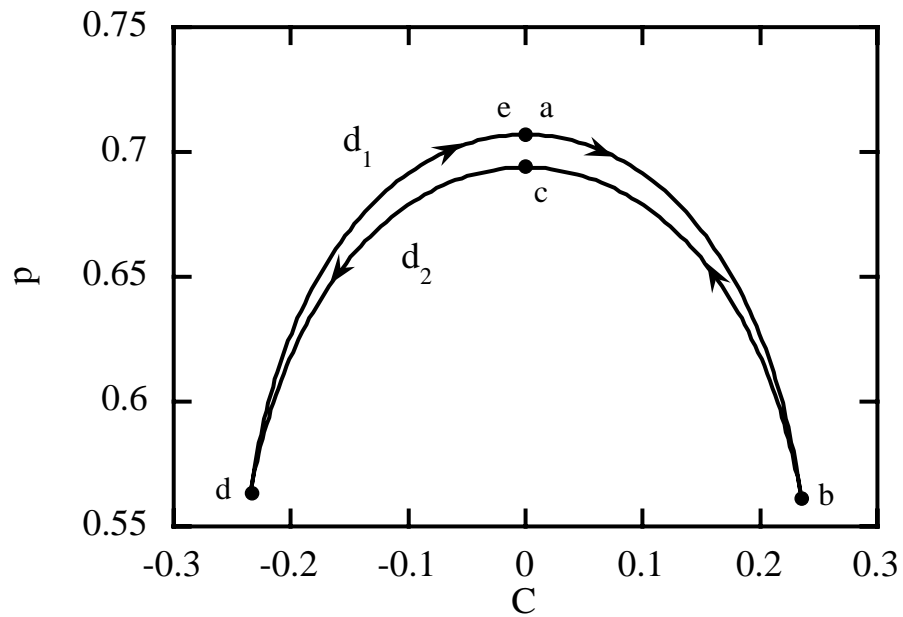


Figure 2.4: A periodic orbit of Fig. 2.2 and Fig. 2.3 in p - C plane.

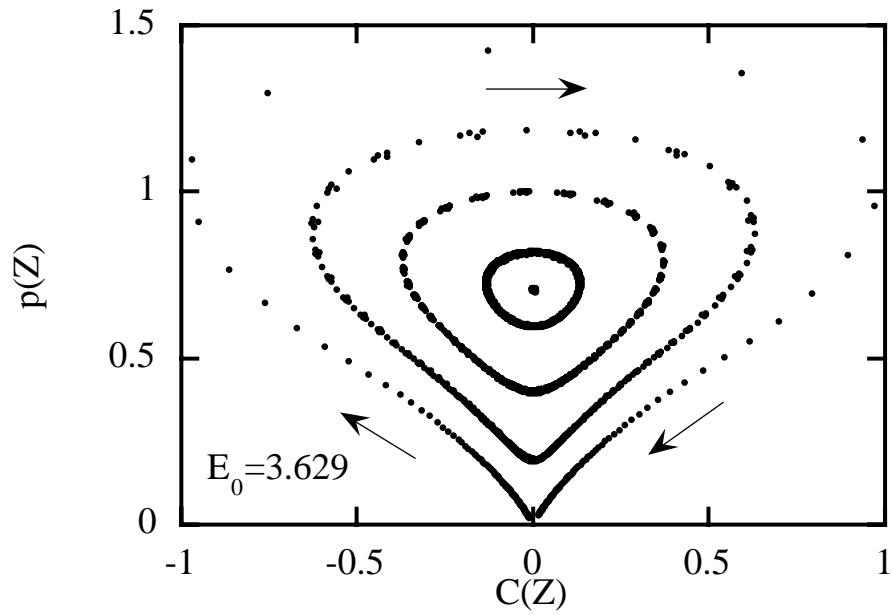


Figure 2.5: Poincaré maps for the solutions of (2.19a) and (2.19b) with several values of $p(0)$ and $C(0)$ and the fixed energy $E_0 = 3.629$.

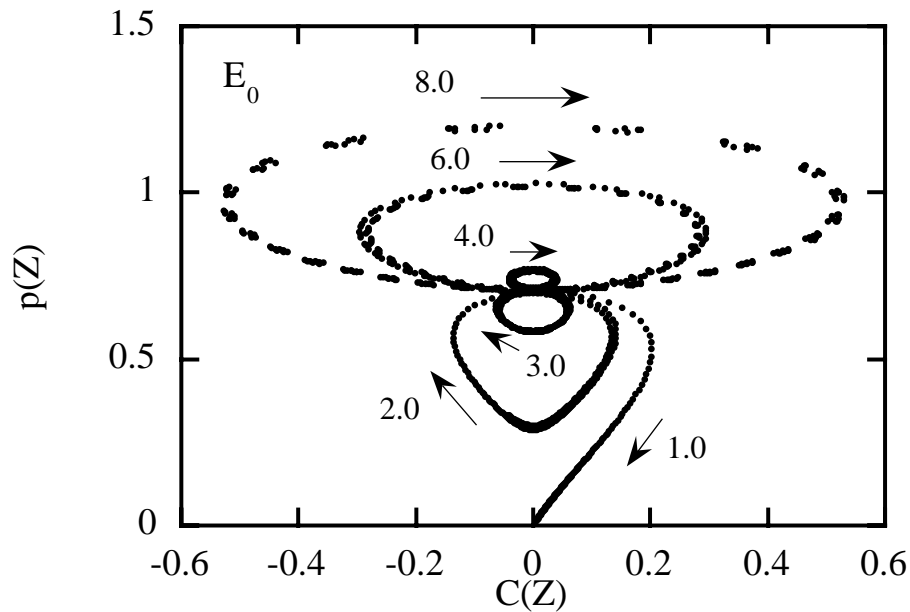


Figure 2.6: Poincaré maps for the solutions of (2.19a) and (2.19b) with several values of E_0 and the fixed initial condition $p(0) = 1/\sqrt{2}$ and $C(0) = 0$.

From the relation $\delta u = (\partial u / \partial r) \delta r$, we have

$$\begin{aligned} \int_{-\infty}^{\infty} \delta L dZ &= \int_{-\infty}^{\infty} \int_{-\infty}^{\infty} \left(\frac{\delta \mathcal{L}}{\delta u} \frac{\partial u}{\partial r} + \frac{\delta \mathcal{L}}{\delta u^*} \frac{\partial u^*}{\partial r} \right) \delta r dT dZ \\ &= \int_{-\infty}^{\infty} \int_{-\infty}^{\infty} \left(\varepsilon R^* \frac{\partial u}{\partial r} + \varepsilon R \frac{\partial u^*}{\partial r} \right) \delta r dT dZ. \end{aligned} \quad (2.30)$$

Compared with (2.13), Euler-Lagrange equation in the presence of the perturbation εR can be written as

$$\frac{\delta L}{\delta r} = \int_{-\infty}^{\infty} \left(\varepsilon R^* \frac{\partial u}{\partial r} + \varepsilon R \frac{\partial u^*}{\partial r} \right) dT. \quad (2.31)$$

We now write down explicitly the equation (2.31) for the each parameter $r = A, p, C, \kappa, T_0$, and θ_0 .

For $r = A$:

$$\begin{aligned} \frac{\partial L}{\partial A} - \frac{d}{dZ} \left(\frac{\partial L}{\partial A_Z} \right) &= -dA \left(p I_D + \frac{4C^2}{p^3} I_C + \frac{\kappa^2}{p} I_L \right) + \frac{2a^2 A^3}{p} I_N - \frac{2A}{p^3} \frac{dC}{dZ} I_C \\ &\quad + \frac{2A}{p} \left(T_0 \frac{d\kappa}{dZ} - \frac{d\theta_0}{dZ} \right) I_L \\ \int_{-\infty}^{\infty} \left(\varepsilon R^* \frac{\partial u}{\partial A} + \varepsilon R \frac{\partial u^*}{\partial A} \right) dT &= \int_{-\infty}^{\infty} \left(\varepsilon R^* e^{i\varphi} + \varepsilon R e^{-i\varphi} \right) f(\tau) dT \\ &= \frac{2}{p} \int_{-\infty}^{\infty} \text{Re}[\varepsilon R e^{-i\varphi}] f(\tau) d\tau. \end{aligned} \quad (2.32a)$$

For $r = p$:

$$\begin{aligned} \frac{\partial L}{\partial p} - \frac{d}{dZ} \left(\frac{\partial L}{\partial p_Z} \right) &= -dA^2 \left(\frac{I_D}{2} - \frac{6C^2}{p^4} I_C - \frac{\kappa^2}{2p^2} I_L \right) - \frac{a^2 A^2}{2p^2} I_N + \frac{3A^2}{p^4} \frac{dC}{dZ} I_C \\ &\quad - \frac{A^2}{p^2} \left(T_0 \frac{d\kappa}{dZ} - \frac{d\theta_0}{dZ} \right) I_L \\ \int_{-\infty}^{\infty} \left(\varepsilon R^* \frac{\partial u}{\partial p} + \varepsilon R \frac{\partial u^*}{\partial p} \right) dT &= \int_{-\infty}^{\infty} \left(\varepsilon R^* e^{i\varphi} + \varepsilon R e^{-i\varphi} \right) \frac{A}{p} \tau \frac{df}{d\tau} dT \\ &= \frac{2A}{p^2} \int_{-\infty}^{\infty} \text{Re}[\varepsilon R e^{-i\varphi}] \tau \frac{df}{d\tau} d\tau. \end{aligned} \quad (2.32b)$$

For $r = C$:

$$\begin{aligned} \frac{\partial L}{\partial C} - \frac{d}{dZ} \left(\frac{\partial L}{\partial C_Z} \right) &= -\frac{4dA^2 C}{p^3} I_C + \frac{2A}{p^3} \frac{dA}{dZ} I_C - \frac{3A^2}{p^4} \frac{dp}{dZ} I_C \\ \int_{-\infty}^{\infty} \left(\varepsilon R^* \frac{\partial u}{\partial C} + \varepsilon R \frac{\partial u^*}{\partial C} \right) dT &= i \int_{-\infty}^{\infty} \left(\varepsilon R^* e^{i\varphi} - \varepsilon R e^{-i\varphi} \right) (T - T_0)^2 A f(\tau) dT \\ &= \frac{2A}{p^3} \int_{-\infty}^{\infty} \text{Im}[\varepsilon R e^{-i\varphi}] \tau^2 f(\tau) d\tau. \end{aligned} \quad (2.32c)$$

For $r = \kappa$:

$$\begin{aligned} \frac{\partial L}{\partial \kappa} - \frac{d}{dZ} \left(\frac{\partial L}{\partial \kappa_Z} \right) &= -\frac{dA^2 \kappa}{p} I_L - \frac{2AT_0}{p} \frac{dA}{dZ} I_L - \frac{A^2}{p} \frac{dT_0}{dZ} I_L + \frac{A^2 T_0}{p^2} \frac{dp}{dZ} I_L \\ \int_{-\infty}^{\infty} \left(\varepsilon R^* \frac{\partial u}{\partial \kappa} + \varepsilon R \frac{\partial u^*}{\partial \kappa} \right) dT &= -i \int_{-\infty}^{\infty} \left(\varepsilon R^* e^{i\varphi} - \varepsilon R e^{-i\varphi} \right) T A f(\tau) dT \\ &= -\frac{2A}{p^2} (1 + pT_0) \int_{-\infty}^{\infty} \text{Re}[\varepsilon R e^{-i\varphi}] f(\tau) d\tau. \end{aligned} \quad (2.32d)$$

For $r = T_0$:

$$\begin{aligned} \frac{\partial L}{\partial T_0} - \frac{d}{dZ} \left(\frac{\partial L}{\partial T_{0Z}} \right) &= \frac{A^2}{p} \frac{d\kappa}{dZ} I_L \\ \int_{-\infty}^{\infty} \left(\varepsilon R^* \frac{\partial u}{\partial T_0} + \varepsilon R \frac{\partial u^*}{\partial T_0} \right) dT &= - \int_{-\infty}^{\infty} \left(\varepsilon R^* e^{i\varphi} + \varepsilon R e^{-i\varphi} \right) A p \frac{df}{d\tau} dT \\ &\quad - 2i \int_{-\infty}^{\infty} \left(\varepsilon R^* e^{i\varphi} - \varepsilon R e^{-i\varphi} \right) AC(T - T_0) f(\tau) dT \\ &= -2A \int_{-\infty}^{\infty} \text{Re}[\varepsilon R e^{-i\varphi}] \frac{df}{d\tau} d\tau - \frac{4AC}{p^2} \int_{-\infty}^{\infty} \text{Im}[\varepsilon R e^{-i\varphi}] \tau f(\tau) d\tau. \end{aligned} \quad (2.32e)$$

For $r = \theta_0$:

$$\begin{aligned} \frac{\partial L}{\partial \theta_0} - \frac{d}{dZ} \left(\frac{\partial L}{\partial \theta_{0Z}} \right) &= \frac{2A}{p} \frac{dA}{dZ} I_L - \frac{A^2}{p^2} \frac{dp}{dZ} I_L \\ \int_{-\infty}^{\infty} \left(\varepsilon R^* \frac{\partial u}{\partial \theta_0} + \varepsilon R \frac{\partial u^*}{\partial \theta_0} \right) dT &= i \int_{-\infty}^{\infty} \left(\varepsilon R^* e^{i\varphi} - \varepsilon R e^{-i\varphi} \right) A f(\tau) dT \\ &= \frac{2A}{p} \int_{-\infty}^{\infty} \text{Im}[\varepsilon R e^{-i\varphi}] f(\tau) d\tau. \end{aligned} \quad (2.32f)$$

In these equations, $\tau \equiv p(Z)\{T - T_0(Z)\}$, $\varphi \equiv C(Z)\{T - T_0(Z)\}^2 - \kappa(Z)\{T - T_0(Z)\} + \theta_0(Z)$. Solving (2.32a)–(2.32f) with respect to dr/dZ ($r = A, p, C, \kappa, T_0, \theta_0$), we obtain

$$\frac{dA}{dZ} = -ACd - \frac{1}{2I_L I_C} \int_{-\infty}^{\infty} \text{Im}[\varepsilon R e^{-i\varphi}] (I_L \tau^2 - 3I_C) f(\tau) d\tau, \quad (2.33a)$$

$$\frac{dp}{dZ} = -2pCd - \frac{p}{I_L I_C A} \int_{-\infty}^{\infty} \text{Im}[\varepsilon R e^{-i\varphi}] (I_L \tau^2 - I_C) f(\tau) d\tau, \quad (2.33b)$$

$$\frac{dC}{dZ} = \left(\frac{I_D}{2I_C} p^4 - 2C^2 \right) d - \frac{I_N}{4I_C} a^2 A^2 p^2 + \frac{p^2}{2I_C A} \int_{-\infty}^{\infty} \text{Re}[\varepsilon R e^{-i\varphi}] \left(f(\tau) + 2\tau \frac{df}{d\tau} \right) d\tau, \quad (2.33c)$$

$$\frac{d\kappa}{dZ} = -\frac{2}{I_L A p} \int_{-\infty}^{\infty} \left\{ p^2 \text{Re}[\varepsilon R e^{-i\varphi}] \frac{df}{d\tau} + 2C \text{Im}[\varepsilon R e^{-i\varphi}] \tau f(\tau) \right\} d\tau, \quad (2.33d)$$

$$\frac{dT_0}{dZ} = -\kappa d + \frac{2}{I_L A p} \int_{-\infty}^{\infty} \text{Im}[\varepsilon R e^{-i\varphi}] \tau f(\tau) d\tau, \quad (2.33e)$$

$$\begin{aligned} \frac{d\theta_0}{dZ} &= \left(\frac{\kappa^2}{2} - \frac{I_D}{I_L} p^2 \right) d + \frac{5I_N}{4I_L} a^2 A^2 \\ &\quad - \frac{1}{2I_L A p} \int_{-\infty}^{\infty} \left\{ p \text{Re}[\varepsilon R e^{-i\varphi}] \left(3f(\tau) + 2\tau \frac{df}{d\tau} \right) - 4\kappa \text{Im}[\varepsilon R e^{-i\varphi}] \tau f(\tau) \right\} d\tau. \end{aligned} \quad (2.33f)$$

2.5 Conclusion

We have derived ordinary differential equations for the characteristic parameters of the DM solitons. Fundamental dynamics of the DM solitons are characterized by their pulse width and frequency chirp. We further studied adiabatic evolution of these parameters to study the behavior of the DM solitons under the perturbations. These equations give useful estimation on the influence of perturbative effects in transmission lines such as amplifier noise, higher-order dispersion, self-induced Raman effect, and nonlinear interaction with other solitons. We refer to these equations frequently in the following chapters.

Chapter 3

Wavelength division multiplexing of dispersion managed solitons

3.1 Introduction

In this chapter, we theoretically analyze the nonlinear interactions among solitons in strongly dispersion managed WDM systems. We employ the perturbation method derived in Chapter 2 to evaluate the frequency shift and the chirp alteration caused by collisions of solitons in different WDM channels.

3.2 Soliton interaction in WDM systems

In soliton based WDM systems, where solitons in different wavelength channels propagate at different speeds, collisions between the solitons take place and induce nonlinear interactions among the colliding solitons such as cross phase modulation and four wave mixing. The cross phase modulation leads to their central frequency shift, and the four wave mixing produces sideband components. In the ideal collision process, the frequency shift arising in the first half of the collision process is offset exactly in the latter half of the collision because of the symmetric picture of the whole collision process. The four wave mixing components, which are generated in the first half of the collision, also diminish completely in the latter half. These properties can be clearly seen in Fig. 3.1, where we plot spectrum of two colliding solitons in a lossless fiber.

However, in the presence of a lumped amplifier in the middle of a collision process, for instance, the symmetric picture breaks down. The effect of the asymmetric collision process is well averaged out if a collision takes place over multiple amplifier spans, whereas a collision over a distance comparable to the amplifier spacing may lead to a residual frequency shift and to time displacement [23].

The temporary frequency shifts that the colliding solitons suffer from are calculated either by the adiabatic perturbation method [23], the inverse scattering transform [25], or the asymptotic expansion of the N soliton solution [26]. For the case of a complete collision of two solitons that takes place in a lossless fiber, the frequency shift at Z is given by

$$\delta\kappa(Z) = \frac{4}{\Delta B} \frac{\Delta B Z \cosh(\Delta B Z) - \sinh(\Delta B Z)}{\sinh^3(\Delta B Z)}, \quad (3.1)$$

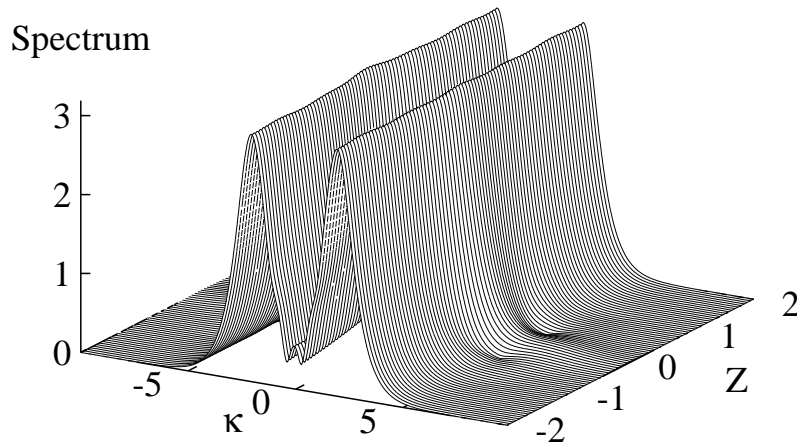


Figure 3.1: Spectrum of two colliding solitons in a lossless fiber. Two solitons collide at $Z = 0$ in time domain. The channel spacing $\Delta B = 4.0$.

where ΔB represents a frequency separation between the solitons[†], and collision is assumed to take place at $Z = 0$. We note that $\delta\kappa(Z)$ in (3.1) has the maximum value at $Z = 0$:

$$\delta\kappa(0) = \frac{4}{3\Delta B}, \quad (3.2)$$

or in real units

$$\delta f(0) = \frac{0.105}{t_s^2 \Delta f}, \quad (3.3)$$

where t_s is the pulse width of a soliton. Thus the frequency shift is inversely proportional to the channel spacing ΔB (Δf) and the square of the pulse width t_s^2 . The frequency shift is offset in a complete collision in a lossless fiber, whereas the initially overlapped solitons suffer from a net frequency shift, the amount of which is given by (3.2) or (3.3). The initial overlap is a significant problem especially for solitons with narrower frequency separation.

The extension of the analysis is discussed in [23] in the presence of damping and lumped amplifications. The effect of the non-adiabatic periodic perturbation depends on the ratio between the walk-off distance of colliding solitons and the amplifier spacing Z_a . The walk-off distance Z_{coll} is defined as the length over which the two solitons begin and end to overlap at their half power points:

$$Z_{\text{coll}} = 2 \frac{1.763}{\Delta B}. \quad (3.4)$$

For $Z_{\text{coll}}/Z_a > 2$, that is for narrow channel spacing, the local events during a collision are well averaged out over the multiple amplifier spans and thus the net frequency shift becomes negligible. On the other hand, for $0.5 < Z_{\text{coll}}/Z_a < 2$, i.e. when the walk-off distance is comparable to the amplifier spacing, effects of the collision are no longer averaged out, resulting in net frequency shift. In contrast to the

[†]In this chapter, we define the frequency separation ΔB to be the central frequency deviation of one channel from the other channel. Thus ΔB is negative for the slower channel with respect to the faster channel.

initial overlap, this problem is significant for relatively wide channel spacing with a fixed value of Z_a , or equivalently, the condition $Z_{\text{coll}}/Z_a > 2$ impose an upper limit on Z_a with a fixed value of ΔB .

It should be noted that the residual frequency shift as well as radiative waves generated during the collision are suppressed considerably by the use of the ‘adiabatic’ dispersion management [62–64], where the stepwise decreasing dispersion is employed to approximate the exponentially decreasing GVD profile so that the balance is maintained between the dispersion and the varied nonlinearity due to loss and amplifications through the propagation in a lossy fiber. As a result of the dispersion tapering, collisions become symmetric regardless of the ratio Z_{coll}/Z_a or the channel spacing.

3.3 Soliton interaction in strongly dispersion managed WDM systems

Soliton WDM systems also benefit from non-adiabatic dispersion management. Although the dispersion managed (DM) soliton system is not integrable and thus careful studies may be necessary to consider their compatibility with WDM transmission, it demonstrates peculiar properties that have not been observed in the classical solitons and even in the adiabatically dispersion managed transmission.

One of the peculiar characteristics of dispersion managed WDM transmission is that the frequency shift that arises in the normal (positive) dispersion regime has a sign opposite from the one in the anomalous (negative) dispersion regime. In addition, the relative direction of propagation with respect to each other in different channels is reversed in the normal dispersion regime, so that collisions between the pulses are expected to take place repeatedly in dispersion managed systems. This indicates the frequency shift produced by a collision might be mostly canceled out under certain conditions, although a residual frequency shift could appear in general even in the absence of loss.

Recognizing this, Sugahara et al. [65] and Devaney et al. [66] derived the optimal design of dispersion compensation that averages out the asymmetric process of collisions in a topological manner. In their analyses, however, a weak dispersion management (i.e. $\Delta D Z_d \ll 1$, where $\Delta D \equiv d_1 - d_2$) was assumed, and the effect of pulse width oscillation and chirp, that characterize the DM solitons, was not taken into account. We apply the perturbation method derived in Section 2.4 to a two-channel WDM system, and elucidate the effect of collisions on dispersion managed WDM soliton transmissions [67].

We assume the frequency separation between the two pulses u_1 and u_2 to be sufficiently large, so that their propagation is described by (2.2), by replacing u with a simple linear superimposition $u_1 + u_2$:

$$i \frac{\partial}{\partial Z} (u_1 + u_2) + \frac{d(Z)}{2} \frac{\partial^2}{\partial T^2} (u_1 + u_2) + a^2(Z) |u_1 + u_2|^2 (u_1 + u_2) = 0. \quad (3.5)$$

Expanding the nonlinear terms and separating them according to their frequencies, we obtain a coupled equation of the form

$$i \frac{\partial u_i}{\partial Z} + \frac{d(Z)}{2} \frac{\partial^2 u_i}{\partial T^2} + a^2(Z) |u_i|^2 u_i = -2a^2(Z) |u_{3-i}|^2 u_i, \quad (3.6)$$

where $i(= 1, 2)$ denotes each WDM channel. In deriving (3.6), we neglected the four wave mixing components $a^2(Z) u_i^2 u_{3-i}^*$, which is well validated for strongly dispersion managed systems. Equation

(3.6) indicates that the propagation of each channel in WDM systems is described by the perturbed equation (2.27) with the perturbation term originating from the cross phase modulation. We thus apply the perturbation analysis in Section 2.4 with the perturbation given by the right hand side of Eq. (3.6): $\varepsilon R = -2a^2(Z)|u_{3-i}|^2u_i$. Inserting this into Eqs. (2.33a)–(2.33e), we have

$$\frac{dA}{dZ} = -ACd, \quad (3.7a)$$

$$\frac{dp}{dZ} = -2pCd, \quad (3.7b)$$

$$\frac{dC}{dZ} = \left(\frac{I_D}{2I_C}p^4 - 2C^2 \right) d - \frac{I_N}{4I_C}a^2A^2p^2 - \frac{a^2A^2p^2}{I_C} \int_{-\infty}^{\infty} f(\tau_i)f^2(\tau_{3-i}) \left\{ f(\tau_i) + 2\tau_i \frac{df}{d\tau_i} \right\} d\tau_i, \quad (3.7c)$$

$$\frac{d\kappa}{dZ} = \frac{4a^2A^2p}{I_L} \int_{-\infty}^{\infty} f(\tau_i)f^2(\tau_{3-i}) \frac{df}{d\tau_i} d\tau_i, \quad (3.7d)$$

$$\frac{dT_0}{dZ} = -\kappa d. \quad (3.7e)$$

We do not write down here the explicit form of the equation for θ_0 , because it has somewhat complicated form and is not directly related to the subject. We notice from Eq. (3.7d) that frequency shift takes place owing to the interaction of the DM solitons. The frequency shift $\delta\kappa$ follows the equation

$$\frac{d(\delta\kappa)}{dZ} = \frac{4a^2\alpha^2p^2}{I_L} \int_{-\infty}^{\infty} f(\tau)f^2(\tau + p\Delta T) \frac{df}{d\tau} d\tau, \quad (3.8)$$

where $\Delta T \equiv T_{0,i} - T_{0,3-i}$, and we used (2.17). The Gaussian ansatz for a pulse shape ($f(\tau) = \exp(-\tau^2)$) reduces Eq. (3.8) to

$$\frac{d(\delta\kappa)}{dZ} = 2\sqrt{2}a^2\alpha^2p^3\Delta T \exp(-p^2\Delta T^2). \quad (3.9)$$

Integrating Eq. (3.8) or (3.9) over a distance Z yields the frequency shift at Z .

In addition to the frequency shift, we can see from Eq. (3.7c) that a collision of dispersion managed WDM solitons also gives rise to the temporary alteration of the frequency chirp, expressed as the following form with the Gaussian ansatz

$$\frac{dC}{dZ} = 2(p^4 - C^2)d - \frac{\sqrt{2}a^2\alpha^2p^3}{2} + \sqrt{2}a^2\alpha^2p^3(2p^2\Delta T^2 - 1) \exp(-p^2\Delta T^2). \quad (3.10)$$

The chirp alteration may be responsible for the temporary modification of the behavior of the DM solitons.

3.4 Numerical results

With the Gaussian ansatz, we study a two-channel dispersion managed WDM soliton transmission in a lossless fiber. The dispersion management period is taken $Z_d = 0.156$, and the average dispersion over Z_d is set $\langle d \rangle = 1.0$. We evaluated the frequency shift as well as the chirp alteration for several different values of dispersion management strength ΔD , the difference between the anomalous GVD d_1 and the normal GVD d_2 . The channel spacing is fixed to be $\Delta B = 24$, which gives the walk-off distance of $Z_{\text{coll}} = 0.147$, and thus $Z_{\text{coll}}/Z_d = 0.94$.

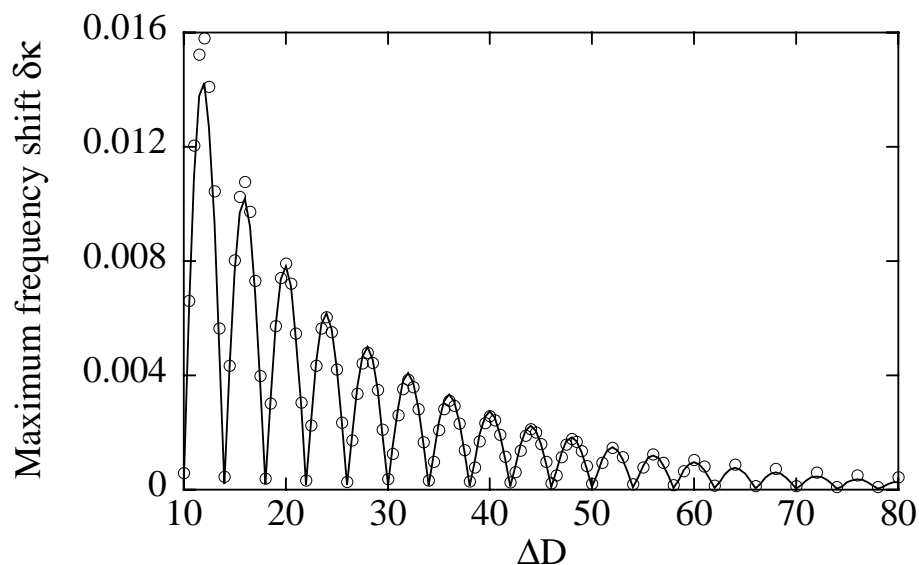


Figure 3.2: Residual frequency shift $\delta\kappa(\infty)$ as a function of ΔD . The solid curve shows the analytical result calculated from Eq. (3.9) and dots are the result obtained from direct numerical simulations. The initial channel spacing is $\Delta B = 24$, which corresponds to 212 GHz for the 20 ps pulse.

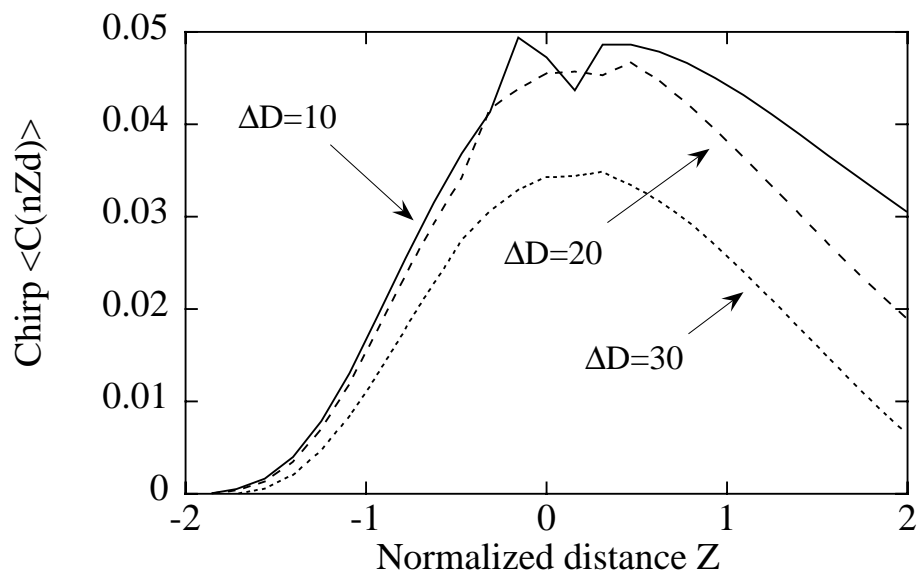


Figure 3.3: The evolution of chirp C at every midpoint of the anomalous GVD segment of the dispersion profile. The initial channel spacing is the same as Fig. 3.2.

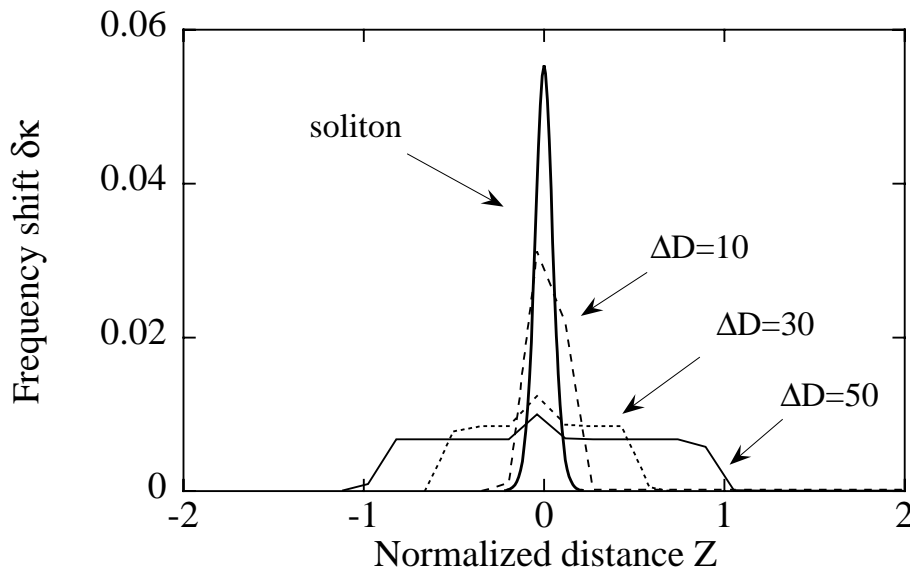


Figure 3.4: Collision-induced frequency shift of a DM soliton and a classical soliton versus normalized distance. Here the classical soliton propagates in a fiber with uniform dispersion equivalent to the averaged value of the dispersion profile.

Figure 3.2 shows plots of the residual frequency shift $\delta\kappa(\infty)$ as a function of ΔD . Here the maxima of $\delta\kappa(\infty)$ for several colliding points with respect to the dispersion profile are plotted for each ΔD , since the amount of frequency shift depends on the colliding points; the maximum frequency shift is given by the collision at the dispersion discontinuity point. For the particular values of ΔD , we can achieve a symmetric collision process regardless of the colliding points, and suppress those residual shifts in the same way as discussed in [65] and [66]. Although the pulses acquire a residual shift of their central frequency even in a lossless fiber, the residual frequency shift, as a whole, is considerably reduced for a large ΔD . This is of particular interest, since in spite of the large variation of pulse width and chirp during the collision, the effect of collision can be well averaged out. This observation is expected to hold also in lossy cases, where the residual shift for the case of $0.5 < Z_{\text{coll}}/Z_a < 2$ in the classical solitons may be suppressed thanks to this averaging effect.

Figure 3.3 shows the chirp C at every midpoint in d_1 segment of the dispersion map, calculated by the direct numerical simulations where a periodic solution is launched. $Z = 0$ represents the complete colliding point. For the stationary state without collisions or any other perturbations, the chirp C is uniformly zero in a lossless case. Collisions, however, give rise to the alteration of C from the stationary state. Unlike the case of the frequency shift, the chirp alteration goes asymptotically back to zero after the collision regardless of the value of ΔD . This result somewhat disagrees with the result obtained from (3.7c); the variational result predicts a residual chirp alteration for the particular values of ΔD as in the case of the residual frequency shift. This discrepancy may be a consequence of radiative effects.

Figure 3.4 shows comparison of the collision-induced frequency shift of a DM soliton and a classical

soliton, both having the same pulse width. In order to eliminate effects of the repeated collisions as a result of periodic dispersion compensations, the frequency shift of the DM soliton is evaluated at each amplifier position. Reduction of the nonlinear interaction within a collision process is clearly seen in this figure. Moreover, we note that a large ΔD increases effective collision length. These observations are of practical importance in reducing the effect of the initial overlap.

Finally we address two additional remarks on the obtained results. First, although the present calculations are restricted to the two-channel case, the analysis for a WDM system with more than two channels is well approximated by the sum of the effect of pairwise collisions especially for larger channel spacing [26]. Second, it should be noted that the timing shift, given by the integral of the temporary frequency shift, may not be suppressed significantly and is still a major limitation in WDM DM soliton transmissions [68, 69].

3.5 Conclusion

We have analytically studied the impact of the cross phase modulation on dispersion managed WDM soliton transmissions. The residual frequency shift is of negligible amount in strongly dispersion managed systems. The analysis shows that a collision also induces chirp degeneration, which is verified by the numerical simulations. For a fixed value of the path averaged GVD and the transform limited pulse width, compared with classical solitons, the DM solitons suffer less nonlinear interaction in a collision process. This result indicates their potential applicability for WDM systems. The analytical results obtained in this chapter can also be applied to make a quick estimate of the timing jitter induced by the frequency shift [68, 69], simply by solving the coupled equations (3.7a)–(3.7e) without carrying out direct numerical simulations of the nonlinear Schrödinger equation.

Chapter 4

Densely dispersion managed soliton transmission

4.1 Introduction

We numerically demonstrate 160 Gbit/s densely dispersion managed soliton transmission in a single channel over 2,000 km in the dispersion-flattened fibers in the presence of polarization mode dispersion (PMD) and of large variation in group-velocity dispersion (GVD). The best performance is achieved by a proper design of the dispersion profile with possible minimum average dispersion so that the soliton interactions are minimized [70].

4.2 Dispersion managed soliton interaction in the same channel

Due to nonlinear interactions between the neighboring solitons in the same channel, they attract each other in time domain and may end up to their complete overlap at a certain propagation distance. In a classical soliton transmission, two in-phase solitons separated over ΔT at the launching point attract and collide at $Z \sim (\pi/4) \exp(\Delta T/2)$ [20, 21, 71], which is obtained by the perturbation method called ‘quasi-particle approach,’ where the well-separated two solitons are individually treated as particles. For a distance typically $\sim 10,000$ km, two solitons need to be separated widely enough (typically $> 6t_s$, where t_s is the pulse width) to avoid the interaction. This significantly degrades spectral efficiency.

Several attempts have been studied to reduce the interaction by means of the introduction of the phase [72, 73] and/or amplitude difference [74] between the neighboring solitons, or the polarization interleaving that takes advantage of the reduction of nonlinear interactions between orthogonally polarized solitons [75]. These schemes, however, may create additional complications in that the former requires precise tuning of phase and amplitude, and the latter may suffer from the PMD-induced relative delay between a pair of orthogonally polarized solitons [76] and the collision-induced depolarization in WDM transmission as a result of the random fluctuation of the orthogonal birefringence axes [77].

Dispersion managed (DM) solitons also suffer from nonlinear interactions between the neighboring slots, but in a different manner. DM soliton interaction has been investigated both analytically and numerically, and as a result, it has been clarified that the interaction is strongly dependent on the

dispersion management strength S defined as

$$S = \frac{|k_1'' z_1 - k_2'' z_2|}{t_s^2}, \quad (4.1)$$

where $k'' = -(\lambda^2/2\pi c)D$, and t_s is the full-width at half-maximum of the pulse when it is transform-limited, and subscripts 1 and 2 denote the anomalous and normal GVD regime, respectively.

In a small S regime, namely in a weak dispersion management regime, the interaction is shown to decrease as S increases, according to the guiding center theory applied to the weak dispersion management [49]. This improvement is a consequence of the faster decrease of the pulse tail whose exact form can be analytically obtained. On the other hand, for large S , namely in a strong dispersion management regime, they exhibit the large oscillation of their pulse width, resulting in strong cross phase modulation (XPM) between the neighboring pulses. As a result, system performance can even be worse than in classical solitons. Note that the cross phase modulation is the major contribution here, since the overlapped tail exhibits a rapid variation of frequency due to the periodically changing chirp, and thus incoherent nonlinear terms such as $q_i^2 q_{3-i}^*$ or $|q_i|^2 q_{3-i}$ with $i = 1$ or 2 are not responsible for the pulse-to-pulse interaction. This indicates that the phase difference does not improve the performance. We also note that we are able to apply the adiabatic perturbation methods to study the interaction just as we discussed in Chapter 3 by imposing the initial conditions $|T_i(0) - T_{3-i}(0)| = \Delta T$ and $\kappa_i(0) = \kappa_{3-i}(0) = 0$ [78, 79]. Overall, the dependence of the collision distance on S is summarized as shown in Fig. 4.1, where we show the numerical results of the collision distance for each value of S in a lossless case. We recognize that the interaction is minimized at $S \sim 1.65$ [80]. This is the most desirable choice in terms of a high-speed single-channel DM soliton transmission.

Before closing the introductory remarks, we briefly comment on the recent trends on the ‘quasi-soliton transmission’ utilizing a properly programmed dispersion profile [81] and the ‘pulse-overlapped DM soliton transmission’ utilizing an extremely strong dispersion management [82], both intended to reduce the pulse-to-pulse interaction.

In the quasi-soliton transmission, the varying dispersion profile provides pulse confinement, resulting in less oscillation of pulse width within one dispersion management period and thus the increase of achievable transmission distance by an order of magnitude compared to the two-step DM soliton systems [83]. Quasi-soliton transmission is studied in detail in Section 5.3.

On the other hand, it has been suggested that sufficiently strong dispersion management may in turn suppress the pulse-to-pulse interaction, based on the observation that the XPM-induced frequency shift, whose derivative is proportional to the temporal profile of the pulse, is reduced considerably for the larger S as a result of considerable pulse spreading [82]. This is based on a completely different philosophy from the design principle of the utilization of the moderate dispersion management with $S = 1.65$ or the quasi-soliton. The pulse-overlapped transmission might be an effective approach to cope with the nonlinear interaction in DM soliton transmission systems where pre-installed standard fibers are upgraded by DCF, having inevitably large S . However the suppression of cross phase modulation critically depends on data pattern, and in some cases it may lead to large amplitude jitter via intra-

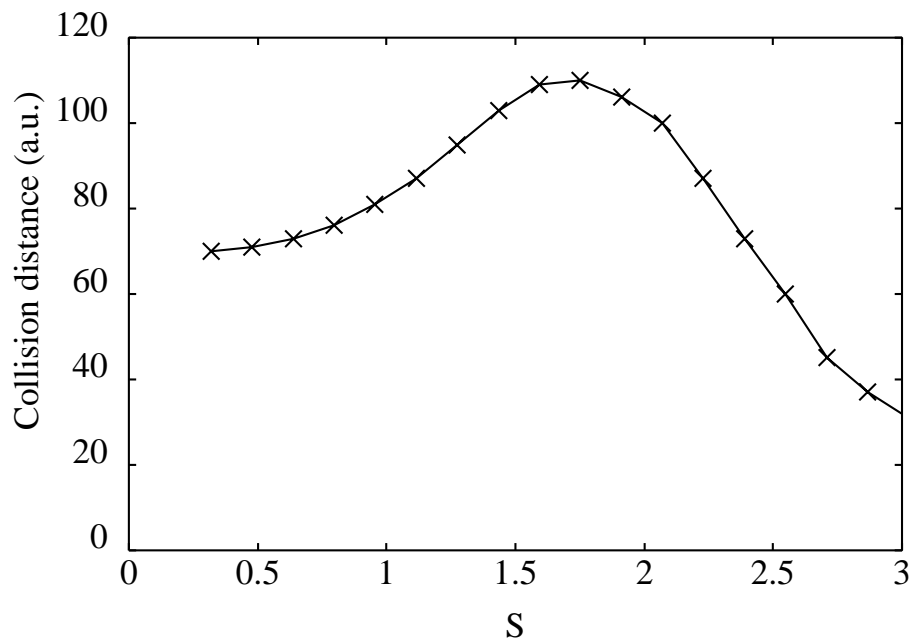


Figure 4.1: Collision distance of two DM solitons for each value of S .

channel four wave mixing [82].

In the following discussions, we focus on the issue of how to realize the optimal dispersion management profile with $S \sim 1.65$.

4.3 Densely dispersion managed soliton

One of the most important properties of dispersion management is that it provides high-capacity soliton transmission over pre-installed standard fibers which are upgraded by connecting dispersion compensating fibers [84]. However there exists a major limitation on the bit rate per single channel in such dispersion managed soliton (DMS) systems caused by soliton interactions between the neighboring pulses induced by the large pulse breathing within one dispersion management period. As we reviewed in Section 4.2, strong dispersion management could lead to system performance even worse than in the classical soliton systems. Moreover, since S depends on t_s^{-2} , the condition $S \sim 1.65$ may not be satisfied for dispersion managed transmission systems even utilizing DSF when they are operated at higher bit rate with much shorter pulses.

To overcome this limitation, densely dispersion managed soliton (DDMS) system was recently proposed in which one amplifier spacing is composed of $n(> 1)$ dispersion management periods [85]. By a proper choice of n , a stationary pulse propagates with less oscillation of pulse width and hence suffers from less interaction with the neighboring pulses compared with the conventional DMS system with the same local and average group-velocity dispersion (GVD). As a result, it is numerically shown that 80 Gbit/s DDMS transmission over 9,000 km may be possible without any active control [85].

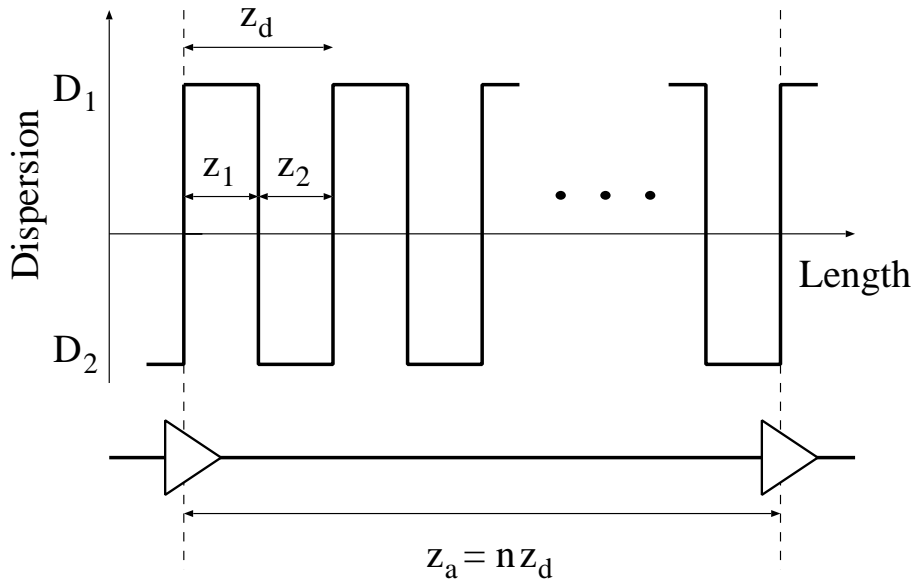


Figure 4.2: Densely dispersion managed system.

We consider a DDMS system schematically shown in Fig. 4.2. It consists of the anomalous (normal) GVD section of D_1 (D_2) over a length of z_1 (z_2), and one amplification period z_a consists of n DM periods. As we described in Section 4.2, the DM soliton interaction can be minimized by arranging the GVD profile such that it satisfies the condition $S = 1.65$ in a lossless case. Such an optimization in conventional DMS systems is equivalent to the proper choice of n in DDMS systems given the amplifier spacing, the local and the average GVD, and the pulse width.

Figure 4.3 shows a dependence of collision distance on n (and corresponding S), when two DDMS's are launched with the initial separation of 6.25 ps. Here we used the parameters $z_a = 40$ km, $D_1 = 2.5$ ps/nm/km, $D_2 = -2.49$ ps/nm/km, $\langle D \rangle = 0.005$ ps/nm/km, $t_s = 2.0$ ps, and introduced the fiber loss of 0.2 dB/km. Dispersion slope and PMD, neglected here for simplicity, are taken into account carefully later in this chapter. From Fig. 4.3, we find the optimum n to be 20 which corresponds to $S \sim 1.6$. A slight difference from the previous condition $S = 1.65$ is due to the fiber loss and amplifications. Note that in classical soliton systems with uniform GVD ($D = 0.005$ ps/nm/km), two sech solitons collide at 2,400 km under the same condition. As we note in Fig. 4.3 that the collision distance asymptotically approaches to 2,400 km for $S < 1.6$, confirming that the soliton interaction in this region originates from the fact that the stationary pulse approaches to the sech soliton [49]. For $S > 1.6$, on the other hand, the interaction forces become stronger (even stronger than sech solitons) because of too much oscillation of pulse width.

To illustrate the impairment of the system arising from soliton interactions for the larger average GVD as well as from the amplifier noise for smaller peak power, we measured Q values for 160 Gbit/s transmission of PRBS (pseudo random bit sequence) 32 bit sequence of DDMS over 2,000 km for each value of $\langle D \rangle$ and initial peak power P_0 , with the fixed DM strength of $S = 1.6$. The noise figure of

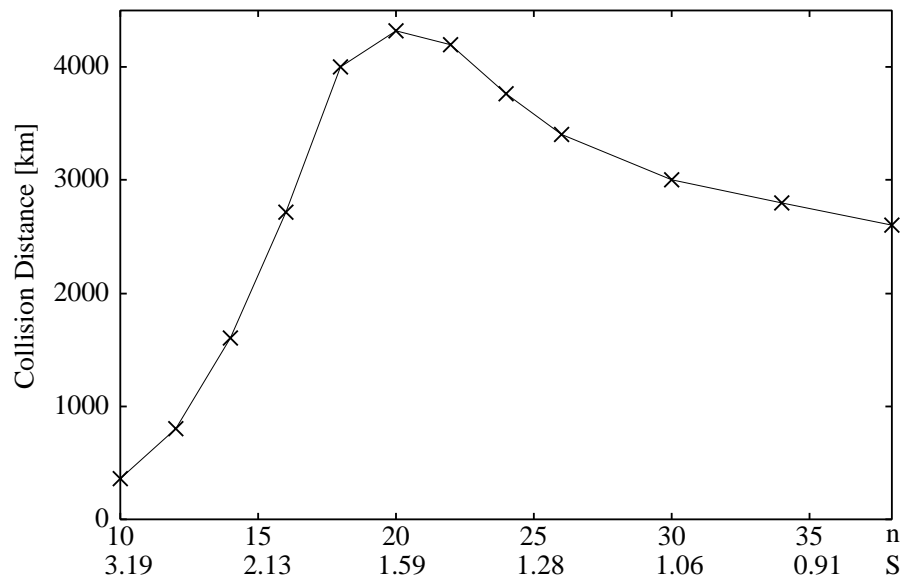


Figure 4.3: Dependence of collision distance on n (and corresponding S parameter). A pair of solitons, whose pulse width is set to be constant (2 ps), are initially separated by 6.25 ps.

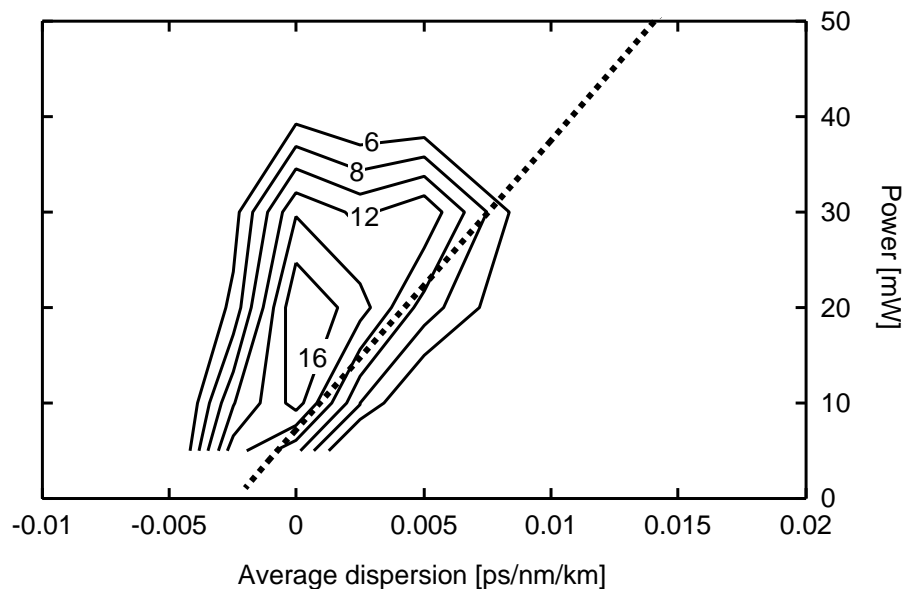


Figure 4.4: Contour map of Q values measured for 160 Gbit/s DDMS transmission over 2,000 km with variable launched power. GVD profile has a variable $\langle D \rangle$ with fixed DM strength of $S = 1.6$.

amplifiers was set 5.0 dB. The Q value is the signal-to-noise ratio of the received eye diagram defined as

$$Q = \frac{\mu_1 - \mu_0}{\sigma_0 + \sigma_1}, \quad (4.2)$$

where μ and σ represent the mean value and the standard derivation of the signal, and the subscripts 1 and 0 denote the bit that corresponds to “1” and “0,” respectively. The dotted line represents a periodic solution evaluated for each $\langle D \rangle$. In Fig. 4.4, we note that $\langle D \rangle$ less than 0.01 ps/nm/km may be necessary to achieve the maximum transmission performance.

Furthermore, the increase of the bit rate in DDMS system up to 160 Gbit/s requires a careful management of dispersion slope and PMD. To cope with dispersion slope, two schemes may be implemented: dispersion slope compensation and dispersion flattening. However, it is not easy to fabricate fibers that have a low GVD and negative dispersion slope simultaneously, whereas dispersion-flattened fibers have normally a large distribution in GVD. Here we consider the utilization of dispersion-flattened fibers having distribution in the value of GVD. It is expected that even when fiber GVD varies, soliton interactions may be minimized by properly connecting fibers with different GVD in a manner such that $S = 1.6$ is maintained. For instance, given a pair of fibers having anomalous and normal GVD D_1 and D_2 respectively, the length of each section z_1 and z_2 may be chosen so that S becomes 1.6 and the average GVD is set as close as to zero along the line. In addition, by connecting fibers in descending value of GVD, we expect further improvement of transmission characteristic [86]. This improvement can be understood by noting that nonlinearity gets weaker in the direction of propagation due to the loss.

Figure 4.5 shows the arrangement of GVD profile based on this principle constructed from the pieces of fibers having Gaussian distribution in GVD with the average $\bar{D} = 0$ ps/nm/km and the variance $\bar{D}^2 = 3.0$ (ps/nm/km)², and the average GVD at each span $\langle D \rangle$ is set as close as to zero. The parameters used in this profile is shown in Table 4.1. An example of DDMS propagation in this GVD profile is plotted in Fig. 4.6. It should be noted that, in practice, it is difficult to design the average GVD to be exactly zero at every span because of the inaccuracy in GVD measurement, especially for shorter

Table 4.1: GVD value [ps/nm/km] and length [km] of each span in GVD profile shown in Fig. 4.5. The average dispersion and DM strength for each span is also listed.

#	D_1	z_1	D_2	z_2	$\langle D \rangle$	S
1	4.50	0.5	-2.60	1.0	-0.233	1.546
2	2.92	1.0	-2.27	1.0	0.325	1.654
3	2.22	1.0	-0.507	5.0	-0.052	1.516
4	1.59	1.5	-0.438	5.5	-0.003	1.529
5	1.15	2.0	-0.280	9.0	-0.020	1.537
6	0.687	4.0	-0.183	13.5	0.035	1.773

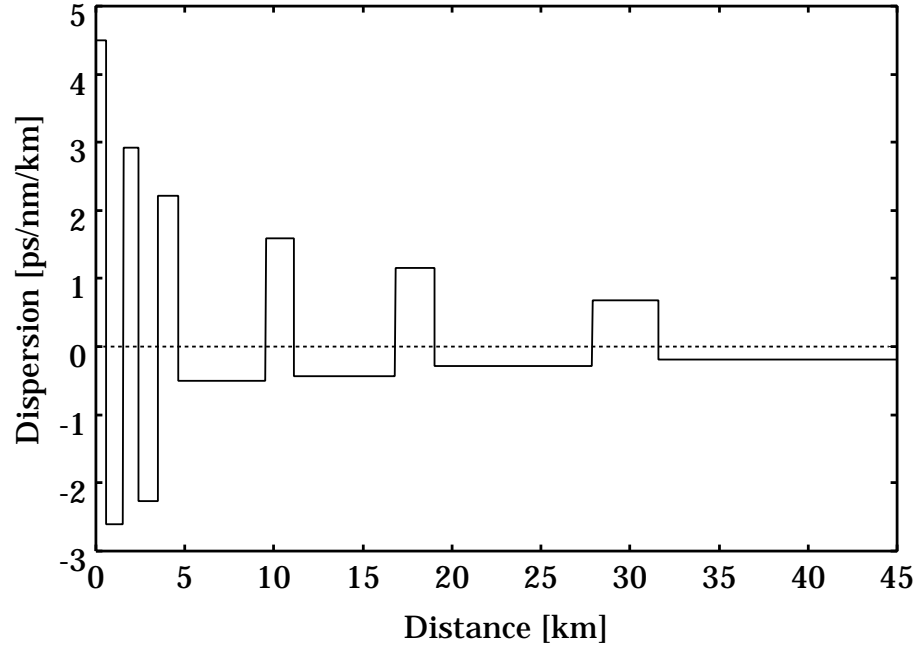


Figure 4.5: An example of dispersion profile in DDMS system.

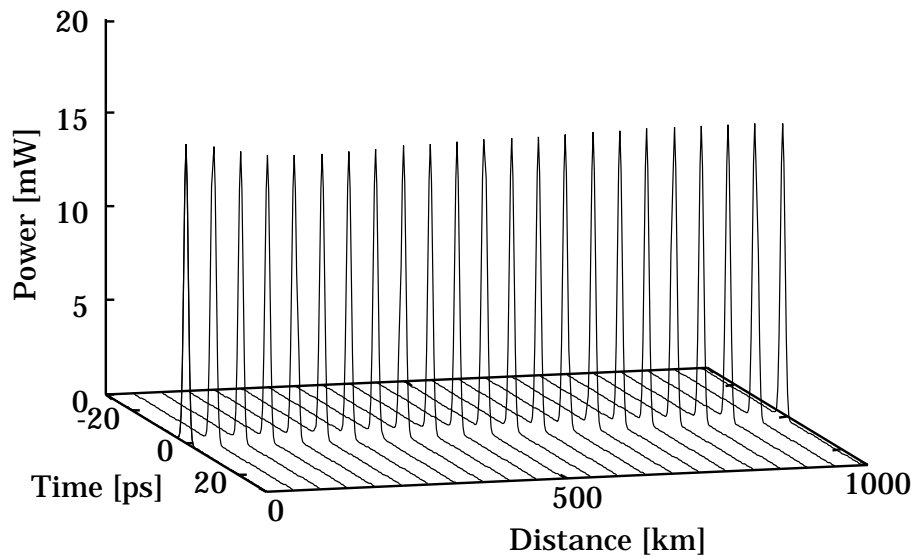


Figure 4.6: Propagation of DDMS in the profile shown in Fig. 4.5.

length. However, we can manage the average GVD over one amplifier spacing as close as to zero simply by arranging the length of the anomalous or normal GVD segment of the final span, depending on the magnitude of $\langle D \rangle$ measured over the whole span except for the final one. For the particular GVD profile in Table 4.1, we increased the length of the anomalous GVD segment of the final span, since the measured $\langle D \rangle$ over the first five segment is negative as a result of the insufficient accuracy of GVD. As a result, $\langle D \rangle$ over the whole span is calculated to be 0.008 ps/nm/km. In other words, although it is impossible to manufacture a fiber with such a small value of the average dispersion, the proper scheme allows one to construct a transmission line with practically any value of $\langle D \rangle$.

4.4 Numerical results

To evaluate the system performance, we carried out numerical simulations of the transmission of PRBS 32 bit sequence at 160 Gbit/s on the dispersion map shown in Fig. 4.5. We assumed fibers having loss of 0.2 dB/km, the nonlinear coefficient $n_2\omega_0/cA_{\text{eff}}$ of $1.86 \text{ W}^{-1}\text{km}^{-1}$, PMD of $0.05 \text{ ps}/\sqrt{\text{km}}$, and the residual dispersion slope of $0.005 \text{ ps}/\text{nm}^2/\text{km}$. Amplifiers are assumed to have the noise figure of 5.0 dB. To reduce the soliton interaction, in-line optical filters with the bandwidth of 1,800 GHz are inserted at every amplifier location (45 km interval). We numerically solved the coupled nonlinear Schrödinger equation that includes the effect of third order dispersion and PMD:

$$\begin{cases} i \left(\frac{\partial u}{\partial Z} + \delta \frac{\partial u}{\partial T} \right) + \frac{d(Z)}{2} \frac{\partial^2 u}{\partial T^2} - i \frac{\beta_3}{6} \frac{\partial^3 u}{\partial T^3} + \left(|u|^2 + \frac{2}{3} |v|^2 \right) u \\ \qquad \qquad \qquad = -i\Gamma u + i \sum_n G_0 \delta(Z - nZ_a) u \\ i \left(\frac{\partial v}{\partial Z} - \delta \frac{\partial v}{\partial T} \right) + \frac{d(Z)}{2} \frac{\partial^2 v}{\partial T^2} - i \frac{\beta_3}{6} \frac{\partial^3 v}{\partial T^3} + \left(|v|^2 + \frac{2}{3} |u|^2 \right) v \\ \qquad \qquad \qquad = -i\Gamma v + i \sum_n G_0 \delta(Z - nZ_a) v \end{cases}, \quad (4.3)$$

where u and v are the two orthogonal components. In order to introduce random variation of the orientation of the fiber birefringence, we rotate the fields by θ (with uniform distribution in $[0: \pi]$) at the interval of 200 m by the transformation of the form [87]

$$\begin{pmatrix} u' \\ v' \end{pmatrix} = \begin{pmatrix} \cos \theta & \sin \theta \exp(i\phi) \\ -\sin \theta \exp(-i\phi) & \cos \theta \end{pmatrix} \begin{pmatrix} u \\ v \end{pmatrix}, \quad (4.4)$$

We also imposed random phase difference ϕ (with uniform distribution in $[0: \pi]$) between u and v .

Figure 4.7 shows the calculated Q value versus transmission distance, obtained by averaging the values over 20 runs with different random number sequences for θ , ϕ , and the ASE noise. Since the residual dispersion slope is kept small, it simply produces a position shift and the degradation may be caused by the PMD. In another simulation without PMD, we have confirmed 160 Gbit/s transmission over $> 3,000$ km. These results demonstrate successful DDMS transmission on a terrestrial scale utilizing practical fibers. Although the simulation is carried out for the particular profile in Fig. 4.5, we expect improved performance similar to Fig. 4.7 for other GVD profile with different pieces of fibers, by following the above arrangement in individual design of GVD profile. We also expect further improvement by employing the polarization interleaving between the neighboring time slots.

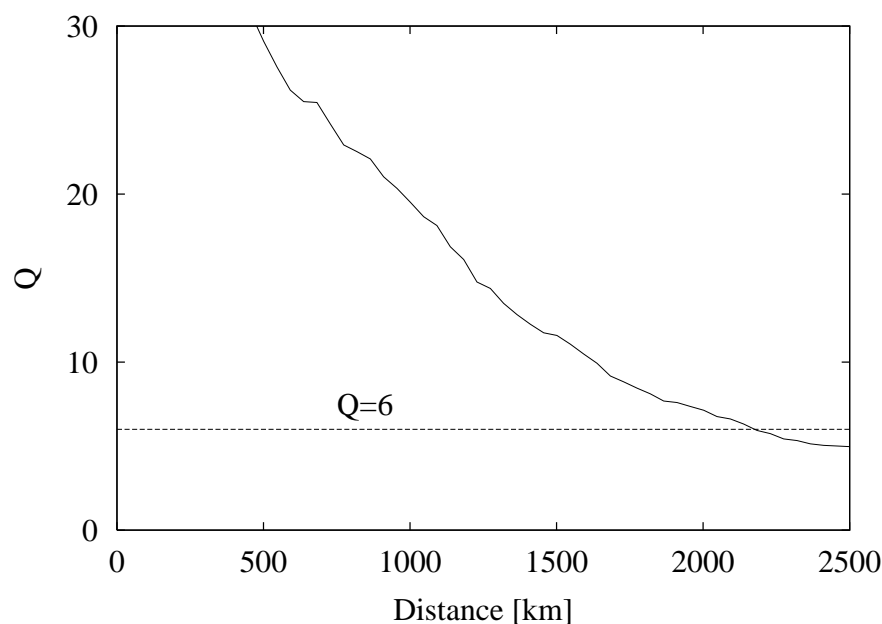


Figure 4.7: The Q factor versus transmission distance for 160 Gbit/s DDMS system with GVD profile shown in Fig. 4.5.

4.5 Conclusion

In conclusion, we have investigated the feasibility of ultra-fast single-channel soliton transmission in a densely dispersion managed fiber. Thanks to the large tolerance of DMS to random distribution of GVD, 160 Gbit/s single-channel soliton transmission is possible on a terrestrial scale by reducing the dispersion slope and the average dispersion, and by a proper arrangement of the dispersion profile. Finally we emphasize that the DDMS systems having well separated RZ pulses at any point in transmission line has a strong advantage over those with chirped RZ pulses in network applications in allowing the installation of add-drop multiplexers at any point in the system.

Chapter 5

Transmission control of dispersion managed solitons

5.1 Introduction

We analyze several schemes, both theoretically and numerically, to improve transmission characteristics in dispersion managed (DM) soliton systems in single-channel transmission as well as multi-wavelength channels.

In Section 5.2, we investigate the stabilizing action of nonlinear gain elements on DM soliton transmissions. By means of a proper combination of the nonlinear gain and filtering, the background and amplitude instability introduced by lumped guiding filters can be controlled. Indeed, radiative background that may not be separated from the signal when the average dispersion is close to zero is shown to be suppressed. Following a theoretical analysis based on the variational method, we present numerical results to demonstrate that nonlinear gain has a strong stabilizing action on the amplitude, frequency, and chirp of the DM soliton. In Section 5.3, we demonstrate that the quasi-soliton supports ultra high-speed single-channel optical transmission over 10^2 Tbit·km/s with a help of the properly programmed dispersion profile and optical phase conjugation. The varying dispersion profile allows less variation of pulse width and thus less interaction between adjacent pulses. In addition, the optical phase conjugation provides strong pulse confinement by producing linear trapping potential that is beneficial for further reduction of the interaction. In Section 5.4, we observe the suppression of noise growth enhanced by the filtering action, with a help of the cross phase modulation of the noise by solitons in different wavelength channels. This may open up the possibility of soliton based massive WDM transmission with considerably improved performance.

5.2 Stabilization of dispersion managed soliton transmissions by nonlinear gain

Dispersion managed (DM) solitons are attracting considerable interest recently in return-to-zero (RZ) format optical communication systems because of their superb characteristics which are not observed in the classical solitons, as we have seen in the preceding chapters. In particular, strong periodic dispersion

management allows for the stationary propagation of nonlinear RZ pulses with finite energy when the average dispersion is close or even equal to zero [55, 88]. This helps suppress the Gordon-Haus effect without sacrificing the signal-to-noise ratio. Dispersion management also plays an important role in high-speed soliton transmissions over pre-installed standard fibers, and it is shown to be compatible with dense wavelength-division-multiplexed (WDM) transmissions [84].

Such strong dispersion management, however, enhances the nonlinear interactions between adjacent pulses because of the large pulse breathing within one management period. Furthermore, for small average dispersions, linear waves may strongly degrade the transmission performance. Indeed, the propagation of nonlinear stationary pulses in real fiber links is always accompanied by radiative background (or linear mode). These dispersive waves originate from the amplifier noise or from the mismatch between the input pulse and the truly stationary pulse. Small average dispersions prevent the separation of the linear wave from the signal, which delays the formation of a stationary pulse.

Transmission control methods such as guiding filters (with its frequency fixed or slid) [89–91] or synchronous modulation [92, 93] were studied in order to stabilize DM soliton transmissions against the above mentioned perturbations. Although the guiding filter is shown to decrease pulse interactions, it requires excess gain in order to compensate for the filter-induced loss, which in turn may enhance the accumulation of such linear mode. In addition, it was recently shown [90, 93] that filtered DM solitons suffer from additional instabilities, depending on the location of lumped filters, owing to the opposite direction of the filter action on stabilizing energy against spectrum fluctuation. Whereas the synchronous modulation may also not be effective as long as the linear wave is not shed away.

On the other hand, nonlinear gain may be an alternative to the above schemes [94–97]. Nonlinear gain is realized by making use of polarization controllers [94], nonlinear amplifying loop mirrors [95], or fast saturable absorbers [96]. Note that sub-picosecond response times are presently achievable with semiconductor saturable absorbers using low temperature growth techniques [98–100]. In the same way as the passive mode-locking in fiber ring lasers, it suppresses the growth of the linear mode and thus avoids soliton instability caused by such linear mode accumulation. Thanks to the DM soliton power enhancement, nonlinear gain is expected to be more beneficial to DM solitons than to classical solitons [96]. A recent experiment [101] demonstrated that passive control by use of saturable absorption, combined with strong filtering, allows for error-free DM soliton transmissions over 200 Mm at 10 Gbit/s, and the growth of the ASE noise is significantly suppressed. We apply the perturbation method in Section 2.4 to the DM soliton system controlled by the nonlinear gain elements and filtering, and analyze their stabilizing effects.

We start from the modified nonlinear Schrödinger (NLS) equation in a dimensionless form including the effect of dispersion management, non-adiabatic loss and lumped amplification, excess gain, filtering, and quadratic and quartic nonlinear gain on the right hand side

$$\frac{\partial u}{\partial Z} = i \frac{d(Z)}{2} \frac{\partial^2 u}{\partial T^2} + i a^2(Z) |u|^2 u + \delta(Z) u + \beta(Z) \frac{\partial^2 u}{\partial T^2} + \gamma_1(Z) |u|^2 u + \gamma_2(Z) |u|^4 u, \quad (5.1)$$

where $d(Z)$ represents the variable group-velocity dispersion and $a^2(Z)$ represents the exponential

variation of the power. We consider the two step GVD profile as usual; for example, whenever $Z_d = Z_1 + Z_2$ denotes the length of the dispersion map, one has $d = d_1$ for $nZ_d < Z < nZ_d + Z_1$, and $d = d_2$ for $nZ_d + Z_1 < Z < (n+1)Z_d$, respectively. Moreover, $a(Z) = A_0 \exp(-\Gamma Z)$ for $nZ_d < Z < (n+1)Z_d$, where Γ is the (supposed constant for simplicity) fiber loss coefficient, and A_0 is the nonlinearity amplitude after the amplifier. Note that the coefficients δ , β , γ_1 , and γ_2 are expressed in terms of delta functions when we consider periodic lumped filters and nonlinear gain elements (e.g. located after every amplifier). In the following, we shall consider $\gamma_1 > 0$ and $\gamma_2 < 0$, that is, the quartic nonlinearity term in (5.1) acts as a key stabilizing nonlinear loss term. We note that this gain profile can be realized by the use of both polarization controllers and fast saturable absorbers. The relation between the real value of the polarization controller components and the dimensionless parameters γ_1 and γ_2 is shown in [94]. The gain profile in (5.1) also corresponds to the Taylor expansion of the nonlinearity of the fast saturable absorbers. The instantaneous response of the saturable absorbers of the form $-\alpha_0/(1+|u|^2/I_s)$ can be expanded, up to the second order, into $-\alpha_0 + (\alpha_0/I_s)|u|^2 - (\alpha_0/I_s^2)|u|^4$, where α_0 and I_s are the loss coefficient and the saturation intensity, respectively. Thus the coefficients of the second and third term give γ_1 and γ_2 respectively.

With the ansatz (2.9) with $f(\tau) = \exp(-\tau^2)$, and from the perturbation method (2.33a)–(2.33f), we obtain equations that describe the adiabatic evolution of each parameter in (2.9) owing to the nonlinear gain and filtering. For example, for the energy $E = (A^2/p)\sqrt{\pi/2}$ and frequency κ , one obtains

$$\frac{dE}{dZ} = 2\delta E - 2\beta\kappa^2 E - 2\beta \left(p^2 + \frac{C^2}{p^2} \right) E + \sqrt{2}\gamma_1 A^2 E + \frac{2\sqrt{3}}{3}\gamma_2 A^4 E, \quad (5.2)$$

$$\frac{d\kappa}{dZ} = -4\beta \left(p^2 + \frac{C^2}{p^2} \right) \kappa. \quad (5.3)$$

When we consider a steady state in (5.2), the excess gain can be evaluated as

$$\delta = \beta B_0 - \frac{\sqrt{2}}{2}\gamma_1 A_0^2 - \frac{\sqrt{3}}{3}\gamma_2 A_0^4, \quad (5.4)$$

where $B \equiv p^2 + C^2/p^2$ is proportional to the square of the spectral bandwidth, and the subscript 0 denotes the evaluation at the location of filter and/or nonlinear gain element in the steady state. As expected, with the aid of nonlinear gain one can reduce the excess gain at the amplifiers, without sacrificing filter strength. If we linearize $B(E)$ and $A(E)$ around the steady state $E = E_0$, the equation for the DM soliton energy fluctuations reads as

$$\frac{dE}{dZ} = \left[-2\beta B'(E_0) + \left\{ 2\sqrt{2}\gamma_1 A_0 + \frac{8\sqrt{3}}{3}\gamma_2 A_0^3 \right\} A'(E_0) \right] (E - E_0)E. \quad (5.5)$$

Without nonlinear gain, the pulse energy fluctuations may not be compensated for, rather they may be even enhanced for large E_0 , since $B'(E_0)$ can be negative in this case [93]. This severely limits the acceptable energy and thus the signal-to-noise ratio in the case of DM soliton transmissions with nearly zero average dispersion. On the other hand, nonlinear gain permits to avoid the above limitation since one may tune the γ_1 and γ_2 parameters so that the coefficient of $(E - E_0)E$ is negative. (Note $A'(E_0)$ is always positive even when $B'(E_0) < 0$.)

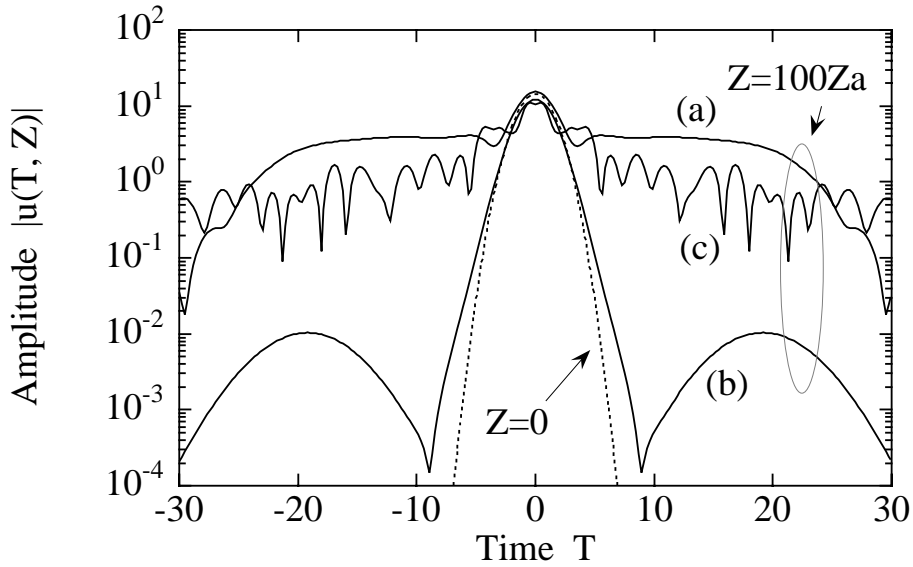


Figure 5.1: Waveforms of a DM soliton at $Z = 0$ (dotted line) and $Z = 100Z_a$ (solid lines). (a) With guiding filter ($\delta = 0.161$, $\beta = 0.6$), (b) With guiding filter and nonlinear gain ($\delta = 0.0$, $\beta = 0.6$, $\gamma_1 = 4.6 \times 10^{-2}$, $\gamma_2 = -1.6 \times 10^{-3}$), (c) Without any control.

In order to demonstrate the stabilizing action of nonlinear gain, we carried out direct numerical simulations of (5.1). We considered a periodic dispersion profile with zero average dispersion, which consists of anomalous dispersion ($d_1 = 100$) fiber spans of length $Z_1 = 0.2$, followed by normal dispersion ($d_2 = -400$) spans with length $Z_2 = 0.05$. The dimensionless loss coefficient in each span was $\Gamma = 11.5$. Amplifiers, filters, and nonlinear gain elements were located after each d_2 span, i.e. they were spaced at an interval of $Z_a = Z_d$. Amplifier ASE noise was not included for simplicity. We considered in-line guiding filters with a Gaussian transfer function $T(\Omega) = \exp[(\delta - \beta\Omega^2)Z_a]$ with $\beta = 0.6$. We further introduced a nonlinear gain element represented by a lumped gain function $G = 1 + \gamma_1 Z_a |u|^2 + \gamma_2 Z_a |u|^4$ with $\gamma_1 = 4.6 \times 10^{-2}$ and $\gamma_2 = -1.6 \times 10^{-3}$. Whenever the guiding filters and the nonlinear gain elements are combined, no excess gain is introduced in the system, which clearly permits to reduce the background instability of filtered DM solitons.

Figure 5.1 shows a comparison of DM soliton waveforms at a propagation distance $Z = 100Z_a$: the propagation was supported by guiding filters alone, by filters combined with nonlinear gain, and without any control. The initial waveform, chosen as a Gaussian pulse, is also plotted in this figure. The substantial suppression of the linear mode by introducing nonlinear gain can be clearly seen in this figure. We also note that filters alone may not be effective in stabilizing the DM soliton transmission.

Figure 5.2 (Figure 5.3) shows the evolution along the link of the energy (chirp and frequency) fluctuations with filtering and nonlinear gain. As can be seen, even if a transform-limited (i.e. unchirped) pulse is launched at the input, the proper frequency chirp is acquired upon propagation.

Note that, as is pointed out in [91], DM solitons may suffer from propagation instability with this

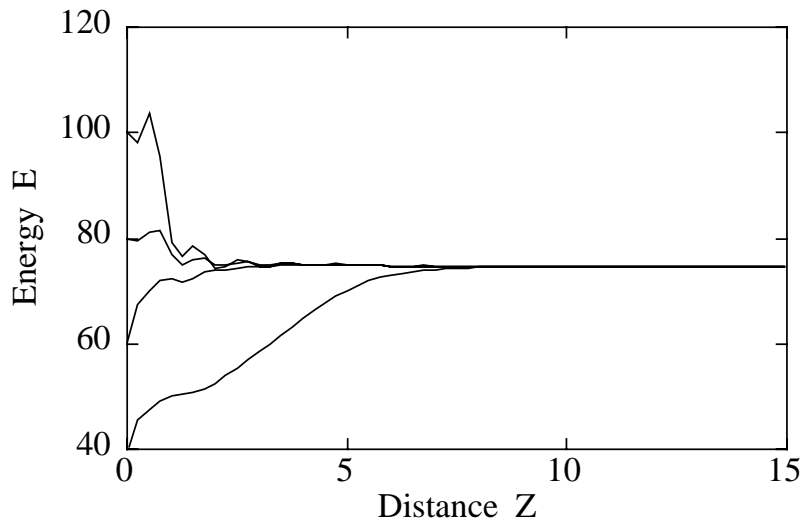


Figure 5.2: Acquisition of the steady state energy E by guiding filter and nonlinear gain. The same parameters are used as (b) in Fig. 5.1. $E(0)=40, 60, 80, 100$.

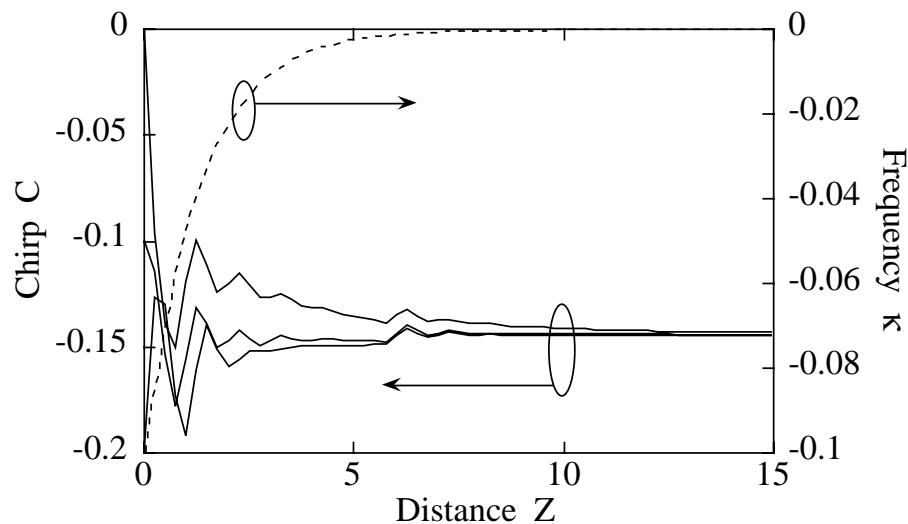


Figure 5.3: Acquisition of the steady state frequency κ and chirp C by guiding filter and nonlinear gain. The same parameters are used as (b) in Fig. 5.1. $\kappa(0) = -0.1$, and $C(0)=-0.2, -0.1, 0$.

filter location, namely at the end of normal dispersion section, owing to the dependence of spectral width on pulse energy which is opposite to the case of classical solitons (i.e. the filters introduce a positive feedback action on the DM soliton bandwidth). One may not be able to suppress the pulse fluctuations without nonlinear gain.

So far we have considered a particular choice for the nonlinear gain coefficients. One may wonder at this point how robust is the control of DM solitons by the nonlinear gain technique whenever the coefficients γ_1 and γ_2 slightly deviate from one saturable absorber to the other. Moreover, another important point to consider is the tolerance of the control method with respect to small deviations in the above nonlinearity coefficients with respect to the ‘optimal values.’ While we leave a detailed analysis of these issues to further work, we may simply note here that even when the nonlinear gain parameters are slightly modified with respect to their original value, the stable pulse amplitude may be kept fixed by just adjusting the excess gain δ such that (5.4) remains satisfied. It should also be noted that the stability of the control technique is not affected as long as negative feedback results whenever the various parameters are inserted in (5.5).

As a concluding remark of this section, we studied the stability of DM soliton propagation supported by nonlinear gain elements. We have shown that nonlinear gain may improve considerably the DM soliton stability. The role of nonlinear gain elements is the suppression of the growth of dispersive waves which is important for nearly-zero average dispersions. Moreover, nonlinear gain allows for a large tolerance with respect to fluctuations in the initial pulse parameters such as energy and chirp. In addition to the recovery of the steady state, nonlinear gain helps avoiding the instability which is caused by lumped filters when these are placed at certain positions in the map such as the midpoint of the normal GVD span. In addition to the several above mentioned improvements introduced by nonlinear gain control, we anticipate that nonlinear gain combined with nonlinear gain saturation may allow to reduce the ASE noise accumulation and waveform distortions caused by polarization mode dispersion (PMD). As a final note, the analysis presented here may also be applied to study DM pulse dynamics in stretched pulse mode-locked lasers [102], where nonlinear polarization rotation is employed as passive mode-locking mechanism.

5.3 Quasi-soliton propagation with periodic optical phase conjugation

Optical phase conjugation (OPC), which compensates for both fiber chromatic dispersion [103] and nonlinear effects [104], is an attractive scheme as a transmission control in fiber-optic communication systems. OPC is an effective technique also for optical soliton transmission [105]; although solitons take advantage of self phase modulation to cancel out the dispersion-induced chirp, OPC is still effective to suppress nonlinear interactions between signal and noise (Gordon-Haus effect) and/or among adjacent pulses, as well as self-induced Raman effect, which are the major limitations on their transmission capacity. No matter which format is employed, ultra high-speed transmission ($\gtrsim 100$ Gbit/s per channel)

requires dense packing of short pulses. Pulse width oscillation observed in dispersion managed densely packed pulses brings about a problem that each bit may not be properly detected in the middle of a transmission line, which presents a serious problem especially in a network application. Although a classical soliton has no variation of pulse width during the transmission, interaction forces between adjacent pulses present a problem when two solitons are packed closely.

In this section, we consider the use of OPC for the quasi-soliton transmission to overcome these difficulties [106]. The quasi-soliton [81] is a nonlinear stationary pulse which is characterized by reduced nonlinearity as a result of the periodic variation of chirp. With a help of the pulse confinement by means of properly programmed dispersion profile, the quasi-soliton is shown to have less variation of pulse width and suffers less interaction between adjacent pulses than a DM soliton [83].

The outline of the quasi-soliton propagation is summarized as follows: the propagation of nonlinear optical pulse in dispersion managed fibers can be described by the modified nonlinear Schrödinger equation (2.2). For a strong dispersion management, the stationary pulse has a periodically varying chirp. We thus assume the solution of (2.2) to have a form similar to (2.9):

$$u(T, Z) = \alpha \sqrt{p(Z)} v(\tau, Z) \exp[iC(Z)T^2/2], \quad \tau \equiv pT. \quad (5.6)$$

The factor 1/2 in the chirp parameter is introduced just to facilitate the arrangement of the following equations. We first tailor the dispersion in proportional to $a^2(Z)$ to remove the non-adiabatic effect owing to the loss and lumped amplifiers. In addition, we further program the dispersion profile such that $d(Z) = 1/p(Z)$. Eq. (5.6) then becomes

$$i \frac{\partial v}{\partial Z''} + \frac{1}{2} \frac{\partial^2 v}{\partial \tau^2} + \alpha^2 |v|^2 v - \frac{K}{2} \tau^2 v = 0, \quad (5.7)$$

where $Z'' \equiv \int_0^{Z'} p(Z') dZ'$, $Z' \equiv \int_0^Z a^2(Z) dZ$, and K is a positive constant. We note that $v(\tau, Z)$ can be interpreted as the wave function confined by self-trapping potential and linear quadratic potential. Assuming $v(\tau, Z) = f(\tau) \exp(i\lambda Z'')$, we obtain

$$\frac{1}{2} \frac{d^2 f}{d\tau^2} + \alpha^2 f^3 - \frac{K}{2} \tau^2 f - \lambda f = 0. \quad (5.8)$$

This gives a localized stationary solution of $f(\tau)$ whose waveform is between the hyperbolic-secant and Gaussian. The dispersion profile is given by

$$d(Z) = d(0) a^2(Z) \left[\cosh(\delta Z') + \frac{C(0)d(0)}{\delta} \sinh(\delta Z') \right], \quad (5.9)$$

where $\delta \equiv \sqrt{K/d(0)^2 + C(0)^2 d(0)^2}$. Quasi-soliton recovers its pulse width at Z'_1 such that $p(Z'_1) = p(0)$ (this means that $C(Z_1) = -C(0)$), where

$$Z'_1 = \frac{1}{\delta} \ln \left(\frac{\delta - C(0)d(0)}{\delta + C(0)d(0)} \right). \quad (5.10)$$

If we reverse the sign of the chirp at every Z_1 , we regain the initial condition.

In the previous works, the chirp is reversed by the use of fiber gratings [81, 107] or dispersion compensating fibers [83]. These schemes, however, produce linear potential with the opposite sign i.e.,

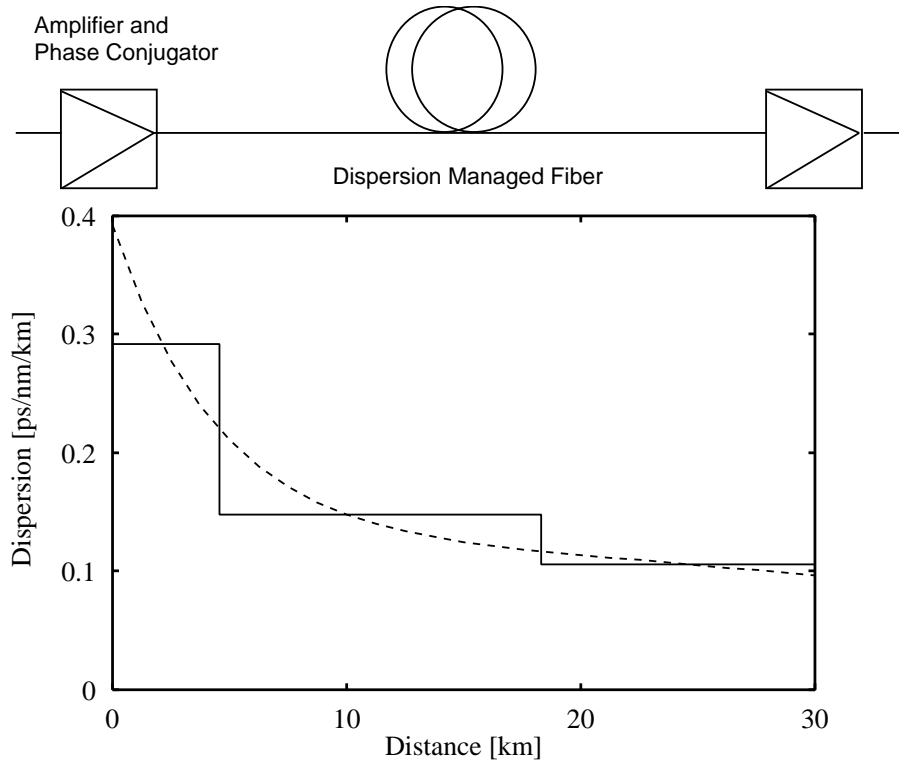


Figure 5.4: Dispersion profile. Solid: stepwise approximation. Dashed: (5.9).

detrapping, when averaged over one period, owing to residual nonlinearity. This may fail to maintain the localized stationary solution [54]. On the other hand, if we employ the OPC, this problem is avoided and the linear potential always contributes to pulse confinement.

We have carried out numerical simulations to show the validity of the proposed scheme. For practical feasibility, we approximate the profile by combination of three fibers with different constant dispersion. Figure 5.4 shows the comparison between the dispersion profile given by (5.9) and the stepwise profile. System parameters are as follows: wavelength = $1.55 \mu\text{m}$, loss = 0.2 dB/km , dispersion slope = $0.02 \text{ ps/nm}^2/\text{km}$, nonlinear refractive index = $3.2 \times 10^{-16} \text{ cm}^2/\text{W}$, core effective area = $40 \mu\text{m}^2$, Raman characteristic time = 3 fs , pulse width = 2.2 ps , bit rate = 80 Gbit/s , input peak power = 12 mW , the amplifier noise figure = 5 dB , amplifier spacing = 30 km , and power penalty at the phase conjugator = 15 dB . In-line filters with 360 GHz bandwidth are inserted at each amplifier. Figure 5.5 shows the received eye diagram after $2,000 \text{ km}$ propagation. In spite of no dispersion slope compensation and insufficient phase conjugation efficiency, successful transmission is achieved over thousands of kilometers. Since OPC does not compensate for the third order dispersion, this is the dominant limiting factor to the transmission capacity. In fact, we have confirmed in simulation, if the dispersion slope is made to zero, 160 Gbit/s data can be transmitted beyond a distance of $4,000 \text{ km}$ in this scheme.

We note that the system is significantly flexible against the fluctuation of dispersion profile or peak pulse power owing to the symmetric property of phase conjugated system. Without the third order dis-

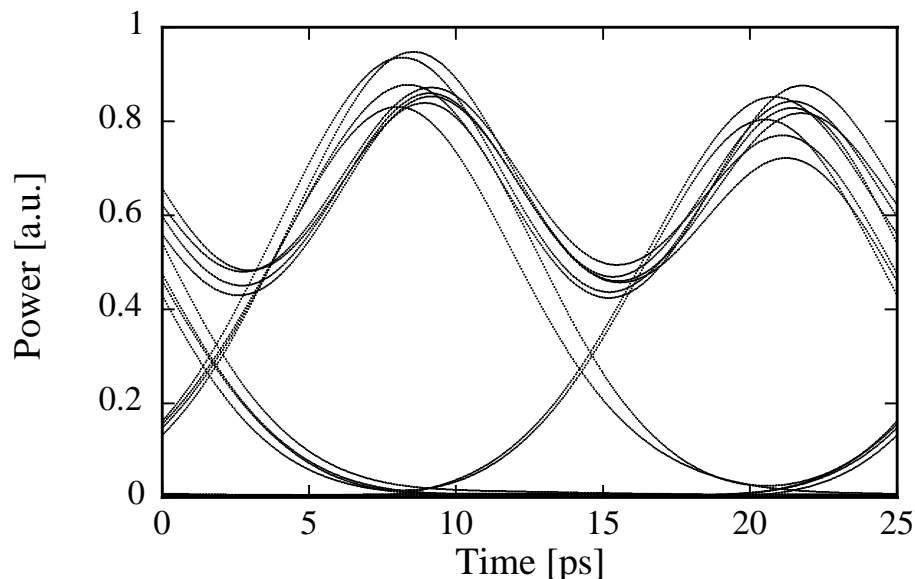


Figure 5.5: Received eye diagram formed from 32 bits data detected by electrical filter with 42 GHz bandwidth.

persion and PMD, the initial condition is completely recovered at every two stages even for mismatched initial conditions. Since OPC can compensate for phase distortion due to group-velocity dispersion and Kerr as well as Raman nonlinearities, the present scheme can also be useful for transmission of NRZ format. However, since NRZ pulses are nonstationary and are less tolerant to the third order dispersion due to interplay with self phase modulation, the resultant transmission capacity is found to be limited than the quasi-soliton.

In summary, it is shown that the quasi-soliton supported by optical phase conjugation can provide ultra-fast single-channel transmission. Combined with WDM technology, it may enable us to construct terabit wide-area networks over thousands of kilometers.

5.4 Stable filter control of wavelength division multiplexed soliton systems

In wavelength division multiplexed (WDM) soliton transmission systems with frequency filter control, the growth of spontaneous emission from amplifiers due to excess gain near the central region of the filter is expected to be suppressed due to the spectral diffusion caused by cross phase modulation by solitons in other WDM channels. We numerically demonstrate that, for a canonical case of the map strength S of about 5, if the number of channels is six or more, the spectral diffusion is sufficient to suppress the growth, and stable filter control is achieved without sliding, phase and/or amplitude modulation [108].

Soliton timing jitter was shown to be effectively controlled by means of a combination of amplifiers

with excess gain δ and frequency filters inserted in the transmission line [30, 31]. However, linear growth of spontaneous emission near the central region of the filter is found eventually to destroy solitons [32]. Several techniques to suppress the growth, such as sliding the filter frequency [33], gain modulation [34] and phase modulation [35], and the amplifiers with nonlinear gain [94, 95] have been proposed. However, these methods complicate the soliton transmission systems, and may not be compatible with dense WDM transmissions.

In WDM soliton transmission systems, however, the cross phase modulation of the linearly unstable mode by solitons in other WDM channels is expected to cause spectral diffusion which transports the unstable spectrum into the stable region of the filter. This process may be described by a phenomenological transport equation for the spontaneous emission spectrum $\bar{v}(\omega, Z)$:

$$\frac{\partial \bar{v}}{\partial Z} = \delta \bar{v} - \frac{\omega^2}{\omega_0^2} \bar{v} + D \frac{\partial^2 \bar{v}}{\partial \omega^2}. \quad (5.11)$$

Here Z is the dimensionless distance of propagation, ω_0 , the characteristic width of the filter, δ , the excess gain at the center of the filter and D is the spectral diffusion rate in distance caused by irreversible phase shifts. Such irreversible phase shifts take place if the soliton amplitude changes during the cross phase modulation due to amplifications and/or collisions with solitons in other channels.

It is noted that Eq. (5.11), which produces exponentially growing spectrum near $\omega = 0$ in the absence of the diffusion term, allows a stationary spectrum given by a Hermite polynomial described by a solution of

$$D \frac{\partial^2 \bar{v}}{\partial \omega^2} + \left(\delta - \frac{\omega^2}{\omega_0^2} \right) \bar{v} = 0. \quad (5.12)$$

In order to confirm this conjecture, we carried out numerical simulations of the evolution of a linear wave envelope by taking into account of the cross phase modulation caused by solitons in a number of WDM channels. We have numerically solved the following equation that describes the evolution of linear wave in time domain:

$$i \frac{\partial w}{\partial Z} + \frac{d(Z)}{2} \frac{\partial^2 w}{\partial T^2} = -i\Gamma w + iG(Z)w + \frac{i}{\omega_0^2} \frac{\partial^2 w}{\partial T^2} + i\delta w - 2 \sum |q_i|^2 w, \quad (5.13)$$

where Γ is normalized damping rate, $d(Z)$ and $G(Z)$ represent periodic variation of the fiber chromatic dispersion and lumped amplification respectively, and q_i denotes the amplitude of the i -th solitons including the soliton in the same channel as w . Note that q_i is a function of time through its $(T + \kappa_i Z - T_i)$ dependence, where κ_i is the frequency difference between w and q_i channels and T_i is the time position of the i -th soliton at $Z = 0$. We further note that T^2 dependence of the statistical average of the last term at $\kappa_i Z = T_i$ produces the spectrum diffusion shown in Eq. (5.11).

We observed the growth of the noise generated at $Z = 0$. For simplicity, we neglect the effect of noise which would be added at every amplifier other than the initial noise. Furthermore, we considered soliton transmission in a strongly dispersion managed line to enhance the suppression of noise, taking advantage of the enhanced power that the solitons acquire. The parameters used in the simulation are as follows: the normalized time t_0 and the dispersion distance z_0 , used for normalization of real

units $T = t/t_0$ and $Z = z/z_0$, is given by the average dispersion of $\langle k'' \rangle = -0.128 \text{ ps}^2/\text{km}$ ($\langle D \rangle = 0.1 \text{ ps/nm/km}$) and pulse width of $t_s = 17.63 \text{ ps}$, thus $t_0 = t_s/1.763 = 10 \text{ ps}$ and $z_0 = -t_0^2/\langle k'' \rangle = 781.25 \text{ km}$. We consider a two-step GVD profile given by (2.23), having the dispersion management strength $S = 5.0$. The average power of the solitons in each channel becomes 4.7 mW. In normalized (real) unit, the amplifier spacing, set equal to the dispersion management period, $Z_a = 0.1$ (78 km), and the loss $\Gamma = 30$ (0.3 dB/km). Solitons have channel spacing of $\Delta\Omega = 7.5$ (120 GHz), where each channel propagates at 10 Gbit/s with a random sequence. Filters are located at every Z_a , having Fabry-Pérot structure with their bandwidth six times larger than the signal bandwidth (25 GHz), accompanied by the excess gain of 0.05 dB.

Figure 5.6 shows the evolution of the noise power within the bandwidth of $-\Delta\Omega/2 < \Omega < \Delta\Omega/2$, for the several number of wavelength channels copropagating with the signal. Without the cross phase modulation, the noise power grows to [95]

$$\int_{-\infty}^{\infty} \frac{N_0}{2\pi} \exp[2(\delta - \beta\Omega^2)Z] d\Omega = \frac{N_0}{2\pi} \sqrt{\frac{\pi}{2\beta Z}} \exp(2\delta Z) \quad (5.14)$$

after propagating over the distance of Z , where N_0 is the power spectrum density of the noise generated at $Z = 0$, and $\beta = 1/\omega_0^2$. The linear growth is successfully suppressed as can be seen in this figure if the number of channels is more than six. The noise spectral densities at $Z = 0$ and $Z = 50Z_a$ obtained in the simulation are shown in Fig. 5.7 with and without the cross phase modulation (XPM). The spectral density with XPM is the results with 12 WDM channels. We can see a substantial reduction of the noise accumulation in the presence of the cross phase modulation. The stationary spectrum obtained has a Gaussian type structure indicating the validity of the conjecture of the diffusion process described by the model equation (5.11). The small peaks at both sides of the spectrum is a consequence of the Fabry-Pérot filter having periodic passbands.

The spectral diffusion constant D is considered to be proportional to the number of WDM channels, while the depth of the filter ω_0^{-2} as well as the excess gain δ needed to control the timing jitter should also be increased as the number of channels. As a result, the stationary spectrum obtained in Fig. 5.7 for a special set of parameters in our numerical simulation is expected to be more or less independent of the number of channels in practical systems.

The remarkable result obtained here presents a substantial advantage for WDM soliton transmission systems since successful massive WDM soliton transmissions have already been experimentally demonstrated without filter control [84, 109].

5.5 Conclusion

We have studied several control schemes to stabilize the DM soliton transmission, which takes advantage of the peculiar features of the DM soliton as a nonlinear stationary pulse.

Nonlinear gain element has been shown to stabilize the amplitude, frequency and chirp of the DM soliton, while suppressing the growth of noise and radiative background even in the transmission line

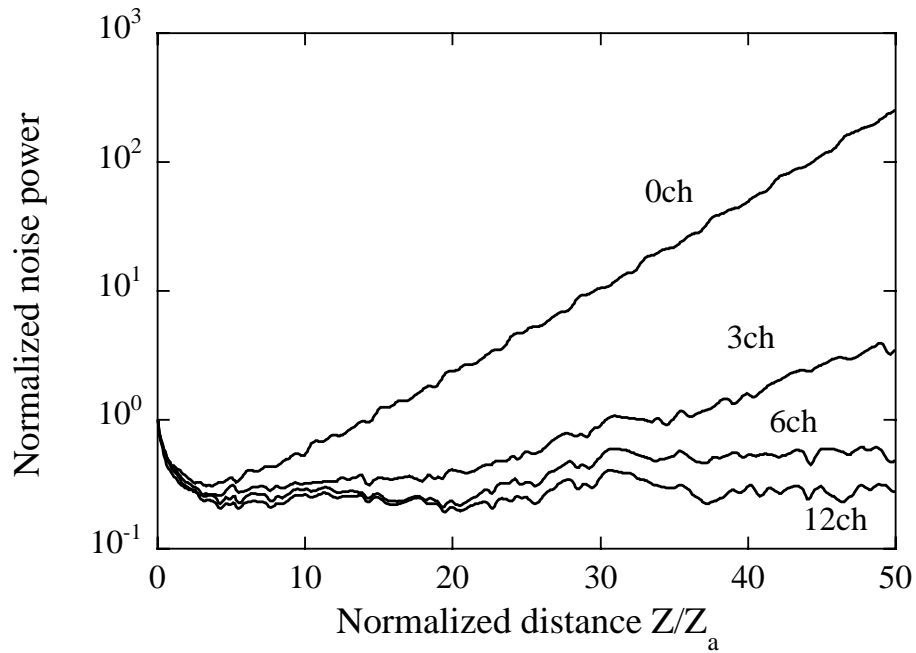


Figure 5.6: The normalized noise power as a function of distance for the several number of wavelength channels copropagating with the signal.

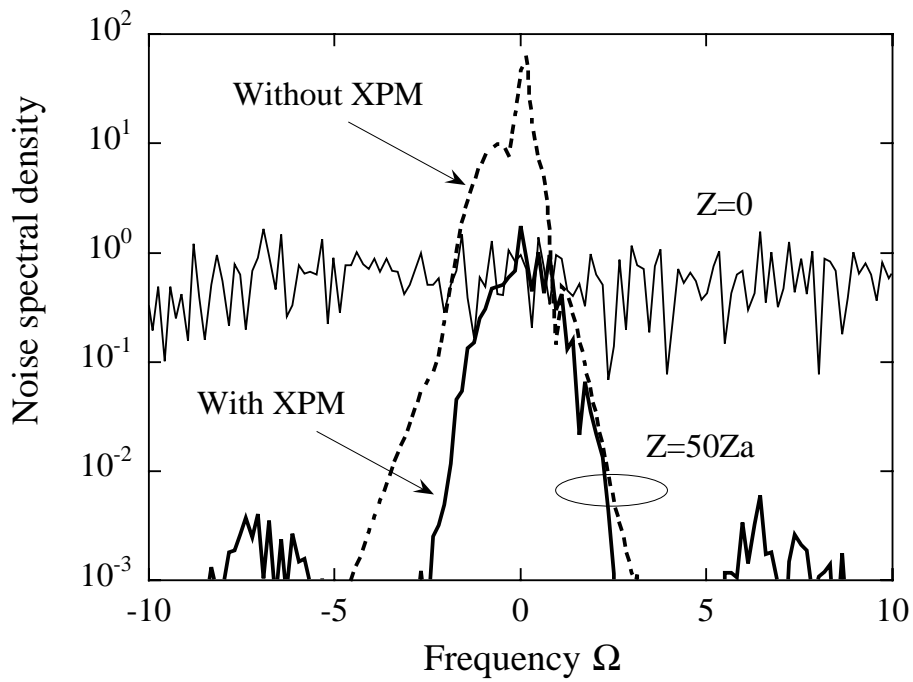


Figure 5.7: The noise spectral densities at $Z = 0$ and $Z = 50Z_a$.

with nearly-zero average dispersion. It is advantageous to improve high-speed single-channel transmissions by evading ASE noise accumulation and PMD induced pulse distortion. On the other hand, in massive WDM systems, a large number of collisions between DM solitons result in the diffusion of noise spectrum and thus avoid the instability, demonstrating the potential advantage of dense WDM transmission with DM solitons. Further stabilization is achieved by the quasi-soliton transmission with properly programmed dispersion profile supported by the optical phase conjugation, which avoids the interaction between neighboring pulses and adjacent wavelength channels. Combined with these control schemes, DM solitons may enable us to construct long-haul high-speed systems as well as terabit wide-area networks.

Chapter 6

Conclusions and discussions

6.1 Conclusions

This thesis has presented theoretical investigation of the feasibility of ultra high-speed optical soliton transmission in dispersion managed fibers. The main results obtained in this thesis can be summarized as follows:

1. In WDM DM soliton transmissions, the nonlinear interaction responsible for the frequency shift and the chirp alteration is significantly suppressed especially for strongly dispersion managed systems (Chap. 3).
2. In single-channel DM soliton transmissions, the interactions are minimized by a proper design of GVD profile with possible minimum average GVD in dispersion-flattened and densely dispersion managed fibers, even in the presence of polarization mode dispersion and of large variation in group-velocity dispersion (Chap. 4).
3. A proper combination of nonlinear gain and filtering can improve DM soliton stability considerably in single-channel transmission, allowing for a large tolerance with respect to fluctuations in the initial pulse parameters and by suppressing the growth of background radiation (Sec. 5.2).
4. The quasi-soliton supported by properly programmed GVD profile combined with periodic optical phase conjugation is demonstrated to provide ultra-fast single-channel transmission with the aid of strong pulse confinement that reduces the nonlinear interactions (Sec. 5.3).
5. The instability in soliton transmission with the conventional transmission control scheme by means of the guiding filter with excess gain can be suppressed due to the spectral diffusion of background radiation with a help of the cross phase modulation by solitons in other WDM channels (Sec. 5.4).

6.2 Discussions

Based on the obtained results, we can conclude that the DM solitons can overcome fundamental challenges that the current fiber-optic communication systems are facing. We clarify their contributions

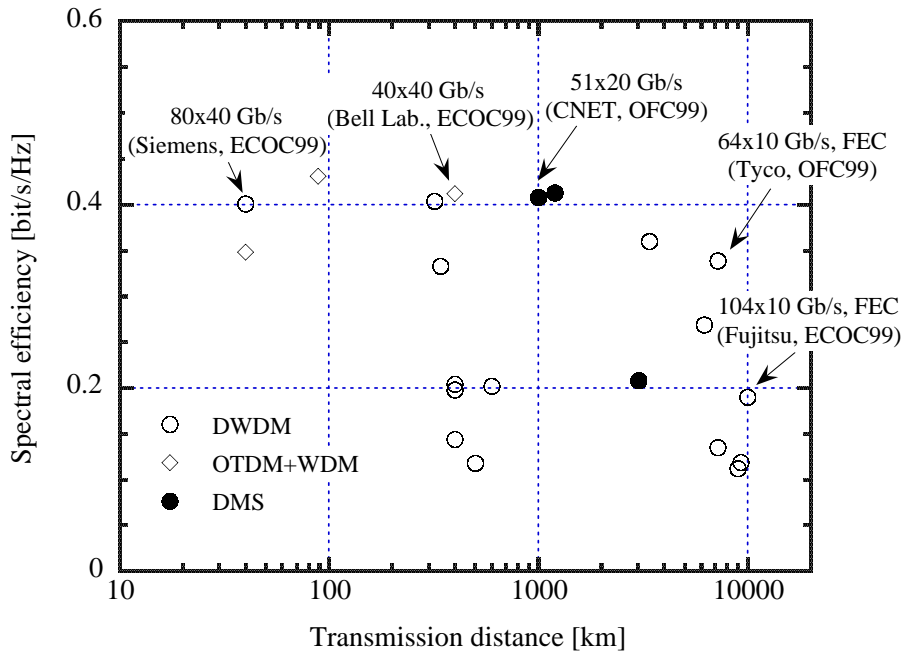


Figure 6.1: Spectral efficiency versus transmission distance in recent experimental results shown in Fig. 1.1. Total capacities are denoted as the number of wavelength channels times the bit-rate per single channel.

OFC: Optical Fiber Communication Conference,

ECOC: European Conference on Optical Communication,

DWDM: Dense Wavelength Division Multiplexing, OTDM: Optical Time Division Multiplexing,

DMS: Dispersion Managed Soliton, FEC: Forward Error Correction.

especially from a point of view of the improvement of spectral efficiency and the construction of OTDM networks.

Technical breakthroughs that have been achieved over the past few years in point-to-point fiber links have been realized by massive WDM transmission, supported by the development of low noise, flat gain erbium-doped fiber amplifiers (EDFAs). By a careful treatment of fiber nonlinearities by means of dispersion managements, Tbit/s transmission experiments over transoceanic distance have already been demonstrated (although with the aid of the forward error corrections). These transmission experiments are typically operated by multiplexing 10 Gbit/s signals over ~ 100 wavelength channels. Nevertheless, the state of the art fiber-optic communication systems have just begun to utilize a small fraction of the 25 THz bandwidth potentially available in optical fibers. Figure 6.1 shows again the recent experimental results appeared in Fig. 1.1 (except for the OTDM transmissions) but from a point of view of spectral efficiency. We note there still remains a large room to improve spectral efficiency up to 1.0 bit/s/Hz.

The scenario for the high spectral efficiency largely depends on the length scale that the transmission link covers, namely whether the system is short-hauled or long-hauled.

On a terrestrial scale, the next generation fiber-optic systems, first of all, have to expand the transmittable bandwidth for further increase of the number of wavelength channels, by developing light source, optical amplifiers, and low-loss fibers that are available over the whole bandwidth. Recent trends are focused on exploiting the bandwidth in the vicinity of $1.58 \mu\text{m}$ referred to as ‘L-band,’ in addition to the conventional bandwidth called ‘C-band’ centered in the vicinity of $1.55 \mu\text{m}$.

Spectral efficiency can be improved either by decreasing the channel spacing or by increasing the bit rate per channel. The channel spacing can be reduced by introducing novel modulation format such as optical duobinary modulation, which allows signal bandwidth compression. Indeed, the spectral efficiency of $\sim 0.6 \text{ bit/s/Hz}$ has been achieved by the duobinary modulation [110]. The narrow spectrum also provides large tolerance to GVD. The reduction of channel spacing is, however, restricted by the resolution of optical filters at the stage of demultiplexing and by the crosstalk between the adjacent channels. These restrictions become considerable when we increase the transmission distance, since the spectrum may be distorted as a result of the cascaded filtering as in the case of the network applications. Nonlinear effects, responsible for inter-channel crosstalk, also limit the channel spacing as they accumulate over distance. It should be noted that the duobinary modulation is sensitive to nonlinear effects even in single-channel transmission.

The increase of capacity within one wavelength channel can also improve the spectral efficiency. The large spectral efficiency up to 0.4 bit/s/Hz seen in Fig. 6.1 is a consequence of multiplexing signals each having the capacity more than 20 Gbit/s . As the bit rate per channel increases, however, optical signal processing techniques beyond the limits in electronically available speed are required. Careful management may also be necessary to avoid signal distortion due to GVD and nonlinear effects. In any case, for relatively short scale, the total capacity is expected to be increased mostly by exploiting the transmittable bandwidth.

For long-haul transmission systems, on the other hand, individual channel suffers from optical signal distortion owing to the physical properties of optical fibers as we discussed in Chapter 1. This becomes a dominant limiting factor when we increase the transmission distance. As shown in Fig. 6.1, for transoceanic distance, spectral efficiency is significantly impaired without the aid of FEC.

Long-haul WDM transmission systems, in the first place, have to achieve the equalization of physical parameters throughout the bandwidth. The most important issues are the gain flattening of optical amplifiers and the equalization of GVD and dispersion slope. A number of attempts have been made to provide the equalization, such as the hybrid amplification over C- and L-band, the development of the reverse dispersion fiber (RDF) that compensates for both GVD and dispersion slope of SMF, or the combination with Raman amplifications to reduce ASE noise. Nonlinear effects, however, are still major limiting factors, since the optical power has to be kept large enough to maintain the optical signal-to-noise ratio. These systems have to sacrifice spectral efficiency to cope with spectral broadening induced by the self phase modulation, and nonlinear interactions between adjacent channels by separating them sufficiently.

Recognizing the fundamental challenges in fiber-optic systems today, we examine the roles that the

DM solitons can play to overcome the difficulties. The potential advantage of DM solitons for short-haul and long-haul systems can be summarized as follows. For long-haul systems, they are more tolerant to nonlinear effects in fibers, namely they do not suffer from the spectral broadening due to the self phase modulation. Moreover, we can take advantage of the self phase modulation to stabilize the DM soliton transmission (Chap. 5). Another advantage of DM solitons, which is not observed in conventional linear transmission, is their intrinsic periodicity discussed in Chapter 2. This is particularly beneficial for both submarine and terrestrial systems, allowing flexibility in system configurations. In the linear systems employing post transmission compensation of the cumulative GVD, signals are not recognized at each amplification period. Furthermore, for terrestrial systems, DM solitons have been demonstrated to provide considerably large spectral efficiency as shown in Fig. 6.1. The two closed circles lying in the vicinity of 0.4 bit/s/Hz over 1,000 km represent the experimental results by CNET presented at the postdeadline sessions of ECOC 98 [111] and OFC 99 [84] respectively. In addition to the high spectral efficiency, the system having the amplifier spacing of ~ 100 km and the gain of EDFA > 20 dB demonstrates large signal-to-noise ratio. This is a consequence of a unique property of DM solitons that GVD and nonlinear effects are positively exploited. This outstanding result indicates the potential benefit of DM solitons in short-haul transmission systems including unrepeated systems.

DM solitons, however, still face fundamental difficulties but in a somewhat different manner from conventional systems. The major limiting factor in DM soliton systems is nonlinear interactions among different WDM channels as well as neighboring pulses in the same channel, as we discussed in Chapters 3 and 4, once the Gordon-Haus effect is overcome by means of the dispersion management. For short-haul transmission, the interaction among the neighboring pulses within one channel impairs the bit rate per channel and thus the spectral efficiency (Chap. 4). In addition, for long-haul transmission, the interaction between the adjacent channels becomes significant (Chap. 3) as the transmission distance increases. A somewhat contradictory observation is that the relatively weak dispersion management is considered to be effective to reduce the interaction within one channel, whereas the relatively strong dispersion management is beneficial to suppress the interaction between the channels.

One scenario to improve the spectral efficiency while minimizing the nonlinear interaction is to adopt the weak dispersion management in terrestrial systems and the strong dispersion management in long-haul systems. Since the increase of bit rate per channel is a crucial issue in terrestrial systems, and taking into account the observation that the DM soliton allows the fluctuation in physical parameters of fibers to some extent, the optimization of transmission line following the $S \sim 1.6$, such as the configuration we introduced in Chapter 4, is expected to meet the requirement. An ultimately superb performance may be realized by making use of the quasi-soliton supported by OPC (Sec. 5.3).

On the other hand, in long-haul systems, the nonlinear inter-channel crosstalk and the channel equalization are the critical issues. In order to provide the channel equalization over the total bandwidth with respect to the physical parameters of fibers, total compensation of GVD and slope by the use of SMF and DCF or RDF may be preferable. This configuration is given by strong dispersion management, which leads to reduced cross phase modulation between adjacent channels (Chap. 3) while inducing

strong interaction within the individual channels at the same time (Chap. 4). In this case, transmission control schemes (Chap. 5) may contribute as a key technology to overcome the limitation, some of which have been shown to be compatible with dense WDM transmission (Sec. 5.4).

Finally we provide some additional remarks on OTDM transmission with DM solitons in high-speed optical data networks operating at a rate > 100 Gbit/s. Research trends in optical data networks are, at present, focused largely on WDM networks, because of their relatively simple configuration and the commercial availability of WDM components required for wavelength routing. Therefore they can meet increasing bandwidth requirements immediately. One of the important features of WDM based networks is their transparency; they can provide independency for each wavelength channels with respect to signal format and bit synchronization and thus demonstrate flexibility in accommodating information packets from individual access nodes. In this sense, WDM networks are intrinsically an ‘analog’ system.

On the other hand, OTDM based networks [112–115] are naturally compatible with the synchronous digital hierarchy that facilitates network management and control, and with sophisticated signal processing at the stage of routing the traffic or 3R regeneration in the optical domain. In this respect, they are intrinsically a ‘digital’ system. Furthermore, OTDM networks provide large scalability in terms of distance and the number of nodes, and considerable flexibility in terms of bandwidth requirements that can vary from ~ 1 Gbit/s to burst traffic at very high data rate such as ~ 100 Gbit/s. OTDM network configuration that takes advantage of this observation is sometimes referred to as slotted TDM or statistically multiplexed TDM [114], which are distinguished from bit-interleaved TDM. In spite of their outstanding property, OTDM networks are still not feasible, mainly because they require advanced photonic technologies operating at ultra fast rates, that include short pulse generation, high-speed transmission, multiplexing and demultiplexing, data processing that is employed to address recognition, clock recovery, buffering, rate conversion, and all-optical switching.

DM solitons are expected to play a vital role in such OTDM networks not only in high-speed transmission but also in other technologies. They are obviously beneficial in terms of high-speed transmission. They allow single-channel transmission > 100 Gbit/s (Chap. 4) and exhibit intrinsic periodicity (Chap 2), which provide huge scalability in network configuration. Recently, 100 Gbit/s soliton transmission in a densely dispersion managed line over 1,000 km has been experimentally demonstrated utilizing a continuously fabricated fiber with built-in GVD and slope compensation [116]. For an ultra high-speed OTDM transmission at 160 Gbit/s or even at 640 Gbit/s, in a more practical situation, optical fibers themselves are required to suppress GVD fluctuation and provide dispersion flattening and lower PMD.

We would like to emphasize that solitons in general may contribute also to various components in OTDM networks which are fabricated based on optical fibers. In particular, DM soliton has been applied to stabilize pulse generation from the fiber ring laser referred to as the stretched pulse laser, whose ring resonator consists of an erbium-doped fiber having normal GVD and a standard fiber with anomalous GVD [102]. Stretched pulse laser eliminates some of the limitations observed in conventional soliton

fiber lasers such as the reduction of nonlinear effects responsible for sideband generation, resulting in improved performance in terms of energy enhancement and pulse compression. Pulse dynamics in ring cavity of stretched pulse lasers with passive mode-locking can be described in the context of DM soliton transmission with the aid of filters and nonlinear gain elements (Sec. 5.2). We also note that the unique property of (classical) solitons to preserve their shape and phase throughout the propagation in fibers is quite attractive to their application to buffering of optical data packets [117] and logic gates by means of interferometric optical switching [118, 119]. These techniques, taking advantage of Kerr effect, namely a nonlinear electric polarization of the silica, can in principle achieve femto-second response.

The maturity of OTDM networks crucially depends on several technological innovations in the future. For extensive development of next generation Internet, solitons will undoubtedly make a remarkable contribution.

Appendix

Nonlinear Schrödinger equation

We derive the nonlinear Schrödinger equation that describes the behavior of solitons in optical fibers, starting from first principles, i.e. Maxwell's equation in isotropic, dispersive, and nonlinear dielectric material. To avoid complexity in computations, we restrict the derivation to the propagation of wave packets in a planer waveguide, where the electric field is taken to be a scalar property. Despite the restriction, the essential idea is the same. The extension of the scalar analysis to the vector case in optical fibers is briefly summarized in Section A.5. (See [120] for detail.)

A.1 Maxwell equation

We begin with Maxwell's equation

$$\nabla \times \mathbf{E} = -\frac{\partial \mathbf{B}}{\partial t}, \quad (\text{A.1})$$

$$\nabla \times \mathbf{B} = \mu_0 \frac{\partial \mathbf{D}}{\partial t}, \quad (\text{A.2})$$

$$\nabla \cdot \mathbf{D} = 0, \quad (\text{A.3})$$

$$\nabla \cdot \mathbf{B} = 0, \quad (\text{A.4})$$

where \mathbf{E} , \mathbf{D} , \mathbf{B} represent electric field, electric flux density, and magnetic flux density, respectively. Since the magnetic properties of silica can be ignored, the permeability is given by μ_0 , namely the one for free space. Eliminating \mathbf{B} in (A.1)–(A.4), we obtain

$$\nabla \times (\nabla \times \mathbf{E}) = -\frac{\partial}{\partial t}(\nabla \times \mathbf{B}) = -\mu_0 \frac{\partial^2 \mathbf{D}}{\partial t^2}. \quad (\text{A.5})$$

In dielectric material, \mathbf{D} is expressed as the sum of the contribution of the electric field in free space $\epsilon_0 \mathbf{E}$ and the effect of the electric polarization of the material \mathbf{P} :

$$\mathbf{D} = \epsilon_0 \mathbf{E} + \mathbf{P}, \quad (\text{A.6})$$

where ϵ_0 is the permittivity of free space. Silica exhibits linear and nonlinear response with retardation. The electric polarization \mathbf{P} has thus two contributions:

$$\mathbf{P} = \mathbf{P}_L + \mathbf{P}_{NL}$$

$$\begin{aligned}
&= \int_{-\infty}^t \epsilon_0 \boldsymbol{\chi}^{(1)}(\mathbf{r}, t - \tau) \cdot \mathbf{E}(\mathbf{r}, \tau) d\tau \\
&\quad + \int_{-\infty}^t \int_{-\infty}^t \int_{-\infty}^t \epsilon_0 \boldsymbol{\chi}^{(3)}(\mathbf{r}, t - \tau_1, t - \tau_2, t - \tau_3) : \mathbf{E}(\mathbf{r}, \tau_1) \mathbf{E}(\mathbf{r}, \tau_2) \mathbf{E}(\mathbf{r}, \tau_3) d\tau_1 d\tau_2 d\tau_3, \quad (\text{A.7})
\end{aligned}$$

where $\boldsymbol{\chi}^{(1)}$ and $\boldsymbol{\chi}^{(3)}$ represent the linear and third order nonlinear susceptibility tensors, respectively, having the dependence of the spatial coordinates \mathbf{r} of the material, and

$$\begin{aligned}
\left(\boldsymbol{\chi}^{(1)} \cdot \mathbf{E} \right)_i &= \sum_j \chi_{ij}^{(1)} E_j \\
\left(\boldsymbol{\chi}^{(3)} : \mathbf{E} \mathbf{E} \mathbf{E} \right)_i &= \sum_{j,k,l} \chi_{ijkl}^{(3)} E_j E_k E_l \quad (i = x, y, z). \quad (\text{A.8})
\end{aligned}$$

Because of the centrosymmetric crystal structure of silica, optical fibers do not exhibit the second order nonlinear effect. Using the following formula of the vector analysis

$$\nabla \times \nabla \times \mathbf{E} = \nabla(\nabla \cdot \mathbf{E}) - \nabla^2 \mathbf{E} \quad (\text{A.9})$$

on the left hand side of (A.5), and assuming a weakly guided mode (i.e. $\nabla \cdot \mathbf{E} = 0$), we have

$$\begin{aligned}
\nabla^2 \mathbf{E} - \frac{1}{c^2} \frac{\partial^2 \mathbf{E}}{\partial t^2} &= \frac{1}{c^2 \epsilon_0} \frac{\partial^2 \mathbf{P}}{\partial t^2} \\
&= \frac{1}{c^2} \frac{\partial^2}{\partial t^2} \int_{-\infty}^t \boldsymbol{\chi}^{(1)}(\mathbf{r}, t - \tau) \cdot \mathbf{E}(\mathbf{r}, \tau) d\tau \\
&\quad + \frac{1}{c^2} \frac{\partial^2}{\partial t^2} \int_{-\infty}^t \int_{-\infty}^t \int_{-\infty}^t \boldsymbol{\chi}^{(3)}(\mathbf{r}, t - \tau_1, t - \tau_2, t - \tau_3) : \mathbf{E}(\mathbf{r}, \tau_1) \mathbf{E}(\mathbf{r}, \tau_2) \mathbf{E}(\mathbf{r}, \tau_3) d\tau_1 d\tau_2 d\tau_3. \quad (\text{A.10})
\end{aligned}$$

A.2 Quasi monochromatic approximation

We introduce two assumptions to derive the nonlinear Schrödinger equation by means of a proper approximation of (A.10). First, we assume the electric field to be a scalar quantity, since the planer waveguide allows a single transverse polarization, unlike the case of the guided modes in optical fibers. Second, we apply the quasi monochromatic approximation, namely we assume that the waveform having slowly varying envelope, or in frequency domain having narrow spectrum with respect to its carrier frequency. The latter approximation leads to slow variation of the lightwave envelope with respect to time and distance. The nonlinear Schrödinger equation is derived as the equation that describes long range evolution of the slowly varying envelope.

Before introducing the quasi monochromatic approximation, we first write down the electric field vector \mathbf{E} as a plane wave in the form

$$\begin{aligned}
\mathbf{E}(x, z, t) &= \hat{\mathbf{y}} E(x, z, t) \\
&= \hat{\mathbf{y}} [AU(x, \omega_0) \exp(ik_0 z - i\omega_0 t) + \text{c.c.}], \quad (\text{A.11})
\end{aligned}$$

where c.c. denotes the complex conjugate, $\hat{\mathbf{y}}$ is the unit vector along y axis, ω_0 and $k_0 \equiv k(\omega_0)$ represent the angular frequency and the wave number of the carrier respectively, and A and U are the wave envelope and the mode distribution over a cross section in the waveguide geometry. We assumed the

waveguide having guiding structure in x and y coordinates, namely optical wave propagates along z axis, and having uniform structure in y direction (i.e. $\partial/\partial y = 0$) so that \mathbf{E} is polarized along y axis. Taking the Fourier transform of (A.11), we obtain the electric field in frequency domain:

$$\begin{aligned}\hat{E}(x, z, \omega) &= \int_{-\infty}^{\infty} E(x, z, t) \exp(i\omega t) dt \\ &= 2\pi\delta(\omega - \omega_0)AU(x, \omega_0) \exp(ik_0z) + \text{c.c.}\end{aligned}\quad (\text{A.12})$$

Note that A is constant with respect to t and z at present, as long as the wave is monochromatic, i.e. the spectrum is given by the delta function standing at the frequency $\omega = \pm\omega_0$. However, as a result of the quasi monochromatic approximation, the envelope A acquires sufficiently slow variation in time domain, whereas in frequency domain it exhibits sufficiently small spectral broadening over the bandwidth $\Delta\omega$ in the vicinity of $\pm\omega_0$. We introduce a small parameter $\varepsilon \sim \Delta\omega/\omega_0$ as a factor characterizing the small scale of the spectral broadening. Long range evolution of A is described in a slow scale coordinate $Z = \varepsilon z$. As a consequence of the long term amplitude modulation, $\hat{E}(x, z, \omega)$ now has the form

$$\hat{E}(x, z, \omega) = \hat{A}(Z, \omega - \omega_0)U(x, \omega_0) \exp(ik_0z) + \text{c.c.}\quad (\text{A.13})$$

By taking the inverse Fourier transform, we have

$$\begin{aligned}E(x, z, t) &= \frac{1}{2\pi} \int_{-\infty}^{\infty} \hat{E}(x, z, \omega) \exp(-i\omega t) d\omega \\ &= \frac{1}{2\pi} \int_{-\infty}^{\infty} \hat{A}(Z, \omega - \omega_0)U(x, \omega_0) \exp(ik_0z - i\omega t) d\omega + \text{c.c.} \\ &= \left(\frac{1}{2\pi} \int_{-\infty}^{\infty} \hat{A}(Z, \omega - \omega_0) \exp[-i(\omega - \omega_0)t] d(\omega - \omega_0) \right) U(x, \omega_0) \exp(ik_0z - i\omega_0 t) \\ &\quad + \text{c.c.} \\ &= \left(\frac{\varepsilon}{2\pi} \int_{-\infty}^{\infty} \hat{A}(Z, \varepsilon\Omega) \exp(-i\Omega T) d\Omega \right) U(x, \omega_0) \exp(ik_0z - i\omega_0 t) + \text{c.c.} \\ &= \varepsilon A(Z, T; \varepsilon)U(x, \omega_0) \exp(ik_0z - i\omega_0 t) + \text{c.c.},\end{aligned}\quad (\text{A.14})$$

where we introduced another independent variable $T = \varepsilon t$ similar to Z to describe long term behavior of A , and

$$A(Z, T; \varepsilon) = \frac{1}{2\pi} \int_{-\infty}^{\infty} \hat{A}(Z, \Omega; \varepsilon) \exp(-i\Omega T) d\Omega, \quad \varepsilon\Omega \equiv \omega - \omega_0.\quad (\text{A.15})$$

A.3 Linear and nonlinear polarization

We impose the quasi monochromatic approximation to the linear and nonlinear polarizations in the scalar Maxwell equation

$$\begin{aligned}\frac{\partial^2 E}{\partial x^2} + \frac{\partial^2 E}{\partial z^2} - \frac{1}{c^2} \frac{\partial^2 E}{\partial t^2} - \frac{1}{c^2} \frac{\partial^2}{\partial t^2} \int_{-\infty}^t \chi^{(1)}(x, t - \tau) E(x, z, \tau) d\tau \\ - \frac{1}{c^2} \frac{\partial^2}{\partial t^2} \iiint \chi^{(3)}(x, t - \tau_1, t - \tau_2, t - \tau_3) E(x, z, \tau_1) E(x, z, \tau_2) E(x, z, \tau_3) d\tau_1 d\tau_2 d\tau_3 = 0,\end{aligned}\quad (\text{A.16})$$

where $\chi^{(1)} = \chi_{yy}^{(1)}$ and $\chi^{(3)} = \chi_{yyyy}^{(3)}$ are scalar functions of x and t and assumed to be independent of z . Since we are interested in the behavior of lightwave electric field in the vicinity of the stationary state ($\varepsilon = 0$), it is natural to introduce an asymptotic expansion of $E(x, z, t)$ with respect to ε :

$$E(x, z, t) = E_0 + \varepsilon E_1 + \varepsilon^2 E_2 + \dots \quad (\text{A.17})$$

Note that, in the frame of the quasi monochromatic approximation, $E_i \sim O(\varepsilon)$ as shown in (A.14).

We apply the quasi monochromatic approximation to the linear and the nonlinear polarization for each $O(\varepsilon^n)$. First we consider $O(\varepsilon)$ contribution in the linear polarization term. Taking the Fourier transform of the $O(\varepsilon)$ component in P_L , we obtain

$$\begin{aligned} \text{F.T.} & \left(\frac{\partial^2}{\partial t^2} \int \chi^{(1)}(x, t - \tau) E_0(x, z, \tau) d\tau \right) \\ &= -\omega^2 \hat{\chi}^{(1)}(x, \omega) \hat{E}_0(x, z, \omega) \\ &= -\omega^2 \hat{\chi}^{(1)}(x, \omega) \hat{A}(Z, \omega - \omega_0) U(x, \omega_0) \exp(ik_0 z) + \text{c.c.}, \end{aligned} \quad (\text{A.18})$$

Following (A.14), the inverse transform (i.e. multiply $(1/2\pi) \exp(-i\omega t)$ and integrate over ω) results in

$$\begin{aligned} & \frac{\partial^2}{\partial t^2} \int \chi^{(1)}(x, t - \tau) E_0(x, z, \tau) d\tau \\ &= -\frac{1}{2\pi} \int \omega^2 \hat{\chi}^{(1)}(x, \omega) \hat{A}(Z, \omega - \omega_0) U(x, \omega_0) \exp(ik_0 z - i\omega t) d\omega + \text{c.c.} \\ &= -\left(\frac{1}{2\pi} \int [\omega_0 + (\omega - \omega_0)]^2 \hat{\chi}^{(1)}(x, \omega_0 + (\omega - \omega_0)) \hat{A}(Z, \omega - \omega_0) \exp[-i(\omega - \omega_0)t] d(\omega - \omega_0) \right) \\ & \quad \times U(x, \omega_0) \exp(ik_0 z - i\omega_0 t) + \text{c.c.} \\ &= -\left(\frac{\varepsilon}{2\pi} \int (\omega_0 + \varepsilon\Omega)^2 \hat{\chi}^{(1)}(x, \omega_0 + \varepsilon\Omega) \hat{A}(Z, \varepsilon\Omega) \exp(-i\Omega T) d\Omega \right) U(x, \omega_0) \exp(ik_0 z - i\omega_0 t) \\ & \quad + \text{c.c.} \\ &= -\varepsilon \left(\omega_0 + i\varepsilon \frac{\partial}{\partial T} \right)^2 \hat{\chi}^{(1)} \left(x, \omega_0 + i\varepsilon \frac{\partial}{\partial T} \right) A(Z, T; \varepsilon) U(x, \omega_0) \exp(ik_0 z - i\omega_0 t) + \text{c.c.}, \end{aligned} \quad (\text{A.19})$$

where we referred to the following relation

$$\left(i\varepsilon \frac{\partial}{\partial T} \right)^n A(Z, T; \varepsilon) = \frac{\varepsilon}{2\pi} \int \varepsilon^n \Omega^n \hat{A}(Z, \Omega; \varepsilon) \exp(-i\Omega T) d\Omega. \quad (\text{A.20})$$

It can be easily verified that the higher order terms of P_L have a form similar to (A.19).

Kerr nonlinearity has a lowest order contribution at $O(\varepsilon^3)$. The quasi monochromatic approximation to the nonlinear electric polarization P_{NL} requires somewhat complicated calculations, but in principle, we just follow the calculation for the linear polarization. We first take the Fourier transform the nonlinear term:

$$\begin{aligned} \text{F.T.} & \left(\frac{\partial^2}{\partial t^2} \iiint \chi^{(3)}(x, t - \tau_1, t - \tau_2, t - \tau_3) E_0(x, z, \tau_1) E_0(x, z, \tau_2) E_0(x, z, \tau_3) d\tau_1 d\tau_2 d\tau_3 \right) \\ &= \text{F.T.} \left(-\frac{1}{(2\pi)^3} \iiint d\omega_1 d\omega_2 d\omega_3 (\omega_1 + \omega_2 + \omega_3)^2 \hat{\chi}^{(3)}(x, \omega_1, \omega_2, \omega_3) \right. \\ & \quad \left. \times \hat{E}_0(x, z, \omega_1) \exp(-i\omega_1 t) \hat{E}_0(x, z, \omega_2) \exp(-i\omega_2 t) \hat{E}_0(x, z, \omega_3) \exp(-i\omega_3 t) \right) \\ &= -\frac{1}{(2\pi)^3} \int dt \exp(i\omega t) \iiint d\omega_1 d\omega_2 d\omega_3 (\omega_1 + \omega_2 + \omega_3)^2 \hat{\chi}^{(3)}(x, \omega_1, \omega_2, \omega_3) \end{aligned}$$

$$\begin{aligned}
& \times \hat{E}_0(x, z, \omega_1) \hat{E}_0(x, z, \omega_2) \hat{E}_0(x, z, \omega_3) \exp(-i(\omega_1 + \omega_2 + \omega_3)t) \\
& = -\frac{1}{(2\pi)^3} \iiint d\omega_1 d\omega_2 d\omega_3 2\pi\delta(\omega - \omega_1 - \omega_2 - \omega_3) (\omega_1 + \omega_2 + \omega_3)^2 \hat{\chi}^{(3)}(x, \omega_1, \omega_2, \omega_3) \\
& \quad \times \hat{E}_0(x, z, \omega_1) \hat{E}_0(x, z, \omega_2) \hat{E}_0(x, z, \omega_3) \\
& = -\frac{1}{(2\pi)^2} \iiint d\omega_1 d\omega_2 d\omega_3 \delta(\omega - \omega_1 - \omega_2 - \omega_3) (\omega_1 + \omega_2 + \omega_3)^2 \hat{\chi}^{(3)}(x, \omega_1, \omega_2, \omega_3) \\
& \quad \times \left(\hat{A}(Z, \omega_1 - \omega_0) U(x, \omega_0) \exp(ik_0 z) + \text{c.c.} \right) \left(\hat{A}(Z, \omega_2 - \omega_0) U(x, \omega_0) \exp(ik_0 z) + \text{c.c.} \right) \\
& \quad \times \left(\hat{A}(Z, \omega_3 - \omega_0) U(x, \omega_0) \exp(ik_0 z) + \text{c.c.} \right), \tag{A.21}
\end{aligned}$$

where we used the formula

$$\int \exp[i(\omega - \omega_1 - \omega_2 - \omega_3)t] dt = 2\pi\delta(\omega - \omega_1 - \omega_2 - \omega_3) \tag{A.22}$$

in the integration over t in (A.21). We note that the nonlinear term (A.21) includes eight contributions in total: three components having the wave number of k_0 and $-k_0$ respectively (i.e. $\propto \exp(ik_0 z)$ and $\propto \exp(-ik_0 z)$), and one harmonic component having the wave number of $3k_0$ and $-3k_0$ respectively (i.e. $\propto \exp(3ik_0 z)$ and $\propto \exp(-3ik_0 z)$). We are interested in $\exp(\pm ik_0 z)$ terms; we consider specifically one of the $\exp(ik_0 z)$ components of the form

$$\begin{aligned}
& -\frac{1}{(2\pi)^2} \iiint d\omega_1 d\omega_2 d\omega_3 \delta(\omega - \omega_1 - \omega_2 - \omega_3) (\omega_1 + \omega_2 + \omega_3)^2 \hat{\chi}^{(3)}(x, \omega_1, \omega_2, \omega_3) \\
& \quad \times \hat{A}^*(Z, -\omega_1 - \omega_0) \hat{A}(Z, \omega_2 - \omega_0) \hat{A}(Z, \omega_3 - \omega_0) U^*(x, \omega_0) U(x, \omega_0) U(x, \omega_0) \exp(ik_0 z) \tag{A.23}
\end{aligned}$$

among the three contributions. Taylor expansion in the vicinity of $\omega_1 = -\omega_0$, $\omega_2 = \omega_0$, and $\omega_3 = \omega_0$ in (A.23) yields

$$\begin{aligned}
\text{(A.23)} & = -\frac{1}{(2\pi)^2} \iiint d\omega_1 d\omega_2 d\omega_3 \delta(\omega - \omega_1 - \omega_2 - \omega_3) \\
& \quad \times \left(\omega_0^2 + 2\omega_0(\omega_1 - (-\omega_0))^2 + 2\omega_0(\omega_2 - \omega_0)^2 + 2\omega_0(\omega_3 - \omega_0)^2 + \dots \right) \\
& \quad \times \left(\hat{\chi}^{(3)}(x, -\omega_0, \omega_0, \omega_0) + \frac{\partial \hat{\chi}^{(3)}}{\partial \omega_1}(x, -\omega_0, \omega_0, \omega_0)(\omega_1 - (-\omega_0)) \right. \\
& \quad \quad \left. + \frac{\partial \hat{\chi}^{(3)}}{\partial \omega_2}(x, -\omega_0, \omega_0, \omega_0)(\omega_2 - \omega_0) + \frac{\partial \hat{\chi}^{(3)}}{\partial \omega_3}(x, -\omega_0, \omega_0, \omega_0)(\omega_3 - \omega_0) + \dots \right) \\
& \quad \times \hat{A}^*(Z, -\omega_1 - \omega_0) \hat{A}(Z, \omega_2 - \omega_0) \hat{A}(Z, \omega_3 - \omega_0) U^3(x, \omega_0) \exp(ik_0 z), \tag{A.24}
\end{aligned}$$

where we assumed U to be real and even in ω ($U^*(x, \omega_0) = U(x, -\omega_0) = U(x, \omega_0)$). Taking the inverse Fourier transform of (A.24), and replacing $\delta(\omega - \omega_1 - \omega_2 - \omega_3)$ with the integration over t' in the same way as (A.22), we have

$$\begin{aligned}
& -\frac{1}{(2\pi)^4} \int d\omega \exp(-i\omega t) \iiint d\omega_1 d\omega_2 d\omega_3 \int dt' \exp[i(\omega - \omega_1 - \omega_2 - \omega_3)t'] \\
& \quad \times \hat{A}^*(Z, -\omega_1 - \omega_0) \hat{A}(Z, \omega_2 - \omega_0) \hat{A}(Z, \omega_3 - \omega_0) U^3(x, \omega_0) \exp(ik_0 z) \\
& \quad \times \left(\omega_0^2 \hat{\chi}^{(3)}(x, -\omega_0, \omega_0, \omega_0) + \omega_0^2 \frac{\partial \hat{\chi}^{(3)}}{\partial \omega_1}(x, -\omega_0, \omega_0, \omega_0)(\omega_1 + \omega_0) \right. \\
& \quad \quad \left. + \omega_0^2 \frac{\partial \hat{\chi}^{(3)}}{\partial \omega_2}(x, -\omega_0, \omega_0, \omega_0)(\omega_2 - \omega_0) + \omega_0^2 \frac{\partial \hat{\chi}^{(3)}}{\partial \omega_3}(x, -\omega_0, \omega_0, \omega_0)(\omega_3 - \omega_0) + \dots \right)
\end{aligned}$$

$$\begin{aligned}
&= -\frac{1}{(2\pi)^4} \int \int \int \int d\omega d\omega_1 d\omega_2 d\omega_3 dt' \exp[-i\omega(t-t')] \exp[-i(\omega_1 + \omega_2 + \omega_3)t'] \\
&\quad \times \left[\omega_0^2 \hat{\chi}^{(3)}(x, -\omega_0, \omega_0, \omega_0) + \dots \right] U^3(x, \omega_0) \hat{A}^*(Z, -\omega_1 - \omega_0) \hat{A}(Z, \omega_2 - \omega_0) \hat{A}(Z, \omega_3 - \omega_0) \\
&\quad \times \exp(ik_0 z). \tag{A.25}
\end{aligned}$$

We note that the integration over ω in (A.25) can be written as

$$\int_{-\infty}^{\infty} \exp[-i\omega(t-t')] d\omega = 2\pi \delta(t-t'), \tag{A.26}$$

and thus the integration over t' is equivalent to simply replacing t' with t . It is also convenient to write

$$\begin{aligned}
\exp[-i(\omega_1 + \omega_2 + \omega_3)t'] &= \exp(-i\omega_0 t') \exp(-i(\omega_1 + \omega_0)t') \exp(-i(\omega_2 - \omega_0)t') \exp(-i(\omega_3 - \omega_0)t') \\
&\equiv \exp(-i\omega_0 t') \exp(-i\Omega_1 T') \exp(-i\Omega_2 T') \exp(-i\Omega_3 T'), \\
\varepsilon\Omega_1 &\equiv \omega_1 + \omega_0, \quad \varepsilon\Omega_2 \equiv \omega_2 - \omega_0, \quad \varepsilon\Omega_3 \equiv \omega_3 - \omega_0. \tag{A.27}
\end{aligned}$$

Consequently (A.25) becomes to leading order

$$\begin{aligned}
(A.25) &= -\frac{\varepsilon^3}{(2\pi)^3} \int \int \int d\Omega_1 d\Omega_2 d\Omega_3 \\
&\quad \times \exp(-i\omega_0 t) \left(\exp(-i\Omega_1 T) \hat{A}^*(Z, -\varepsilon\Omega_1) \right) \left(\exp(-i\Omega_2 T) \hat{A}(Z, \varepsilon\Omega_2) \right) \\
&\quad \times \left(\exp(-i\Omega_3 T) \hat{A}(Z, \varepsilon\Omega_3) \right) \omega_0^2 \hat{\chi}^{(3)}(x, -\omega_0, \omega_0, \omega_0) U^3(x, \omega_0) \exp(ik_0 z) \\
&= -\frac{\varepsilon^3}{(2\pi)^3} \exp(ik_0 z - i\omega_0 t) \omega_0^2 \hat{\chi}^{(3)}(x, -\omega_0, \omega_0, \omega_0) U^3(x, \omega_0) \\
&\quad \times \int d\Omega_1 \hat{A}^*(Z, -\varepsilon\Omega_1) \exp(-i\Omega_1 T) \int d\Omega_2 \hat{A}(Z, \varepsilon\Omega_2) \exp(-i\Omega_2 T) \\
&\quad \times \int d\Omega_3 \hat{A}(Z, \varepsilon\Omega_3) \exp(-i\Omega_3 T) \\
&= -\varepsilon^3 \omega_0^2 \hat{\chi}^{(3)}(x, -\omega_0, \omega_0, \omega_0) A^2(Z, T; \varepsilon) A^*(Z, T; \varepsilon) U^3(x, \omega_0) \exp(ik_0 z - i\omega_0 t). \tag{A.28}
\end{aligned}$$

The extension of the calculation to other nonlinear terms in (A.21) proportional to $\exp(\pm ik_0 z)$ is straightforward. We finally obtain the nonlinear polarization of the form

$$\begin{aligned}
&-3\varepsilon^3 \omega_0^2 \hat{\chi}^{(3)}(x, -\omega_0, \omega_0, \omega_0) A^2(Z, T) A^*(Z, T) U^3(x, \omega_0) \exp(ik_0 z - i\omega_0 t) \\
&\quad -3\varepsilon^3 \omega_0^2 \hat{\chi}^{(3)}(x, -\omega_0, \omega_0, \omega_0) A^{*2}(Z, T) A(Z, T) U^3(x, \omega_0) \exp(-ik_0 z + i\omega_0 t) \tag{A.29}
\end{aligned}$$

as a result of the quasi monochromatic approximation.

A.4 Asymptotic expansion

With these preparation, we now return to the Maxwell's equation (A.16) and apply the multiple scale method to derive an approximate equation that describes the long range evolution of the slowly varying wave envelope. We asymptotically expand the electric field E as (A.17), and introduce multiple scales with respect to z :

$$Z_1 = \varepsilon z, \quad Z_2 = \varepsilon^2 z, \quad \dots, \quad Z_n = \varepsilon^n z. \tag{A.30}$$

Note that we do not observe the role of the nonlinear polarization until we proceed to $O(\varepsilon^3)$. At the lowest order $O(\varepsilon)$, we expect (A.16) simply gives the guiding mode of optical wave packets. At the second lowest order $O(\varepsilon^2)$, where the nonlinearity is still out of scope, (A.16) is expected to give rise to the long term behavior of the guided wave propagation along z with the group velocity of $1/k'_0$ where $k'_0 \equiv \partial k / \partial \omega|_{\omega=\omega_0}$.

It is convenient to introduce the linear operator L to represent the linear response of the electric field:

$$L \left(\frac{d}{dx}, ik, -i\omega \right) \equiv \frac{d^2}{dx^2} - k^2 + \frac{n^2(x, \omega)\omega^2}{c^2}, \quad (\text{A.31})$$

where $n(x, \omega)$ and c represent the refractive index of silica and the velocity of light for free space, respectively. As far as the linear response has no retardation, L is written as

$$L \left(\frac{d}{dx}, ik_0, -i\omega_0 \right) = \frac{d^2}{dx^2} - k_0^2 + \frac{n_0^2 \omega_0^2}{c^2}, \quad (\text{A.32})$$

where $n_0 \equiv n(x, \omega_0)$. With the operator L , the linear component of (A.16) has the form

$$\begin{aligned} & \left(\frac{\partial^2}{\partial x^2} + \frac{\partial^2}{\partial z^2} - \frac{1}{c^2} \frac{\partial^2}{\partial t^2} - \frac{1}{c^2} \frac{\partial^2}{\partial t^2} \int d\tau \chi^{(1)}(x, t - \tau) \right) (E_0 + \varepsilon E_1 + \dots) \\ &= L \left(\frac{d}{dx}, ik_0 + \varepsilon \frac{\partial}{\partial Z_1} + \varepsilon^2 \frac{\partial}{\partial Z_2} + \dots, -i\omega_0 + \varepsilon \frac{\partial}{\partial T} \right) \\ & \quad \times [\varepsilon A(Z_1, Z_2, \dots, T) U(x, \omega_0) \exp(ik_0 z - i\omega_0 t) + \text{c.c.}], \end{aligned} \quad (\text{A.33})$$

where we referred to (A.19). Note that the dispersion relation $k = k(\omega)$, obtained as the eigenvalue in solving the boundary value problem of the form $LV = 0$ (where $E = \varepsilon V \exp(ik_0 z - i\omega_0 t) + \text{c.c.}$, $V \equiv U(x, \omega_0) A(Z, T)$), is given by the relation

$$D([V], k, \omega) \equiv \langle V, LV \rangle = 0, \quad (\text{A.34})$$

where the brackets denote the inner product:

$$\langle A, B \rangle \equiv \int A^* B dx. \quad (\text{A.35})$$

Taking the integration by parts, we obtain

$$\begin{aligned} k^2 &= \frac{\frac{\omega^2}{c^2} \int n^2(x, \omega) |V|^2 dx - \int \left| \frac{\partial V}{\partial x} \right|^2 dx}{\int |V|^2 dx} \\ &= \frac{\frac{\omega^2}{c^2} \int n^2(x, \omega) U^2(x, \omega_0) dx - \int \left(\frac{dU}{dx}(x, \omega_0) \right)^2 dx}{\int U^2(x, \omega_0) dx}. \end{aligned} \quad (\text{A.36})$$

$O(\varepsilon)$: the transverse structure

Extracting $O(\varepsilon)$ contributions from (A.16), we have

$$\left(\frac{\partial^2}{\partial x^2} + \frac{\partial^2}{\partial z^2} - \frac{1}{c^2} \frac{\partial^2}{\partial t^2} - \frac{1}{c^2} \frac{\partial^2}{\partial t^2} \int d\tau \chi^{(1)}(x, t - \tau) \right) E_0 = 0. \quad (\text{A.37})$$

With (A.33), we obtain

$$L\left(\frac{d}{dx}, ik_0, -i\omega_0\right) AU(x, \omega_0) \exp(ik_0 z - i\omega_0 t) + \text{c.c.} = 0. \quad (\text{A.38})$$

We set E_0 as the following form

$$E_0 = \varepsilon U_0 \exp(ik_0 z - i\omega_0 t) + \text{c.c.} \quad (\text{A.39})$$

and find

$$L\left(\frac{d}{dx}, ik_0, -i\omega_0\right) U_0 = \frac{d^2 U_0}{dx^2} - k_0^2 U_0 + \frac{n_0^2 \omega_0^2}{c^2} U_0 = 0, \quad (\text{A.40})$$

which simply gives the transverse structure of E_0 .

$O(\varepsilon^2)$: linear propagation of wave packets

Before studying the $O(\varepsilon^2)$ contributions, we expand L in a Taylor series in advance:

$$\begin{aligned} L &= L\left(\frac{d}{dx}, ik_0 + \varepsilon \frac{\partial}{\partial Z_1} + \varepsilon^2 \frac{\partial}{\partial Z_2} + \dots, -i\omega_0 + \varepsilon \frac{\partial}{\partial T}\right) \\ &\equiv L(X, K, \Omega) \\ &= L_1 \\ &\quad + \left.\frac{\partial L}{\partial K}\right|_{K_0} (K - K_0) + \left.\frac{\partial L}{\partial \Omega}\right|_{\Omega_0} (\Omega - \Omega_0) \\ &\quad + \frac{1}{2} \left.\frac{\partial^2 L}{\partial K^2}\right|_{K_0} (K - K_0)^2 + \frac{1}{2} \left.\frac{\partial^2 L}{\partial \Omega^2}\right|_{\Omega_0} (\Omega - \Omega_0)^2 + \left.\frac{\partial^2 L}{\partial K \partial \Omega}\right|_{K_0, \Omega_0} (K - K_0)(\Omega - \Omega_0) \\ &\quad + \dots \\ &= L_1 \\ &\quad + L_2\left(\varepsilon \frac{\partial}{\partial Z_1}\right) + L_3\left(\varepsilon \frac{\partial}{\partial T}\right) \\ &\quad + L_2\left(\varepsilon^2 \frac{\partial}{\partial Z_2}\right) + \frac{1}{2} L_{22}\left(\varepsilon^2 \frac{\partial^2}{\partial Z_1^2}\right) + \frac{1}{2} L_{33}\left(\varepsilon^2 \frac{\partial^2}{\partial T^2}\right) + L_{23}\left(\varepsilon^2 \frac{\partial^2}{\partial Z_1 \partial T}\right) \\ &\quad + \dots, \end{aligned} \quad (\text{A.41})$$

where we define the following parameters for convenience

$$\begin{aligned} X &\equiv \frac{d}{dx} \\ K - K_0 &\equiv ik - ik_0 = \varepsilon \frac{\partial}{\partial Z_1} + \varepsilon^2 \frac{\partial}{\partial Z_2} + \dots, \\ \Omega - \Omega_0 &\equiv -i\omega - (-i\omega_0) = \varepsilon \frac{\partial}{\partial T}, \\ L_1 &\equiv L(X, K_0, \Omega_0), \quad L_2 \equiv \left.\frac{\partial L}{\partial K}\right|_{K_0}, \quad L_3 \equiv \left.\frac{\partial L}{\partial \Omega}\right|_{\Omega_0}, \quad L_{22} \equiv \left.\frac{\partial^2 L}{\partial K^2}\right|_{K_0}, \quad \dots \end{aligned} \quad (\text{A.42})$$

We also calculate the differentiation of the dispersion relation $D([V], k, \omega) = \langle V, LV \rangle = 0$ with respect to ω , which is used to obtain relations between certain inner products. Since (A.34) holds for all ω , we have

$$\frac{dD}{d\omega} = \left\langle \frac{dV}{d\omega}, LV \right\rangle + \left\langle V, L \frac{dV}{d\omega} \right\rangle + \left\langle V, \frac{dL}{d\omega} V \right\rangle = 0. \quad (\text{A.43})$$

Note in (A.43) that $\langle V, LX \rangle = \langle X, LV \rangle$ for L being a self-adjoint operator. Thus we obtain

$$2 \left\langle \frac{dV}{d\omega}, LV \right\rangle + \left\langle V, \frac{dL}{d\omega} V \right\rangle = 0. \quad (\text{A.44})$$

Recall that on a solution U at $O(\varepsilon)$, $L_1 U = 0$ in (A.44), so that for $k = k_0$ and $\omega = \omega_0$

$$\begin{aligned} \left\langle U, \frac{dL}{d\omega} \Big|_{k_0, \omega_0} U \right\rangle &= \left\langle U, \left(L_2 \frac{d(ik)}{d\omega} \Big|_{\omega_0} + L_3 \frac{d(-i\omega)}{d\omega} \Big|_{\omega_0} \right) U \right\rangle \\ &= \langle U, (ik'_0 L_2 - iL_3) U \rangle \\ &= ik'_0 \langle U, L_2 U \rangle - i \langle U, L_3 U \rangle \\ &= 0. \end{aligned} \quad (\text{A.45})$$

At $O(\varepsilon^2)$, we have from (A.16)

$$\left(\frac{\partial^2}{\partial x^2} + \frac{\partial^2}{\partial z^2} - \frac{1}{c^2} \frac{\partial^2}{\partial t^2} - \frac{1}{c^2} \frac{\partial^2}{\partial t^2} \int d\tau \chi^{(1)}(x, t - \tau) \right) \varepsilon E_1 = 0. \quad (\text{A.46})$$

With (A.41), we obtain the following relation

$$L_1(\varepsilon E_1) + \varepsilon^2 \left(L_2 U(x, \omega_0) \frac{\partial A}{\partial Z_1} + L_3 U(x, \omega_0) \frac{\partial A}{\partial T} \right) \exp(ik_0 z - i\omega_0 t) + \text{c.c.} = 0. \quad (\text{A.47})$$

We put $E_1 = \varepsilon U_1 \exp(ik_0 z - i\omega_0 t) + \text{c.c.}$, so that we have

$$L_1 U_1 = F_1 \equiv - \left(L_2 U(x, \omega_0) \frac{\partial A}{\partial Z_1} + L_3 U(x, \omega_0) \frac{\partial A}{\partial T} \right). \quad (\text{A.48})$$

Solvability condition of E_1 requires that the transverse component $U(x)$ is a smooth solution that vanishes at the boundary $|x| \rightarrow \infty$. In mathematical literature, the requirement is described as the Fredholm alternative theorem; the inhomogeneous boundary value problem $\Lambda X = F$, with the singular operator Λ having nontrivial homogeneous solutions V such that $\Lambda V = 0$, has the bound state solution when the right hand side F is orthogonal to V :

$$\langle V, F \rangle = \langle V, \Lambda X \rangle = 0. \quad (\text{A.49})$$

The brackets denote the inner product defined by (A.35). For the problem (A.48), the Fredholm theorem demands thereby

$$\langle U, F_1 \rangle = \langle U, -L_2 U \rangle \frac{\partial A}{\partial Z_1} + \langle U, -L_3 U \rangle \frac{\partial A}{\partial T} = 0. \quad (\text{A.50})$$

From (A.45), we have

$$\langle U, -L_2 U \rangle \left(\frac{\partial A}{\partial Z_1} + k'_0 \frac{\partial A}{\partial T} \right) = 0. \quad (\text{A.51})$$

Note that

$$\langle U, -L_2 U \rangle = -2ik_0 \langle U, U \rangle \neq 0, \quad (\text{A.52})$$

consequently the solvability condition leads to the following equation

$$\frac{\partial A}{\partial Z_1} + k'_0 \frac{\partial A}{\partial T} = 0, \quad (\text{A.53})$$

which describe the propagation of a wave packet at the group velocity of $1/k'_0$.

The solvability condition gives rise to the slow variation of the mode distribution $U(x)$ with respect to ω . This can be clearly seen by evaluating the forcing function F_1 , namely

$$\begin{aligned} F_1 &= - \left(L_2 U \frac{\partial A}{\partial Z_1} + L_3 U \frac{\partial A}{\partial T} \right) \\ &= (L_2 k'_0 - L_3) U \frac{\partial A}{\partial T} \\ &= (-i L_2 k'_0 + i L_3) U \left(i \frac{\partial A}{\partial T} \right) \\ &= - \left(\frac{\partial L}{\partial k} \frac{dk}{\omega_0} + \frac{\partial L}{\partial \omega_0} \right) U \left(i \frac{\partial A}{\partial T} \right) \\ &= -i \frac{dL}{\omega_0} U \frac{\partial A}{\partial T}, \end{aligned} \quad (\text{A.54})$$

where we used (A.53) and $d/d\omega_0 \equiv d/d\omega|_{\omega_0}$. On the other hand, differentiation of $L_1 U = 0$ with respect to ω leads to $dL/d\omega_0 = 0$ and thus $F_1 = 0$, unless U has ω dependency. Therefore (A.54) can now be written as

$$F_1 = iL \frac{\partial U}{\partial \omega_0} \frac{\partial A}{\partial T}, \quad (\text{A.55})$$

This gives rise to nonzero U_1 :

$$U_1 = i \frac{\partial U}{\partial \omega_0} \frac{\partial A}{\partial T}. \quad (\text{A.56})$$

Thus we have at $O(\varepsilon^2)$

$$E_0 + \varepsilon E_1 = \varepsilon \left(U(x, \omega_0) + i\varepsilon \frac{\partial U}{\partial \omega}(x, \omega_0) \frac{\partial}{\partial T} \right) A(Z, T) \exp(ik_0 z - i\omega_0 t) + \text{c.c.} \quad (\text{A.57})$$

$O(\varepsilon^3)$: the nonlinear Schrödinger equation

Before proceeding to the next order, we make several preparation again. We differentiate (A.43) again with respect to ω . Using (A.45), we find

$$\frac{d^2 D}{d\omega^2} = \left\langle \frac{dV}{d\omega}, \frac{dL}{d\omega} V \right\rangle + \left\langle V, \frac{dL}{d\omega} \frac{dV}{d\omega} \right\rangle + \left\langle V, \frac{d^2 L}{d\omega^2} V \right\rangle = 2 \left\langle V, \frac{dL}{d\omega} \frac{dV}{d\omega} \right\rangle + \left\langle V, \frac{d^2 L}{d\omega^2} V \right\rangle = 0, \quad (\text{A.58})$$

which gives (on a solution U for $k = k_0$ and $\omega = \omega_0$)

$$2 \left\langle U, (ik'_0 L_2 - iL_3) \frac{\partial U}{\partial \omega_0} \right\rangle + ik''_0 \langle U, L_2 U \rangle - k'^2_0 \langle U, L_{22} U \rangle + 2k'_0 \langle U, L_{23} U \rangle - \langle U, L_{33} U \rangle = 0, \quad (\text{A.59})$$

where we used

$$\frac{dL}{d\omega_0} = ik'_0 L_2 - iL_3, \quad \frac{d^2 L}{d\omega_0^2} = ik''_0 L_2 - k'^2_0 L_{22} + 2k'_0 L_{23} - L_{33}. \quad (\text{A.60})$$

At $O(\varepsilon^3)$, we have to take into consideration the nonlinear polarization. Extracting the $O(\varepsilon^3)$ contributions from (A.16), we obtain

$$\left(\frac{\partial^2}{\partial x^2} + \frac{\partial^2}{\partial z^2} - \frac{1}{c^2} \frac{\partial^2}{\partial t^2} - \frac{1}{c^2} \frac{\partial^2}{\partial t^2} \int d\tau \chi^{(1)}(x, t - \tau) \right) \varepsilon^2 E_2 - \frac{1}{c^2} \frac{\partial^2}{\partial t^2} \iiint \chi^{(3)}(x, t - \tau_1, t - \tau_2, t - \tau_3) E_0(x, z, \tau_1) E_0(x, z, \tau_2) E_0(x, z, \tau_3) d\tau_1 d\tau_2 d\tau_3 = 0. \quad (\text{A.61})$$

E_2 has the phase components $\exp(\pm ik_0 z \mp i\omega_0 t)$ as well as $\exp(\pm 3ik_0 z \mp 3i\omega_0 t)$, which we explicitly represent as

$$E_2 = \varepsilon U_2 \exp(ik_0 z - i\omega_0 t) + \varepsilon^3 V_2 \exp(3ik_0 z - 3i\omega_0 t) + \text{c.c.} \quad (\text{A.62})$$

The nonlinear polarization term contains the component proportional to $\exp(ik_0 z - i\omega_0 t)$ given by

$$-\varepsilon^3 \frac{3\omega_0^2}{c^2} \hat{\chi}^{(3)}(x, -\omega_0, \omega_0, \omega_0) A^2(Z, T) A^*(Z, T) U^3(x, \omega_0) \exp(ik_0 z - i\omega_0 t), \quad (\text{A.63})$$

where we referred to (A.29). As a consequence, using the linear operator L , (A.61) can be written as the following arranged form:

$$L(\varepsilon^2 E_2) = \varepsilon^3 F_2 \exp(ik_0 z - i\omega_0 t) + \varepsilon^3 G_2 \exp(3ik_0 z - 3i\omega_0 t) + \text{c.c.}, \quad (\text{A.64})$$

namely, for the frequency ω_0 and the wave number k_0 , we have

$$L_1 U_2 = F_2, \quad (\text{A.65})$$

where

$$\begin{aligned} F_2 = & -L_2 U \frac{\partial A}{\partial Z_2} - \frac{1}{2} L_{22} U \frac{\partial^2 A}{\partial Z_1^2} - \frac{1}{2} L_{33} U \frac{\partial^2 A}{\partial T^2} - L_{23} U \frac{\partial^2 A}{\partial Z_1 \partial T} \\ & - i L_2 \frac{\partial U}{\partial \omega_0} \frac{\partial^2 A}{\partial Z_1 \partial T} - i L_3 \frac{\partial U}{\partial \omega_0} \frac{\partial^2 A}{\partial T^2} \\ & - \frac{3\omega_0^2}{c^2} \hat{\chi}^{(3)}(x, -\omega_0, \omega_0, \omega_0) A^2(Z, T) A^*(Z, T) U^3(x, \omega_0). \end{aligned} \quad (\text{A.66})$$

In terms of the linear electric polarization, the first line of (A.66) originates from εE_0 and the $O(\varepsilon^2)$ contributions of L , whereas the second line is obtained from $\varepsilon^2 E_1$ and the $O(\varepsilon)$ contributions of L . (See (A.41) and (A.57).)

Following the analysis at $O(\varepsilon^2)$, we apply the Fredholm's theorem to (A.65):

$$\langle U, F_2 \rangle = 0, \quad (\text{A.67})$$

where the left hand side of (A.67) can be written as

$$\begin{aligned} \langle U, F_2 \rangle = & \langle U, -L_2 U \rangle \frac{\partial A}{\partial Z_2} + \frac{1}{2} \langle U, -L_{22} U \rangle \frac{\partial^2 A}{\partial Z_1^2} + \frac{1}{2} \langle U, -L_{33} U \rangle \frac{\partial^2 A}{\partial T^2} + \langle U, -L_{23} U \rangle \frac{\partial^2 A}{\partial Z_1 \partial T} \\ & + i \left\langle U, -L_2 \frac{\partial U}{\partial \omega_0} \right\rangle \frac{\partial^2 A}{\partial Z_1 \partial T} + i \left\langle U, -L_3 \frac{\partial U}{\partial \omega_0} \right\rangle \frac{\partial^2 A}{\partial T^2} - \frac{3\omega_0^2}{c^2} \langle U, \hat{\chi}^{(3)} U^3 \rangle A^2 A^* \\ = & \langle U, -L_2 U \rangle \frac{\partial A}{\partial Z_2} + \left(\frac{1}{2} k'_0 \langle U, L_{22} U \rangle - \langle U, L_{23} U \rangle \right) \frac{\partial^2 A}{\partial Z_1 \partial T} + \frac{1}{2} \langle U, -L_{33} U \rangle \frac{\partial^2 A}{\partial T^2} \\ & + \left(-i \left\langle U, L_2 \frac{\partial U}{\partial \omega_0} \right\rangle + \frac{i}{k'_0} \left\langle U, L_3 \frac{\partial U}{\partial \omega_0} \right\rangle \right) \frac{\partial^2 A}{\partial Z_1 \partial T} - \frac{3\omega_0^2}{c^2} \langle U, \hat{\chi}^{(3)} U^3 \rangle A^2 A^* \end{aligned}$$

$$\begin{aligned}
&= \langle U, -L_2 U \rangle \frac{\partial A}{\partial Z_2} - i \frac{k_0''}{2k_0'} \langle U, -L_2 U \rangle \frac{\partial^2 A}{\partial Z_1 \partial T} + \frac{1}{2k_0'} \langle U, -L_{33} U \rangle \left(\frac{\partial^2 A}{\partial Z_1 \partial T} + k_0' \frac{\partial^2 A}{\partial T^2} \right) \\
&\quad - \frac{3\omega_0^2}{c^2} \langle U, \hat{\chi}^{(3)} U^3 \rangle A^2 A^* \\
&= \langle U, -L_2 U \rangle \left(\frac{\partial A}{\partial Z_2} + i \frac{k_0''}{2} \frac{\partial^2 A}{\partial T^2} \right) - \frac{3\omega_0^2}{c^2} \langle U, \hat{\chi}^{(3)} U^3 \rangle A^2 A^* \\
&= -2ik_0 \langle U, U \rangle \left(\frac{\partial A}{\partial Z_2} + i \frac{k_0''}{2} \frac{\partial^2 A}{\partial T^2} \right) - \frac{3\omega_0^2}{c^2} \langle U, \hat{\chi}^{(3)} U^3 \rangle A^2 A^* \\
&= -2ik_0 \int U^2(x, \omega_0) dx \left(\frac{\partial A}{\partial Z_2} + i \frac{k_0''}{2} \frac{\partial^2 A}{\partial T^2} \right) \\
&\quad - \frac{3\omega_0^2}{c^2} A^2 A^* \int \hat{\chi}^{(3)}(x, -\omega_0, \omega_0, \omega_0) U^4(x, \omega_0) dx. \tag{A.68}
\end{aligned}$$

We have referred to (A.59) and the following relations

$$\frac{\partial^2 A}{\partial Z_1 \partial T} + k_0' \frac{\partial^2 A}{\partial T^2} = 0, \quad \frac{\partial^2 A}{\partial Z_1^2} + k_0' \frac{\partial^2 A}{\partial Z_1 \partial T} = 0, \tag{A.69}$$

which are obtained by the differentiation of (A.53) with respect to T and Z_1 respectively. We now have

$$-2ik_0 \int U^2(x, \omega_0) dx \left(\frac{\partial A}{\partial Z_2} + i \frac{k_0''}{2} \frac{\partial^2 A}{\partial T^2} \right) - \frac{3\omega_0^2}{c^2} A^2 A^* \int \hat{\chi}^{(3)}(x, -\omega_0, \omega_0, \omega_0) U^4(x, \omega_0) dx = 0. \tag{A.70}$$

or simply,

$$\frac{\partial A}{\partial Z_2} + i \frac{k_0''}{2} \frac{\partial^2 A}{\partial T^2} + \frac{-\frac{3\omega_0^2}{c^2} \int \hat{\chi}^{(3)} U^4 dx}{-2ik_0 \int U^2 dx} A^2 A^* = 0. \tag{A.71}$$

We hereafter assume for simplicity the nonlinear susceptibility $\hat{\chi}^{(3)}$ having negligibly small dependence on the transverse coordinate x . We define the following parameters

$$n_0 \equiv \frac{ck_0}{\omega_0}, \quad n_2 \equiv \frac{3\hat{\chi}^{(3)}(\omega_0)}{2n_0}, \quad g \equiv \frac{\int U^4 dx}{\int U^2 dx}, \tag{A.72}$$

so that we have

$$\frac{\partial A}{\partial Z_2} + i \frac{k_0''}{2} \frac{\partial^2 A}{\partial T^2} - i \frac{gn_2\omega_0}{c} A^2 A^* = 0. \tag{A.73}$$

Note that in the definition in (A.72), n_0 and n_2 corresponds to the linear and the third order nonlinear coefficients of the refractive index:

$$n(\omega_0, |\mathbf{E}|) = n_0 + n_2 |\mathbf{E}|^2. \tag{A.74}$$

Combining (A.53) and (A.73), and introducing the new coordinates

$$\tau = \varepsilon(t - k_0' z), \quad \zeta = \varepsilon^2 z, \tag{A.75}$$

we finally obtain the canonical form of the nonlinear Schrödinger equation

$$\frac{\partial A}{\partial \zeta} + i \frac{k_0''}{2} \frac{\partial^2 A}{\partial \tau^2} - i \frac{gn_2 \omega_0}{c} A^2 A^* = 0. \quad (\text{A.76})$$

The established nonlinear Schrödinger equation describes the long range propagation of the envelope A which is modestly modulated in a slow scale time coordinate $\tau = \varepsilon t$ over an extended length $\zeta = \varepsilon^2 z$.

Note that, as a result of the solvability condition, E is now written as

$$\begin{aligned} & E_0 + \varepsilon E_1 + \varepsilon^2 E_2 \\ &= \varepsilon \left(U(x, \omega_0) + i\varepsilon \frac{\partial U}{\partial \omega_0} \frac{\partial}{\partial T} - \frac{\varepsilon^2}{2} \frac{\partial^2 U}{\partial \omega_0^2} \frac{\partial^2}{\partial T^2} \right) A(Z, T) \exp(ik_0 z - i\omega_0 t) \\ & \quad + \varepsilon^3 V_2 \exp(3ik_0 z - 3i\omega_0 t) + \text{c.c.} \end{aligned} \quad (\text{A.77})$$

A.5 Nonlinear Schrödinger equation in optical fibers

So far, we have considered nonlinear optical pulse propagation in a planer waveguide, where an electric field has been treated as a scalar quantity. To understand the behavior of optical pulses in fibers, however, we have to take into account their physical properties, such as their material and geometric features. In this section, we point out a couple of remarks on these issues. We assume the polarization preserving fibers in the following; the generalization to birefringent fibers is studied in [122].

Attenuation

One of the major corrections required is the effect of material absorption which originates from the imaginary part of the linear and nonlinear susceptibilities, $\text{Im}[\chi^{(1)}]$ and $\text{Im}[\chi^{(3)}]$, respectively. Including the former contribution in the linear polarization, we have

$$\begin{aligned} \mathbf{P}_L &= \int_{-\infty}^t \epsilon_0 \chi^{(1)}(\mathbf{r}, t - \tau) \cdot \mathbf{E}(\mathbf{r}, \tau) d\tau \\ &\equiv \int_{-\infty}^t \epsilon_0 \left(\chi_R^{(1)}(\mathbf{r}, t - \tau) + i\chi_I^{(1)}(\mathbf{r}, t - \tau) \right) \cdot \mathbf{E}(\mathbf{r}, \tau) d\tau. \end{aligned} \quad (\text{A.78})$$

As a result, we have the following form of the additional term at leading order in (A.18):

$$-i\omega^2 \hat{\chi}_I^{(1)}(x, \omega) \hat{A}(Z, \omega - \omega_0) U(x, \omega_0) \exp(ik_0 z) + \text{c.c.} \quad (\text{A.79})$$

We further assume that $\hat{\chi}_I^{(1)}(x, \omega_0) \sim O(\varepsilon^2)$ and thus (A.79) has $O(\varepsilon^3)$ contribution as a result of the quasi monochromatic approximation. By taking the inverse Fourier transform of (A.79) and the quasi monochromatic approximation, F_2 has now an additional term in (A.66), which is given by

$$-i \frac{\omega_0^2}{c^2} \hat{\chi}_I^{(1)}(x, \omega_0) A(Z, T) U(x, \omega_0). \quad (\text{A.80})$$

The solvability condition (A.68) now reads

$$\begin{aligned} \langle U, F_2 \rangle &= -2ik_0 \int U^2(x, \omega_0) dx \left(\frac{\partial A}{\partial Z_2} + i \frac{k_0''}{2} \frac{\partial^2 A}{\partial T^2} \right) \\ & \quad - \frac{3\omega_0^2}{c^2} A^2 A^* \int \hat{\chi}^{(3)}(x, -\omega_0, \omega_0, \omega_0) U^4(x, \omega_0) dx - i \frac{\omega_0^2}{c^2} A \int \hat{\chi}_I^{(1)}(x, \omega_0) U^2(x, \omega_0) dx \\ &= 0. \end{aligned} \quad (\text{A.81})$$

We finally obtain the modified equation including the material absorption

$$\frac{\partial A}{\partial \zeta} + i \frac{k_0''}{2} \frac{\partial^2 A}{\partial \tau^2} - i \frac{gn_2 \omega_0}{c} A^2 A^* + \frac{n_I \omega_0}{c} A = 0, \quad (\text{A.82})$$

where we neglect the x dependency of $\hat{\chi}_I^{(1)}$ and define

$$n_I \equiv \frac{\hat{\chi}_I^{(1)}(\omega_0)}{2n_0}. \quad (\text{A.83})$$

The last term of (A.82), in both physical and mathematical literature, is responsible for the attenuation of optical power. We can similarly calculate the nonlinear attenuation correction, but its contribution is negligible in practice.

Higher order corrections

Another effects that have been ignored so far are higher order corrections such as third order dispersion, nonlinear dispersion, and delayed response of the nonlinear polarization, which originate from $O(\varepsilon^4)$ contributions in the asymptotic expansion of (A.16). The solvability condition at $O(\varepsilon^4)$ leads to

$$\frac{\partial A}{\partial Z_3} = -\frac{2\pi n_I \omega_0}{\varepsilon c} A + \frac{k_0'''}{6} \frac{\partial^3 A}{\partial T^3} - \varepsilon \beta_1 \frac{\partial}{\partial T} (|A|^2 A) - \varepsilon i \beta_2 A \frac{\partial}{\partial T} |A|^2, \quad (\text{A.84})$$

where $Z_3 \equiv \varepsilon^3 z$. The first term on the right hand side is a consequence of the imaginary part of the linear susceptibility we have just introduced above, and the second term represents the third order dispersion which is obtained by expanding the dispersion relation $k = k(\omega)$ in a Taylor series. The last two terms come from the higher order correction to the nonlinear polarization in (A.25). Noting that $(\omega_1 + \omega_0)$, $(\omega_2 - \omega_0)$, $(\omega_3 - \omega_0)$ are $O(\varepsilon)$, the next order correction is obtained by multiplying them respectively with $\hat{A}^*(-\omega_1 - \omega_0)\hat{A}(\omega_2 - \omega_0)\hat{A}(\omega_3 - \omega_0)$, which is expressed as

$$\begin{aligned} & \frac{\partial \hat{\chi}^{(3)}}{\partial \omega_1}(x, -\omega_0, \omega_0, \omega_0) \omega_0^2 (\omega_1 + \omega_0) \hat{A}^*(-\omega_1 - \omega_0) \hat{A}(\omega_2 - \omega_0) \hat{A}(\omega_3 - \omega_0) \\ & + \frac{\partial \hat{\chi}^{(3)}}{\partial \omega_2}(x, -\omega_0, \omega_0, \omega_0) \omega_0^2 (\omega_2 - \omega_0) \hat{A}^*(-\omega_1 - \omega_0) \hat{A}(\omega_2 - \omega_0) \hat{A}(\omega_3 - \omega_0) \\ & + \frac{\partial \hat{\chi}^{(3)}}{\partial \omega_3}(x, -\omega_0, \omega_0, \omega_0) \omega_0^2 (\omega_3 - \omega_0) \hat{A}^*(-\omega_1 - \omega_0) \hat{A}(\omega_2 - \omega_0) \hat{A}(\omega_3 - \omega_0). \end{aligned} \quad (\text{A.85})$$

After taking the inverse Fourier transform and following the computation in (A.28), we have one term proportional to $A^2 \partial A^* / \partial T$ and two terms proportional to $|A|^2 \partial A / \partial T$. Using the relation

$$\frac{\partial}{\partial T} (|A|^2 A) = A^2 \frac{\partial A^*}{\partial T} + 2|A|^2 \frac{\partial A}{\partial T}, \quad A \frac{\partial |A|^2}{\partial T} = A^2 \frac{\partial A^*}{\partial T} + |A|^2 \frac{\partial A}{\partial T}, \quad (\text{A.86})$$

we finally obtain these contributions in (A.84). The resultant equation is

$$\frac{\partial A}{\partial \zeta} + i \frac{k_0''}{2} \frac{\partial^2 A}{\partial \tau^2} - \varepsilon \frac{k_0'''}{6} \frac{\partial^3 A}{\partial \tau^3} - i \frac{\omega_0}{c} gn_2 |A|^2 A + \frac{\omega_0}{c} n_I A + \varepsilon \beta_1 \frac{\partial}{\partial \tau} (|A|^2 A) + \varepsilon i \beta_2 A \frac{\partial}{\partial \tau} |A|^2 = 0. \quad (\text{A.87})$$

Among the last two terms of higher order nonlinear effects, the former term represents the nonlinear dispersion which originates from the frequency dependence of n_2 , whereas the latter term describes the retarded response of the nonlinear refractive index.

Geometric property

Finally we briefly summarize the procedure on the derivation of the nonlinear Schrödinger equation for single mode optical fibers, by taking into account their geometric properties. In this case, an electric field becomes vector, thus the linear operator L has a matrix form that contains the differentiation operator with respect to y , in addition to $\partial/\partial x$. The inner product of two complex vectors $u = \{u_i\}^t$ and $v = \{v_i\}^t$, $i = 1, 2, 3$, that is necessary to impose the solvability condition (the Fredholm alternative theorem), is extended to the integral over a surface (x, y) and now defined as

$$\langle u, v \rangle \equiv \int (u_1^* v_1 + u_2^* v_2 + u_3^* v_3) dS. \quad (\text{A.88})$$

As a result of this generalization, the dispersion relation (A.36) is now written as

$$k^2 = \frac{\frac{\omega^2}{c^2} \int n^2(x, y, \omega) U^2 dS - \int |\nabla_t U|^2 dS}{\int U^2 dS}, \quad \nabla_t \equiv \hat{\mathbf{x}} \frac{\partial}{\partial x} + \hat{\mathbf{y}} \frac{\partial}{\partial y} \quad (\text{A.89})$$

and g in (A.72) is expressed as

$$g = \frac{\int U^4 dS}{\int U^2 dS}. \quad (\text{A.90})$$

For the fundamental mode of the step-index fiber HE_{11} , U is given by the Bessel functions J_0 and K_0 but well approximated as a Gaussian distribution of the form [121]

$$U(x, y) = \exp\left(-\frac{x^2 + y^2}{w^2}\right), \quad (\text{A.91})$$

where w ($2w$) is the parameter referred to as the spot size (the mode field diameter).

A.6 Normalization of the nonlinear Schrödinger equation

For convenience for mathematical treatments, we normalize the established equation (A.76) by using the normalizing time, distance, and power: t_0 , z_0 , and P_0 , respectively. This normalization may also give quick estimate on system performance [123].

First of all, we normalize the amplitude A into \mathcal{E} so that $|\mathcal{E}|^2$ represents the optical power:

$$|\mathcal{E}|^2 = |A|^2 \int U^2 dS. \quad (\text{A.92})$$

Using the new amplitude \mathcal{E} , we have the following form of the nonlinear Schrödinger equation

$$i \frac{\partial \mathcal{E}}{\partial \zeta} - \frac{k''}{2} \frac{\partial^2 \mathcal{E}}{\partial \tau^2} + \nu |\mathcal{E}|^2 \mathcal{E} = -i\gamma \mathcal{E} + i \frac{k'''}{6} \frac{\partial^3 \mathcal{E}}{\partial \tau^3}, \quad (\text{A.93})$$

where we included the effects of fiber loss and third order dispersion on the right hand side, and

$$\nu \equiv \frac{n_2 \omega_0}{c A_{\text{eff}}}, \quad A_{\text{eff}} \equiv \frac{\int U^2 dS}{g} = \frac{\left(\int U^2 dS\right)^2}{\int U^4 dS}, \quad \gamma \equiv \frac{n_I \omega_0}{c}. \quad (\text{A.94})$$

A_{eff} is known as the effective core area. Now we define the following normalized parameters using t_0 , z_0 , and P_0 :

$$T = \frac{\tau}{t_0}, \quad Z = \frac{\zeta}{z_0}, \quad q = \frac{\mathcal{E}}{\sqrt{P_0}}. \quad (\text{A.95})$$

With these new parameters, the nonlinear Schrödinger equation (A.93) reads

$$i \frac{\partial q}{\partial Z} + \frac{d(Z)}{2} \frac{\partial^2 q}{\partial T^2} + \alpha |q|^2 q = -i\Gamma q + i \frac{\beta_3}{6} \frac{\partial^3 q}{\partial T^3}, \quad (\text{A.96})$$

where the new coefficients given by

$$d(Z) = -\frac{k'' z_0}{t_0^2}, \quad \alpha = \nu P_0 z_0, \quad \Gamma = \gamma z_0, \quad \beta_3 = \frac{k''' z_0}{t_0^3}. \quad (\text{A.97})$$

Although the normalizing parameters t_0 , z_0 , and P_0 can be chosen arbitrary, we can represent Eq. (A.96) in a simplified and practically convenient form by their proper choice. Consider two such examples. First, if we take $z_0 = -t_0^2 / \langle k'' \rangle$ and $P_0 = -\langle k'' \rangle / \alpha t_0^2$ with arbitrary t_0 , then we have (we assume $\langle k'' \rangle < 0$)

$$\begin{aligned} i \frac{\partial q}{\partial Z} + \frac{d(Z)}{2} \frac{\partial^2 q}{\partial T^2} + |q|^2 q &= -i\Gamma q + i \frac{\beta_3}{6} \frac{\partial^3 q}{\partial T^3}, \\ d(Z) = \frac{k''(Z)}{\langle k''(Z) \rangle}, \quad \Gamma &= -\frac{t_0^2 \gamma}{\langle k'' \rangle}, \quad \beta_3 = -\frac{k'''}{\langle k'' \rangle t_0}, \end{aligned} \quad (\text{A.98})$$

which gives the average of the dispersion coefficient $\langle d(Z) \rangle = 1$. We usually define t_0 to be t_s / T_s , where t_s and T_s represent the full-width at half-maximum (FWHM) of the pulse measured in real and normalized unit, respectively, so that it is convenient to treat the problem technically. The normalizing distance z_0 defined above is called the dispersion distance. On the other hand, if we take $z_0 = 1 / \alpha P_0$ and $t_0 = \sqrt{-\langle k'' \rangle / \alpha P_0}$ with arbitrary P_0 , then we have again Eq. (A.98) but with $\Gamma = \gamma / \alpha P_0$ and $\beta_3 = k''' / \alpha P_0 t_0^3$. We usually define P_0 to be the peak power of the pulse also for technical convenience. In this case the normalizing distance z_0 is referred to as the nonlinear distance.

Bibliography

- [1] G. P. Agrawal, *Fiber-Optic Communication Systems* (2nd ed.), John Wiley & Sons, New York (1997).
- [2] I. P. Kaminow and T. L. Koch (Eds.), *Optical Fiber Telecommunications IIIA*, Academic Press, San Diego, CA (1997).
- [3] N. S. Kapaney, *Fiber Optics: Principles and Applications*, Academic Press, San Diego, CA (1967).
- [4] D. Marcuse, *Theory of Dielectric Optical Waveguides* (2nd ed.), Academic Press, San Diego, CA (1991).
- [5] A. C. Newell and J. P. Moloney, *Nonlinear Optics*, Addison-Wesley, Redwood City, CA (1992).
- [6] G. P. Agrawal, *Nonlinear Fiber Optics* (2nd ed.), Academic Press, San Diego, CA (1995).
- [7] F. Forghieri, R. W. Tkach, and A. R. Chraplyvy, “Fiber nonlinearities and their impact on transmission systems,” in *Optical Fiber Telecommunications IIIA* (I. P. Kaminow and T. L. Koch, eds.), Academic Press, San Diego, CA, pp. 196–264 (1997).
- [8] T. Miya, Y. Terumura, T. Hosaka, T. Miyasita, “Ultimate low-loss single-mode fibre at 1.55 μm ,” *Electron. Lett.* **15**, 106 (1979).
- [9] R. J. Mears, L. Reekie, I. M. Jauncey, and D. N. Payne, “Low-noise erbium-doped fibre amplifier operating at 1.54 μm ,” *Electron. Lett.* **23**, 1026 (1987).
- [10] E. Desurvire, J. R. Simpson, and P. C. Becker, “High-gain erbium-doped traveling-wave fiber amplifier,” *Opt. Lett.* **12**, 888 (1987).
- [11] A. Hasegawa and F. Tappert, “Transmission of stationary nonlinear optical pulses in dispersive dielectric fibers. I. Anomalous dispersion,” *Appl. Phys. Lett.* **23**, 142 (1973).
- [12] A. Hasegawa, *Optical Solitons in Fibers* (2nd ed.), Springer-Verlag, Berlin (1989).
- [13] J. R. Taylor (Ed.), *Optical Solitons — Theory and Experiment*, Cambridge Univ. Press, Cambridge (1992).
- [14] A. Hasegawa and Y. Kodama, *Solitons in Optical Communications*, Oxford Univ. Press, Oxford (1995).

- [15] V. E. Zakharov and A. B. Shabat, "Exact theory of two-dimensional self-focusing and one-dimensional self-modulation of waves in nonlinear media," *Sov. Phys. JETP* **34**, 62 (1972).
- [16] A. Hasegawa and Y. Kodama, "Guiding-center soliton in optical fibers," *Opt. Lett.* **15**, 1443 (1990).
- [17] A. Hasegawa and Y. Kodama, "Guiding-center soliton," *Phys. Rev. Lett.* **66**, 161 (1991).
- [18] A. Hasegawa and Y. Kodama, "Guiding-center soliton in fibers with periodically varying dispersion," *Opt. Lett.* **16**, 1385 (1991).
- [19] J. P. Gordon and H. A. Haus, "Random walk of coherently amplified solitons in optical fiber transmission," *Opt. Lett.* **11**, 665 (1986).
- [20] K. J. Blow and N. J. Doran, "Bandwidth limits of nonlinear (soliton) optical communication systems," *Electron. Lett.* **19**, 429 (1983).
- [21] J. P. Gordon, "Interaction forces among solitons in optical fibers," *Opt. Lett.* **8**, 596 (1983).
- [22] P. A. Andrekson, N. A. Olsson, J. R. Simpson, T. Tanbun-Ek, R. A. Logan, P. C. Beaker, and K. W. Wecht, "Observation of multi-wavelength soliton collisions in optical systems with fibre amplifiers," *Appl. Phys. Lett.* **57**, 1715 (1990).
- [23] L. F. Mollenauer, S. G. Evangelides, Jr. and J. P. Gordon, "Wavelength division multiplexing with solitons in ultra-long distance transmission using lumped amplifiers," *J. Lightwave Technol.* **9**, 362 (1991).
- [24] P. A. Andrekson, N. A. Olsson, J. R. Simpson, T. Tanbun-Ek, R. A. Logan, and K. W. Wecht, "Observation of collision induced temporary soliton carrier frequency shifts in ultra-long fiber transmission systems," *J. Lightwave Technol.* **9**, 1132 (1991).
- [25] Y. Kodama and A. Hasegawa, "Effect of initial overlap on the propagation of optical solitons at different wavelengths," *Opt. Lett.* **16**, 208 (1991).
- [26] S. Chakravarty, M. J. Ablowitz, J. R. Sauer, and R. B. Jenkins, "Multisoliton interactions and wavelength-division multiplexing," *Opt. Lett.* **20**, 136 (1995).
- [27] P. V. Mamyshev and L. F. Mollenauer, "Pseudo-phase-matched four-wave mixing in soliton wavelength-division multiplexing transmission," *Opt. Lett.* **21**, 396 (1996).
- [28] M. J. Ablowitz, G. Biondini, S. Chakravarty, R. B. Jenkins, and J. R. Sauer, "Four-wave mixing in wavelength-division-multiplexed soliton systems: damping and amplification," *Opt. Lett.* **20**, 1646 (1996).

- [29] M. J. Ablowitz, G. Biondini, S. Chakravarty, R. B. Jenkins, and J. R. Sauer, "Four-wave mixing in wavelength-division-multiplexed soliton systems: ideal fibers," *J. Opt. Soc. Am. B* **14**, 1788 (1997).
- [30] A. Mecozzi, J. D. Moores, H. A. Haus, and Y. Lai, "Soliton transmission control," *Opt. Lett.* **16**, 1841 (1991).
- [31] Y. Kodama and A. Hasegawa, "Generation of asymptotically stable optical solitons and suppression of the Gordon-Haus effect," *Opt. Lett.* **17**, 31 (1992).
- [32] M. Matsumoto and A. Hasegawa, "Numerical study of the reduction of instability in bandwidth-limited amplified soliton transmission," *Opt. Lett.* **18**, 897 (1993).
- [33] L. F. Mollenauer, J. P. Gordon, and S. G. Evangelides, "The sliding-frequency guiding filter: an improved form of soliton jitter control," *Opt. Lett.* **17**, 1575 (1992).
- [34] M. Nakazawa, E. Yamada, H. Kubota, and K. Suzuki, "10 Gbit/s soliton data transmission over one million kilometers," *Electron. Lett.* **27**, 1270 (1991).
- [35] S. Wabnitz, "Suppression of soliton interactions by phase modulation," *Electron. Lett.* **29**, 1711 (1993).
- [36] L. F. Mollenauer, E. Lichtman, M. J. Neubelt, and G. T. Harvey, "Demonstration, using sliding-frequency guiding filters, of error-free soliton transmission over more than 20 Mm at 10 Gbit/s, single channel, and over more than 13 Mm at 20 Gbit/s in a two channel WDM," *Electron. Lett.* **29**, 1270 (1993).
- [37] M. Nakazawa, K. Suzuki, E. Yamada, H. Kubota, Y. Kimura, and M. Takaya, "Experimental demonstration of soliton data transmission over unlimited distances with soliton control in time and frequency domains," *Electron. Lett.* **29**, 729 (1993).
- [38] W. Forysiak, K. J. Blow, and N. J. Doran, "Reduction of Gordon-Haus jitter by post-transmission dispersion compensation," *Electron. Lett.* **29**, 1225 (1993).
- [39] M. Suzuki, I. Morita, N. Edagawa, S. Yamamoto, H. Taga, and S. Akiba, "Reduction of Gordon-Haus timing jitter by periodic dispersion compensation in soliton transmission," *Electron. Lett.* **31**, 2027 (1995).
- [40] F. M. Knox, W. Forysiak, and N. J. Doran, "10 Gbit/s soliton communication systems over standard fiber at 1.55 μm and the use of dispersion compensation," *J. Lightwave Technol.* **13**, 1955 (1995).
- [41] N. J. Smith, F. M. Knox, N. J. Doran, K. J. Blow, and I. Bennion, "Enhanced power solitons in optical fibres with periodic dispersion management," *Electron. Lett.* **32**, 54 (1996).

- [42] N. J. Smith, W. Forysiak, and N. J. Doran, "Reduced Gordon-Haus jitter due to enhanced power solitons in strongly dispersion managed systems," *Electron. Lett.* **32**, 208 (1996).
- [43] A. Hasegawa, Y. Kodama, and A. Maruta, "Recent progress in dispersion managed soliton transmission technologies," *Opt. Fiber Technol.* **3**, 197 (1997).
- [44] A. Hasegawa (Ed.), *New Trends in Optical Soliton Transmission Systems*, Kluwer Academic Publishers, Dordrecht (1998).
- [45] V. E. Zakharov and S. Wabnitz (Eds.), *Optical Solitons: Theoretical Challenges and Industrial Perspectives*, Springer-Verlag, Berlin (1999).
- [46] I. Gabitov, E. G. Shapiro, and S. K. Turitsyn, "Optical pulse dynamics in fiber links with dispersion compensation," *Opt. Commun.* **134**, 317 (1997).
- [47] M. Matsumoto and H. A. Haus, "Stretched-pulse optical fiber communications," *IEEE Photon. Technol. Lett.* **9**, 785 (1997).
- [48] I. Gabitov and S. K. Turitsyn, "Breathing solitons in optical fiber links," *JETP Lett.* **63**, 861 (1996).
- [49] T. Okamawari, Y. Ueda, A. Maruta, Y. Kodama, and A. Hasegawa, "Interaction between guiding centre solitons in periodically dispersion compensated optical transmission line," *Electron. Lett.* **33**, 1063 (1997).
- [50] M. J. Ablowitz and G. Biondini, "Multiscale pulse dynamics in communication systems with dispersion management," *Opt. Lett.* **23**, 1668 (1998).
- [51] D. Anderson, "Variational approach to nonlinear pulse propagation in optical fibers," *Phys. Rev. A* **27**, 3135 (1983).
- [52] M. J. Ablowitz and H. Segur, *Solitons and the Inverse Scattering Transform*, SIAM Publication, Philadelphia (1981).
- [53] H. Goldstein, *Classical Mechanics*, Addison-Wesley, Redwood City, CA (1950).
- [54] Y. Kodama, S. Kumar, and A. Maruta, "Chirped nonlinear pulse propagation in a dispersion-compensated systems," *Opt. Lett.* **22**, 1689 (1997).
- [55] J. H. B. Nijhof, N. J. Doran, W. Forysiak, and F. M. Knox, "Stable soliton-like propagation in dispersion managed systems with net anomalous, zero and normal dispersion," *Electron. Lett.* **33**, 1726 (1997).
- [56] Y. Kodama, "Nonlinear chirped RZ and NRZ pulses in optical transmission lines," in *New Trends in Optical Soliton Transmission Systems* (A. Hasegawa, ed.), Kluwer Academic Publishers, Dordrecht, pp. 131–153 (1998).

- [57] J. H. B. Nijhof, W. Forysiak, and N. J. Doran, "Dispersion-managed solitons in the normal dispersion regime: a physical interpretation," *Opt. Lett.* **23**, 1674 (1998).
- [58] A. Berntson, D. Anderson, M. Lisak, and B. Malomed, "Slow dynamics of dispersion-managed solitons," in *Nonlinear Guided Waves and Their Applications* (NLGW'99), Dijon, France, ThD9 (1999).
- [59] S. B. Medvedev and S. K. Turitsyn, "Hamilton averaging and integrability in nonlinear systems with periodically varying dispersion," *JETP Lett.* **69**, 465 (1999).
- [60] V. E. Zakharov, "Propagation of optical pulses in nonlinear systems with varying dispersion," in *Optical Soliton: Theoretical Challenges and Industrial Perspectives* (V. E. Zakharov and S. Wabnitz, eds.), Springer-Verlag, Berlin, pp. 73–89 (1999).
- [61] T. I. Lakoba, "Non-integrability of equations governing pulse propagation in dispersion-managed optical fibers," *Phys. Lett. A* **260**, 68 (1999).
- [62] W. Forysiak, F. M. Knox, and N. J. Doran, "Average soliton propagation in periodically amplified systems with stepwise dispersion profiled fibre," *Opt. Lett.* **19**, 174 (1994).
- [63] W. Forysiak, F. M. Knox, and N. J. Doran, "Stepwise dispersion profiling of periodically amplified soliton systems," *J. Lightwave Technol.* **12**, 1330 (1994).
- [64] A. Hasegawa, S. Kumar, and Y. Kodama, "Reduction of collision induced time jitters in dispersion managed soliton transmission systems," *Opt. Lett.* **21**, 39 (1996).
- [65] H. Sugahara, H. Kato, and Y. Kodama, "Maximum reductions of collision induced frequency shift in soliton-WDM systems with dispersion compensation," *Electron. Lett.* **33**, 1065 (1997).
- [66] J. F. L. Devaney, W. Forysiak, A. M. Niculae, and N. J. Doran, "Soliton collisions in dispersion-managed wavelength-division-multiplexed systems," *Opt. Lett.* **22**, 1695 (1997).
- [67] T. Hirooka and A. Hasegawa, "Chirped soliton interaction in strongly dispersion-managed wavelength-division-multiplexing systems," *Opt. Lett.* **23**, 768 (1998).
- [68] D. J. Kaup, B. A. Malomed, and J. Yang, "Collision-induced pulse timing jitter in a wavelength-division-multiplexing system with strong dispersion management," *J. Opt. Soc. Am. B* **16**, 1628 (1999).
- [69] H. Sugahara and A. Maruta, "Timing jitter of a strongly dispersion managed soliton in a wavelength-division-multiplexed system," in *Nonlinear Guided Waves and Their Applications* (NLGW'99), Dijon, France, ThA4 (1999).
- [70] T. Hirooka, T. Nakada, A. Liang, and A. Hasegawa, "160 Gb/s soliton transmission in a densely dispersion-managed fiber in the presence of variable dispersion and polarization-mode dispersion," in *Nonlinear Guided Waves and Their Applications* (NLGW'99), Dijon, France, ThA2 (1999).

- [71] K. I. Karpman and V. V. Solov'ev, "A perturbational approach to the two-soliton systems," *Physica* **3D**, 487 (1981).
- [72] B. Hermansson and D. Yevick, "Numerical investigation of soliton interaction," *Electron. Lett.* **19**, 570 (1983).
- [73] D. Anderson and M. Lisak, "Bandwidth limits due to mutual pulse interaction in optical soliton communication systems," *Opt. Lett.* **11**, 174 (1986).
- [74] P. L. Chu and C. Desem, "Mutual interaction between solitons of unequal amplitudes in optical fibre," *Electron. Lett.* **21**, 1133 (1985).
- [75] S. G. Evangelides, L. F. Mollenauer, J. P. Gordon, and N. S. Bergano, "Polarization multiplexing with solitons," *J. Lightwave Technol.* **10**, 28 (1992).
- [76] L. F. Mollenauer and J. P. Gordon, "Birefringence-mediated timing jitter in soliton transmission," *Opt. Lett.* **19**, 375 (1994).
- [77] L. F. Mollenauer, J. P. Gordon, and F. Heismann, "Polarization scattering by soliton-soliton collisions," *Opt. Lett.* **20**, 2060 (1995).
- [78] M. Matsumoto, "Analysis of interaction between stretched pulses propagating in dispersion-managed fibers," *IEEE Photon. Technol. Lett.* **10**, 373 (1998).
- [79] T. Georges, "Soliton interaction in dispersion managed links," *J. Opt. Soc. Am. B* **15**, 1553 (1998).
- [80] T. Yu, E. A. Golovchenko, A. N. Pilipetskii, and C. R. Menyuk, "Dispersion-managed soliton interactions in optical fibers," *Opt. Lett.* **22**, 793 (1997).
- [81] S. Kumar and A. Hasegawa, "Quasi-soliton propagation in dispersion-managed optical fibers," *Opt. Lett.* **22**, 372 (1997).
- [82] P. V. Mamyshev and N. A. Mamysheva, "Pulse-overlapped dispersion-managed data transmission and intrachannel four-wave mixing," *Opt. Lett.* **24**, 1454 (1999).
- [83] S. Kumar, M. Wald, F. Lederer, and A. Hasegawa, "Soliton interaction in strongly dispersion-managed optical fibers," *Opt. Lett.* **23**, 1019 (1998).
- [84] D. Le Guen, S. Del Burgo, M. L. Moulinard, D. Grot, M. Henry, F. Favre, and T. Georges, "Narrow band 1.02 Tbit/s (50×21 Gbit/s) soliton DWDM transmission over 1000 km of standard fiber with 100 km amplifier spans," in *Optical Fiber Communication Conference (OFC'99)*, San Diego, CA, PD4 (1999).
- [85] A. Liang, H. Toda, and A. Hasegawa, "High-speed soliton transmission in dense periodical fibers," *Opt. Lett.* **24**, 799, (1999).

- [86] R. Ohhira, A. Hasegawa, and Y. Kodama, "Methods of stable optical soliton transmission in fiber with distributed dispersion," *Opt. Lett.* **20**, 701 (1995).
- [87] M. Matsumoto, Y. Akagi, and A. Hasegawa, "Propagation of solitons in fibers with randomly varying birefringence: effects of soliton transmission control," *J. Lightwave Technol.* **15**, 584 (1997).
- [88] S. K. Turitsyn and E. G. Shapiro, "Dispersion-managed solitons in optical amplifier transmission systems with zero average dispersion," *Opt. Lett.* **23**, 682 (1998).
- [89] G. M. Carter and J. M. Jacob, "Dynamics of solitons in filtered dispersion-managed systems," *IEEE Photon. Technol. Lett.* **10**, 546 (1998).
- [90] F. Merlaud and T. George, "Influence of filtering on jitter and amplitude fluctuations for dispersion managed solitons," in *24th European Conference on Optical Communication (ECOC'98)*, Madrid, Spain, WdB22 (1998).
- [91] M. Matsumoto, "Instability of dispersion-managed solitons in a system with filtering," *Opt. Lett.* **23**, 1901 (1998).
- [92] M. Nakazawa, K. Suzuki, H. Kubota, H. Sahara, and E. Yamada, "160 Gbit/s WDM (20 Gbit/s \times 8 channels) soliton transmission over 10000 km using in-line synchronous modulation and optical filtering," *Electron. Lett.* **34**, 103 (1998).
- [93] M. Matsumoto, "Time-domain transmission control of dispersion-managed solitons," *Electron. Lett.* **34**, 2155 (1998).
- [94] Y. Kodama, M. Romangnoli, and S. Wabnitz, "Soliton stability and interactions in fiber lasers," *Electron. Lett.* **28**, 1981 (1992).
- [95] M. Matsumoto, H. Ikeda, T. Uda, and A. Hasegawa, "Stable soliton transmission in the system with nonlinear gain," *IEEE J. Lightwave Technol.* **13**, 658 (1995).
- [96] D. S. Govan, N. J. Smith, F. M. Knox, and N. J. Doran, "Stable propagation of solitons with increased energy through the combined action of dispersion-management and periodic saturable absorption," *J. Opt. Soc. Am. B* **14**, 2960 (1997).
- [97] T. Hirooka and S. Wabnitz, "Stabilization of dispersion-managed soliton transmission by nonlinear gain," *Electron. Lett.* **35**, 655 (1999).
- [98] P. W. Juodawlkis, D. T. McInturff, and S. E. Ralph, "Ultrafast carrier dynamics and optical nonlinearities of low-temperature-grown InGaAs/InAlAs multiple quantum wells," *Appl. Phys. Lett.* **69**, 4062 (1996).
- [99] P. W. E. Smith, S. D. Benjamin, and H. S. Loka, "Tailoring of trap-related carrier dynamics in low-temperature-grown GaAs," *Appl. Phys. Lett.* **71**, 1156 (1997).

- [100] M. Haiml, U. Siegner, F. Morier-Genoud, U. Keller, M. Luysberg, P. Specht, and E. R. Weber, "Femtosecond response times and high optical nonlinearity in beryllium-doped low-temperature grown GaAs," *Appl. Phys. Lett.* **74**, 1269 (1999).
- [101] P. Harper, I. S. Penketh, S. B. Alleston, I. Bennion, N. J. Doran, "10 Gbit/s dispersion managed soliton propagation over 200 Mm without active control," *Electron. Lett.* **34**, 1997 (1998).
- [102] H. A. Haus, K. Tamura, L. E. Nelson, and E. P. Ippen, "Stretched-pulse additive pulse mode-locking in fiber ring lasers: theory and experiment," *IEEE J. Quantum Electron.* **31**, 591 (1995).
- [103] A. Yariv, D. Fekete, and D. M. Pepper, "Compensation for channel dispersion by nonlinear optical phase conjugation," *Opt. Lett.* **4**, 52 (1979).
- [104] R. A. Fischer, B. R. Suydam, and D. Yevick, "Optical phase conjugation for time-domain undoing of dispersive self-phase-modulation effects," *Opt. Lett.* **8**, 611 (1983).
- [105] W. Forsysiak and N. J. Doran, "Conjugate solitons in amplified optical fibre transmission systems," *Electron. Lett.* **30**, 154 (1994).
- [106] T. Hirooka and A. Hasegawa, "Quasi-soliton propagation with periodic optical phase conjugation," *Electron. Lett.* **34**, 2056 (1998).
- [107] S. K. Turitsyn, and V. K. Mezentsev, "Chirped solitons with strong confinement in transmission links with in-line fiber Bragg gratings," *Opt. Lett.* **23**, 600 (1998).
- [108] A. Hasegawa and T. Hirooka, "Stable filter control of wavelength division multiplexed soliton systems," *Electron. Lett.* in press.
- [109] K. Fukuchi, M. Kakui, A. Sasaki, T. Ito, Y. Inada, T. Tsuzaki, T. Shitomi, K. Fujii, S. Shikii, H. Sugahara, and A. Hasegawa, "1.1-Tb/s (55×20-Gb/s) dense WDM soliton transmission over 3,020-km widely dispersion-managed transmission line employing 1.55/1.58- μ m hybrid repeaters," in *25th European Conference on Optical Communication (ECOC'99)*, Nice, France, PD2-10 (1999).
- [110] Y. Yano, T. Ono, K. Fukuchi, T. Ito, H. Yamazaki, M. Yamaguchi, and K. Emura, "2.6 terabit/s WDM transmission experiment using optical duobinary coding," in *22th European Conference on Optical Communication (ECOC'96)*, Oslo, Norway, ThB3-1 (1996).
- [111] D. Le Guen, A. O'Hare, S. Del Burgo, D. Grot, F. Favre, and T. Georges, "Narrow band 640 Gbit/s soliton WDM transmission over 1200 km of standard fibre with 100 km-21 dB amplifier spans," in *24th European Conference on Optical Communication (ECOC'98)*, Madrid, Spain, Postdeadline papers, pp. 61–63 (1999).
- [112] S. W. Seo, K. Bergman, and P. R. Prucnal, "Transparent optical networks with time-division multiplexing," *IEEE J. Select. Areas Commun.* **14**, 1039 (1996).

- [113] D. Cotter and A. D. Ellis, "Asynchronous digital optical regeneration and networks," *J. Lightwave Technol.* **16**, 2068 (1998).
- [114] V. W. S. Chan, K. L. Hall, E. Modiano, and K. A. Rauschenbach, "Architectures and technologies for high-speed optical data networks," *J. Lightwave Technol.* **16**, 2146 (1998).
- [115] A. Hasegawa and H. Toda, "A feasible all optical soliton based inter-LAN network using time division multiplexing," *IEICE Trans. Commun.* **E81-B**, 1681 (1998).
- [116] H. Anis, G. Berkey, G. Bordogna, M. Cavallari, B. Charbonnier, A. Evans, I. Hardcastle, M. Jones, G. Pettitt, B. Shaw, V. Srikant, and J. Wakefield, "Continuous dispersion managed fiber for very high speed soliton systems," in *25th European Conference on Optical Communication (ECOC'99)*, Nice, France, TuA3.4 (1999).
- [117] H. A. Haus and A. Meccozi, "Long-term storage of a bit stream of solitons," *Opt. Lett.* **17**, 1500 (1992).
- [118] N. J. Doran and D. Wood, "Nonlinear optical loop mirror," *Opt. Lett.* **13**, 56 (1988).
- [119] J. D. Moores, K. Bergman, H. A. Haus, and E. Ippen "Demonstration of optical switching by means of solitary wave collisions in a fiber ring reflector," *Opt. Lett.* **16**, 138 (1991).
- [120] Y. Kodama and A. Hasegawa, "Nonlinear pulse propagation in a monomode dielectric guide," *IEEE J. Quantum Electron.* **23**, 510 (1987).
- [121] D. Marcuse, *Light Transmission Optics*, Van Nostrand Reinhold, New York (1982).
- [122] C. R. Menyuk, "Nonlinear pulse propagation in birefringent optical fibers," *IEEE J. Quantum Electron.* **23**, 174 (1987).
- [123] D. Marcuse and C. R. Menyuk, "Simulation of single-channel optical systems at 100 Gb/s," *J. Lightwave Technol.* **17**, 564 (1999).